100 ap
8/14/72

289

AI-AEC-13087

ZIRCONIUM HYDRIDE REACTOR
CORE HYDRAULIC STUDIES
SUMMARY REPORT

AEC Research and Development Report

MASTER

Atomics International Division
Rockwell International

P.O. Box 309
Canoga Park, California 91304

MASTER

DISTRIBUTION OF THIS DOCUMENT IS UNLIMITED

DISCLAIMER

This report was prepared as an account of work sponsored by an agency of the United States Government. Neither the United States Government nor any agency Thereof, nor any of their employees, makes any warranty, express or implied, or assumes any legal liability or responsibility for the accuracy, completeness, or usefulness of any information, apparatus, product, or process disclosed, or represents that its use would not infringe privately owned rights. Reference herein to any specific commercial product, process, or service by trade name, trademark, manufacturer, or otherwise does not necessarily constitute or imply its endorsement, recommendation, or favoring by the United States Government or any agency thereof. The views and opinions of authors expressed herein do not necessarily state or reflect those of the United States Government or any agency thereof.

DISCLAIMER

Portions of this document may be illegible in electronic image products. Images are produced from the best available original document.

NOTICE

This report was prepared as an account of work sponsored by the United States Government. Neither the United States nor the United States Atomic Energy Commission, nor any of their employees, nor any of their contractors, subcontractors, or their employees, makes any warranty, express or implied, or assumes any legal liability or responsibility for the accuracy, completeness or usefulness of any information, apparatus, product or process disclosed, or represents that its use would not infringe privately owned rights.

AI-AEC-13087
SNAP REACTOR
SNAP PROGRAM
M-3679-R69
C-92b

ZIRCONIUM HYDRIDE REACTOR
CORE HYDRAULIC STUDIES
SUMMARY REPORT

B. J. OSTERMIER

NOTICE

This report was prepared as an account of work sponsored by the United States Government. Neither the United States nor the United States Atomic Energy Commission, nor any of their employees, nor any of their contractors, subcontractors, or their employees, makes any warranty, express or implied, or assumes any legal liability or responsibility for the accuracy, completeness or usefulness of any information, apparatus, product or process disclosed, or represents that its use would not infringe privately owned rights.

Atomics International Division
Rockwell International

P O Box 309
Canoga Park California 91304

CONTRACT: AT(04-3)-701
ISSUED: JUNE 30, 1973

DISTRIBUTION OF THIS DOCUMENT IS UNLIMITED

DISTRIBUTION

This report has been distributed according to the category "Systems for Nuclear Auxiliary Power (SNAP) Reactor – SNAP Program," as given in the Standard Distribution for Classified Scientific and Technical Reports, M-3679.

CONTENTS

TABLES

FIGURES

FIGURES

FIGURES

ABSTRACT

A summary is presented for the series of water-hydraulic tests performed to evaluate the flow characteristics of the various zirconium hydride reactors. Test models, test methods, instrumentation, and results are described. Tests were conducted to develop inlet plenum configurations and fuel element fin configurations. Inlet plenum configurations were evaluated on their ability to produce desired in-core flow distributions, and to provide a uniform pressure at the inlet grid plate surface without any undesirable flow characteristics. A series of inlet plenum tests was also conducted to determine any flow behavior which might have contributed to the operational problems of the S8DR. Fuel element fin configurations were evaluated on their ability to produce interchannel flow mixing within the reactor core. Pressure drop determinations were made for all plenum and fuel element fin configurations.

I. INTRODUCTION

The zirconium hydride (ZrH) reactor designs used compact lightweight arrays of ZrH fuel elements cooled by a flowing liquid metal (NaK) at temperatures, generally, of 1100 to 1300° F.

The coolant flowing past a fuel element is not only the heat transfer medium required by the power generation system, it is also the mechanism used for core temperature control and is thereby an important factor in fuel performance. Proper distribution of the coolant within the core is thus an important parameter for the design and operational performance of the Reactor Power System.

Coolant distribution in the core is obtained by proper design of the core coolant flow system, primarily the inlet plenum and core coolant flow channels. The inlet plenum provides the deceleration and redirection of flow required so that the mixing or flow distribution capability of the core elements will insure adequate cooling of all fuel elements. The coolant flow distribution should also be obtained with a minimum system pressure drop to minimize pump size and weight.

The geometry constraints on the ZrH flow systems arrangements were such that flow could not be channeled directly into the reactor with an optimum flow distribution. Typically, in the ZrH reactors the NaK coolant enters a shallow inlet plenum from a direction roughly perpendicular to the long axis of the reactor core. Analytical methods of predicting flow behavior in the reactor cores were not entirely adequate. The non-ideal, i. e. viscous, flow occurring in the inlet plenum meant that when potential flow solutions to flow behavior in the proposed plenum were attempted, they only provided guidance, not direct design information. Also, for some reactors, the plenum configurations were not easily analyzed. These inadequacies in the purely analytical approach, coupled with operating experience with the early reactor designs, indicated that an experimental effort was required to determine and demonstrate the adequate hydraulic performance of the proposed reactor designs prior to their fabrication and operation. Extensive experimental studies of inlet plenum flow behavior, flow distribution in the core, and pressure drop were performed in order to select the core design.

II. INLET PLENUM STUDIES

The ZrH reactors required reactor inlet plenums which could meet the requirements of providing optimum flow distribution in a restricted amount of space. The ability of plenum designs to meet these requirements was determined by hydraulic testing with full- scale core models and the NaK coolant simulated by flowing water. From the results of these tests, similarity relations based on Reynolds number could be used to predict plenum performance with the NaK coolant.

A. SNAP 8 REACTOR

The inlet plenum studies for the SNAP 8 reactors were conducted to determine those inlet plenum configurations which would produce the desired flow distribution in the core. In addition, for the SNAP 8 Developmental Reactor (S8DR) a series of post-operation tests were conducted to determine if there were flow conditions in the inlet plenum which could have contributed to the operational problems encountered with this reactor.

Preoperational tests for the SNAP 8 reactors were designed to select that inlet plenum configuration which would give the desired flow distribution in the reactor core with a minimum core pressure drop. Therefore, instrumentation for these tests was designed to provide measurements of core pressure drop and of flow distribution in the reactor core. The core flow distribution was determined by making measurements in the core itself or at the core exit plane.

Flow settings for all tests were determined to provide Reynolds number similarity between the model and the prototype. For the SNAP 8 reactors, the 100% flow condition was 48,800 lb/hr of NaK-78 entering at 1100°F and leaving at 1300°F. The water flow required to simulate this condition was 272 gpm at 160°F. Other prototype flow conditions were duplicated by using 160°F water and determining the water flow by proportion to the flow simulating 100% prototype flow.

The full-scale core models used in these tests had 211 simulated fuel elements. The elements were arranged in a hexagonal array giving 420 tricusp coolant channels (Figure 1). For those tests using $NaNO_3$ injection to determine

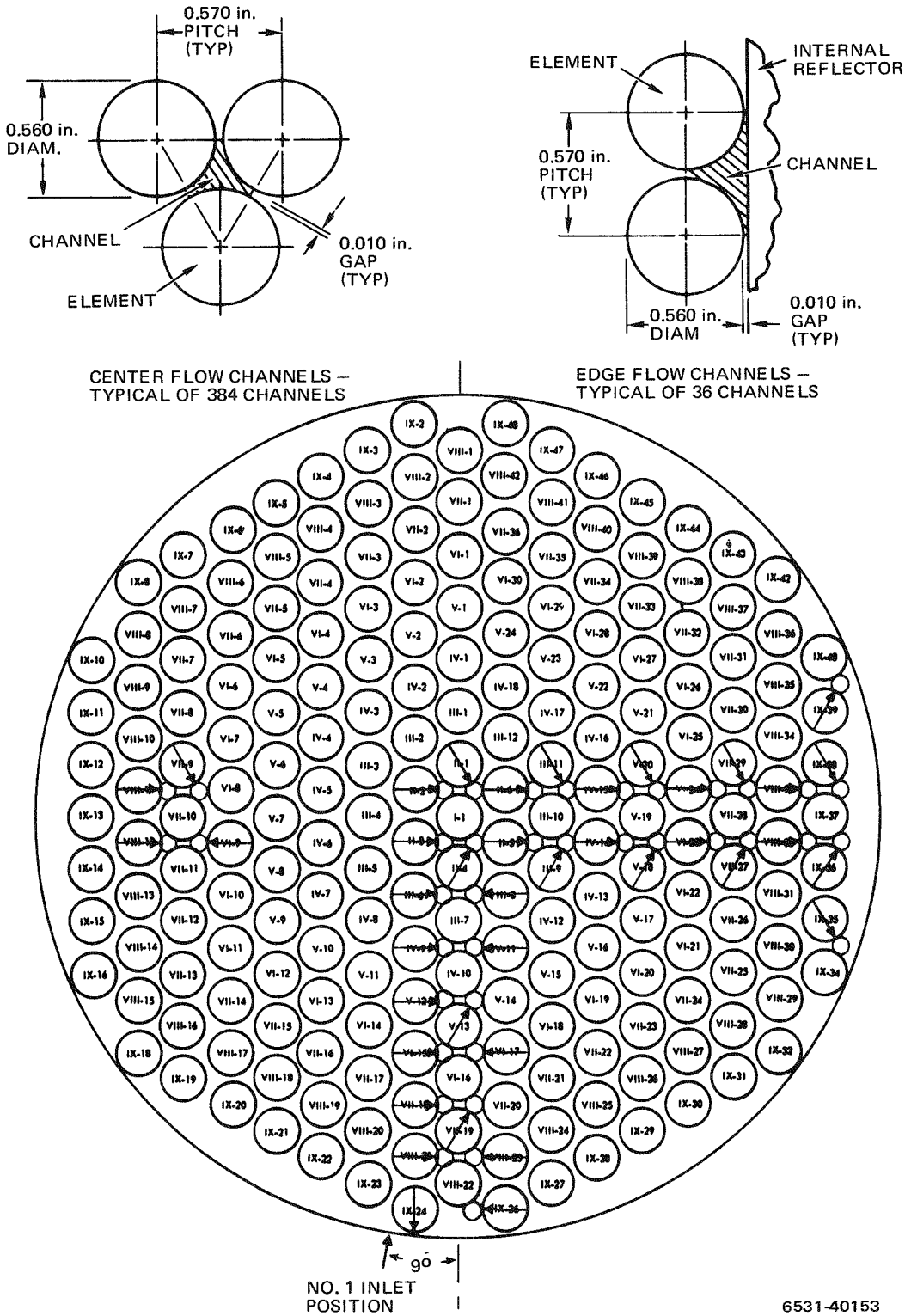

Figure 1. Typical Fuel Element Arrangement

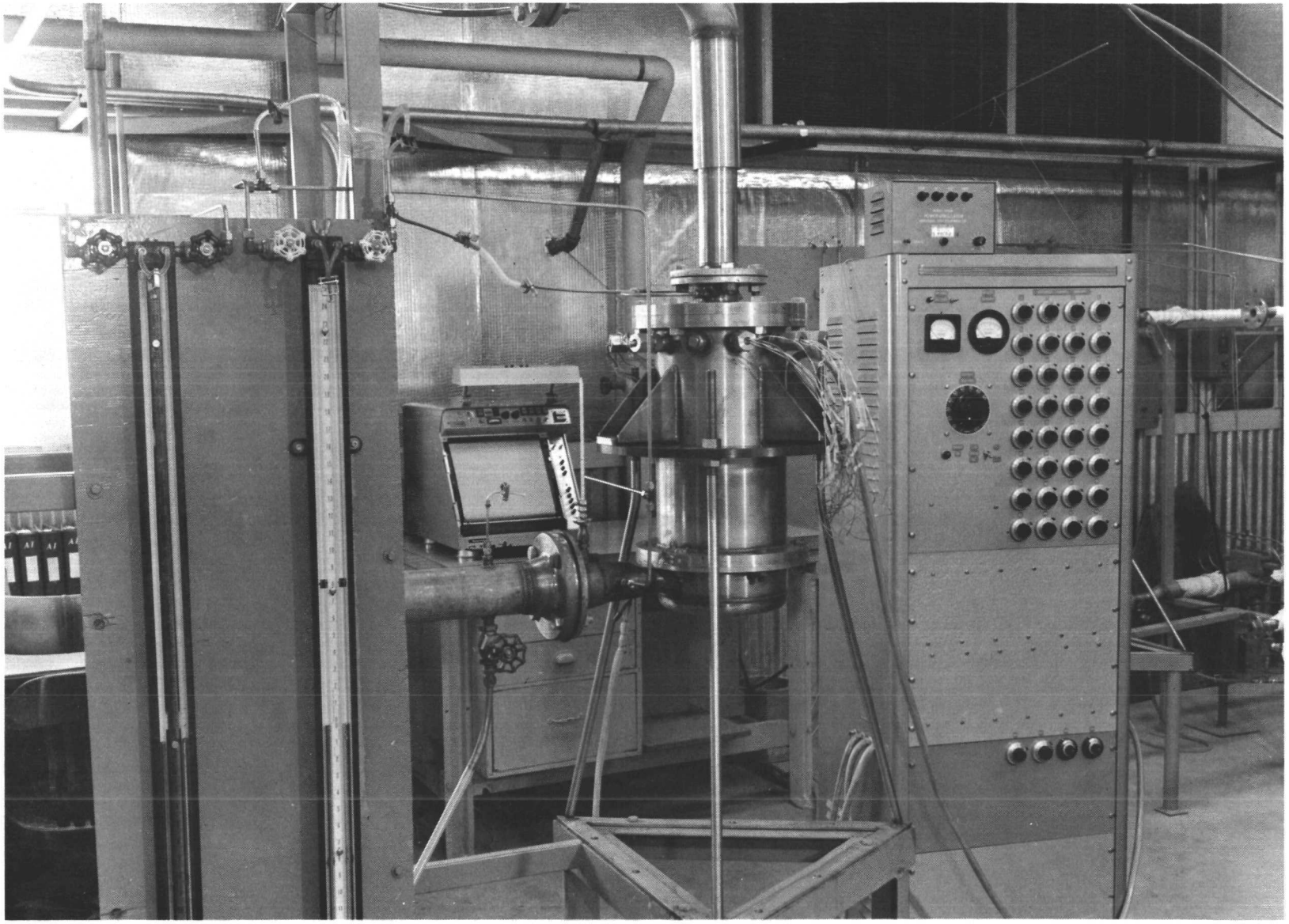

8-15-61

7570-5002A

Figure 2. S8ER Core-Model Test Installation

the core velocity variation, instrumented elements were positioned to monitor selected core flow channels. Instrumentation leads for these elements were generally routed out of the core through a hollow exit grid plate.

The initial plenum tests (Figure 2) were conducted to design the SNAP 8 Experimental Reactor (S8ER) inlet plenum baffle configuration. This series of tests used a technique in which a saturated $NaNO_3$ solution was introduced into the flowing water upstream of the plenum inlet. Sensors (see Figure 3) installed flush with the surface of mockup fuel elements detected the instant that the salt-induced conductivity change occurred in the adjacent flow channel. Two sensors were located 1 ft apart in each instrumented element and were each connected to a Wheatstone bridge circuit. The time for the salt to traverse this 1-ft flow channel distance could be determined from an oscillograph record showing the time between deflection of the Wheatstone bridge galvanometers. The channel average velocity could then be calculated from the sensor spacing and the salt transit time. The data produced by this salt velocity technique had poor reproducibility, and an additional series of tests were conducted in which flow samples were captured at the exit of the core model outlet grid plate. This series of tests was run with the core model inverted and an indexing system used to locate a sample tube (Figure 4) at the exit of selected core channels. The time required for this tube to collect a given weight of water was measured to give the channel exit flowrate. The inlet plenum core internals were varied and flow samples made across core diameters at 90 degrees to each other for each test setup. Results of these tests were used to select the inlet plenum baffle plate design for the S8ER.

As the S8DR reactor preliminary design progressed it was decided to simplify the plenum baffle plate from that for the S8ER. An additional series of tests was run with a full-scale model of the S8DR-inlet plenum and core internals. Instrumentation for these tests consisted of six flush conductivity sensors spaced along mockup fuel elements (Figure 5). The intent was to determine in-core velocity distribution at several axial locations using the salt velocity technique. A preliminary set of tests was conducted to improve the techniques of the salt velocity measurement method by introducing the salt solution into individual core coolant channels. The mechanism for this injection could not be adequately determined, however, and attempts at generalized salt injection in the

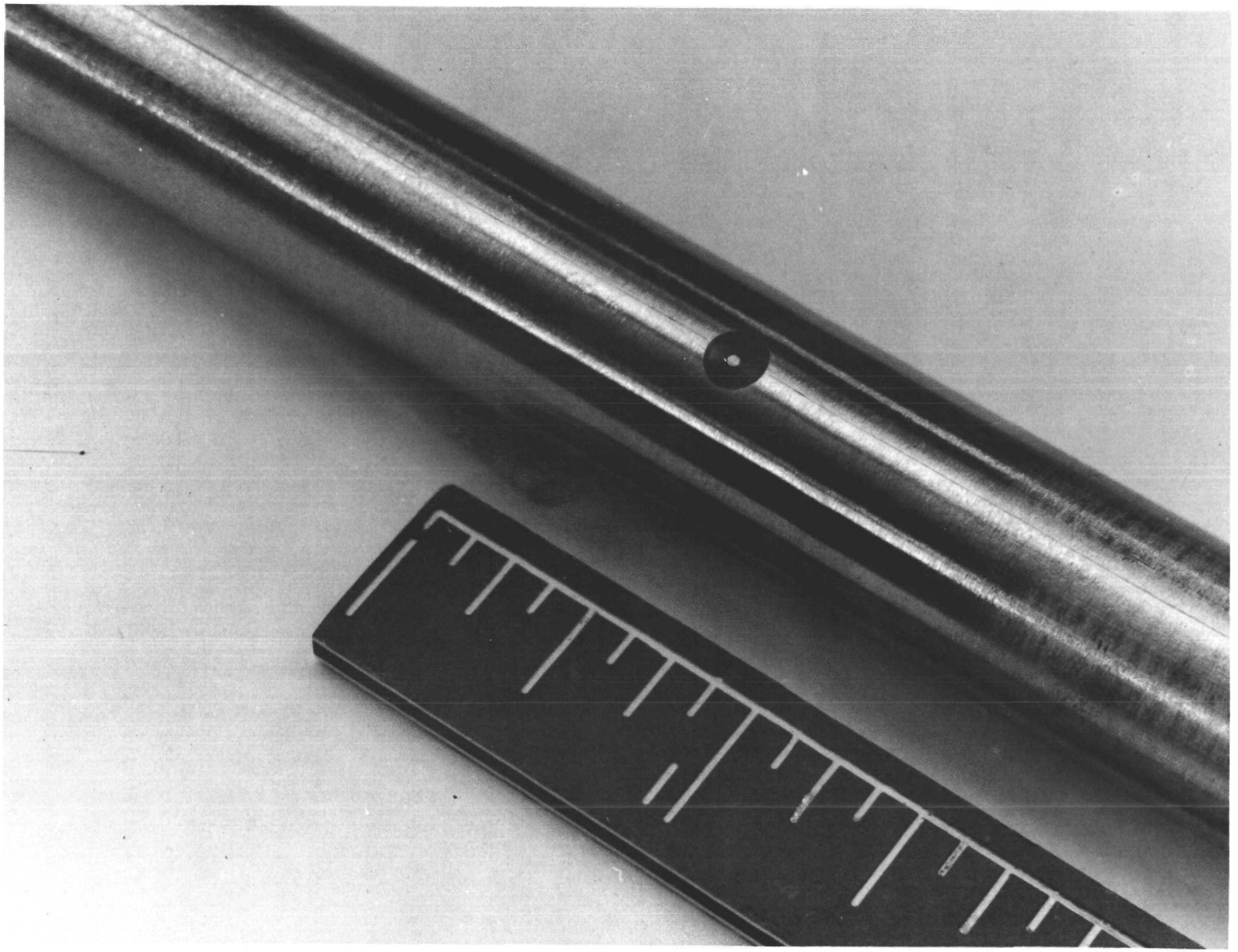

7570-5115C

Figure 3. Typical Installation of Sensor in an S8ER Fuel Element

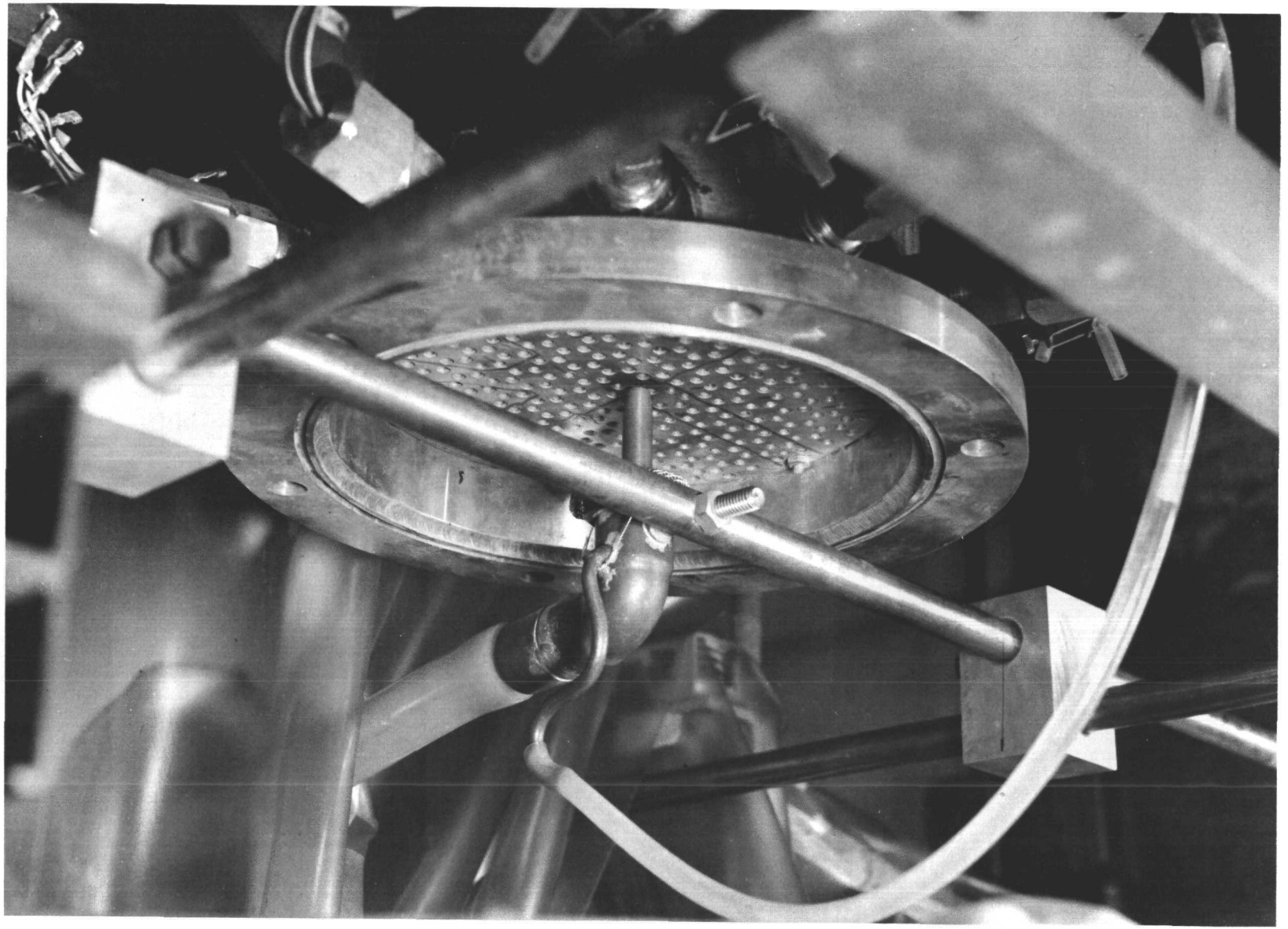

6-14-62

7570-54114A

Figure 4. S8ER Exit Plane "Catch Tube"

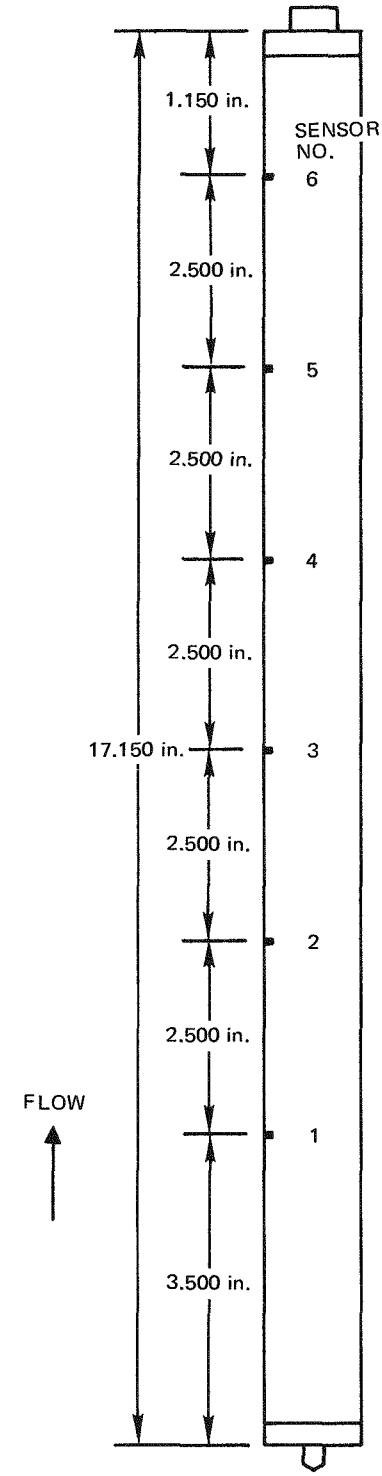

Figure 5. Sensor Locations in S8DR Instrumented Elements

inlet plenum, although showing promise, had problems of data scatter and decreasing sensitivity due to salt accumulation in the system water. Attempts to use the salt velocity technique were terminated, therefore, and an alternate measurement technique, the noise analysis method, was used.

The noise analysis technique measured the average time for a perturbation in a continuously injected stream of salt to move from one sensor to another. This measurement was accomplished using the same sensors as those installed in the core for use in the salt velocity tests. The salt was injected into the inlet flow upstream of the plenum. The recording and data analysis method was entirely different than that for the salt velocity approach. The heart of the noise analysis method was the use of a cross-correlation computer. * This computer was used to determine the delay time, giving a maximum positive value for the cross-correlation function between the signals from two conductivity sensors. If these two sensors were monitoring the same core flow channel, the signals from these sensors would be random coherent signals caused by turbulence-induced variations in the injected $NaNO_3$ concentration. Through suitable calibration, the delay time, as determined with this computer, could be related to the coolant transit time and the average velocity determined for the channel section between sensors.

The sequence of operations used in recording data began with the injection of $NaNO_3$ into the 160° F system water. The resulting randomly occurring conductivity variations in the water flowing through the core flow channels were detected by the sensor circuitry and processed to allow recording on magnetic tape (Figure 6). The signals on this magnetic tape could then be analyzed* to provide the flow transit time between sensor locations. Analysis of these data required calibration data relating the signal transit time measurement to velocity in the core flow channel. This was accomplished using data from an instrumented mockup of a single core channel. This single-channel model was fabricated by soldering together three simulated fuel elements, one of which was instrumented, with suitable spacers between elements to simulate a single core channel. The salt transit times for known channel velocities were then determined from data obtained when this model was installed in a flow loop and sensor

*R. L. Randall, P. J. Pekrul and G. R. Grayham, "Development of Noise Analysis Techniques for Measuring Reactor Coolant Velocities," NAA-SR-11193 (March 5, 1966)

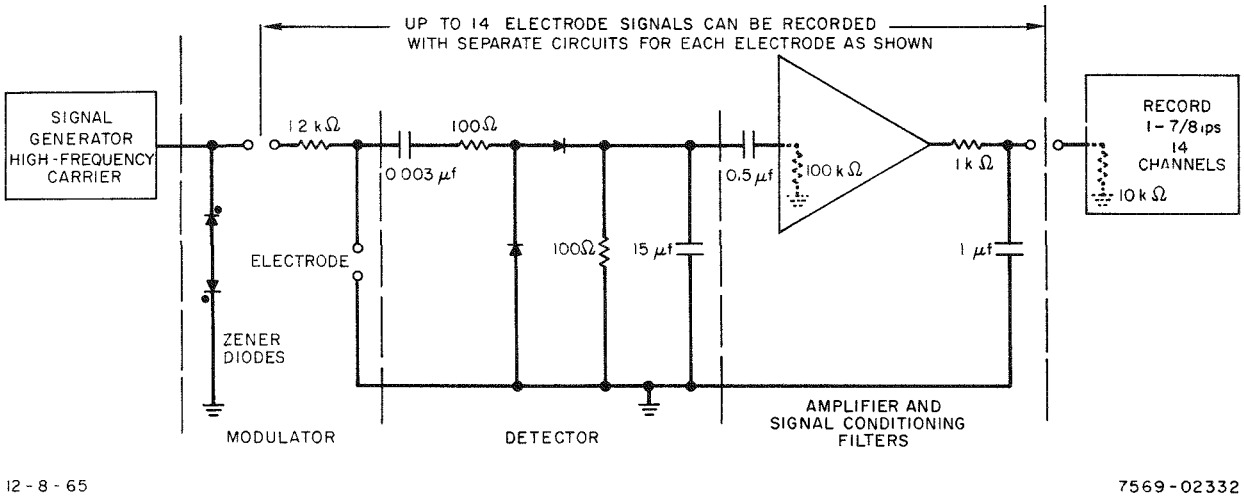

a. Data Acquisition Circuitry

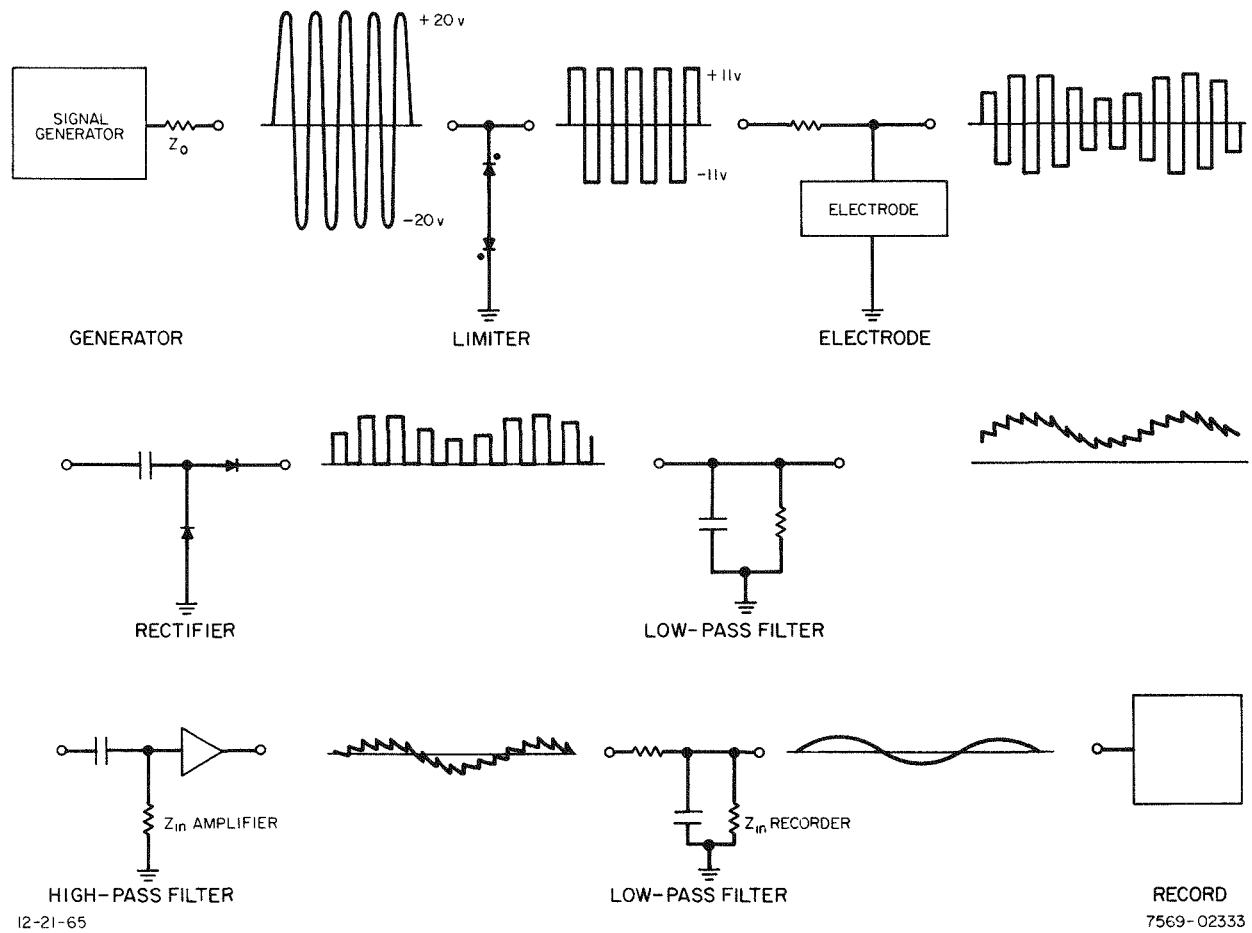

b. Data Acquisition Circuit Waveforms

Figure 6. Noise Analysis Data System

signals recorded for $NaNO_3$ injections into each of several known flowrates ranging over the expected core channel flow rates.

The basic noise analysis technique used in obtaining the experimental data was used to evaluate various flow-shaping devices for the S8DR. Instrumented elements having only four sensors were located in a core model (Figure 7). Using the results of a single channel calibration test the noise analysis measurements from these elements were interpreted to give adjacent channel flowrates.

In the salt injection system, the $NaNO_3$ solution was contained in a tank under N_2 pressure and injected into the core inlet pipe through a needle injector. Injection of the $NaNO_3$ solution was controlled by a solenoid valve which was opened and closed at a random rate (Figure 8). This modulation of the injection rate apparently caused the salt solution to divide into smaller "packets," resulting in variations of sensor conductivity signals with higher frequencies than those normally created by hydraulic mixing. The higher-frequency components in the sensor signal tended to improve the statistical accuracy and time resolution of the cross-correlation measurements.

Some difficulty was experienced with the epoxy used to support and insulate the center electrodes of the conductivity sensors. During tests, some electrode insulators tended to "grow" out of the instrumented elements, partially block the adjacent flow channel, sometimes pressing against elements, and leave the center electrode recessed. These occurrences produced increased scatter in the noise analysis data and were corrected by disassembling the core model and refinishing the insulators to be flush with the element surface.

B. TEST RESULTS

1. SNAP 8 Experimental Reactor

In the preliminary S8ER tests, the measured channel water velocities were converted to predicted NaK velocities using Reynolds number similarity relations. These predicted NaK velocities were then plotted versus the actual radial position of the flow channel. A baffle with an upturned lip (Figure 9) was found to give a measured flow velocity distribution within the allowable variations about the ideal profile (Figure 10) at 100% flow simulation. The flow profiles were then determined for flow simulations ranging from 4% to 138% of the design flow.

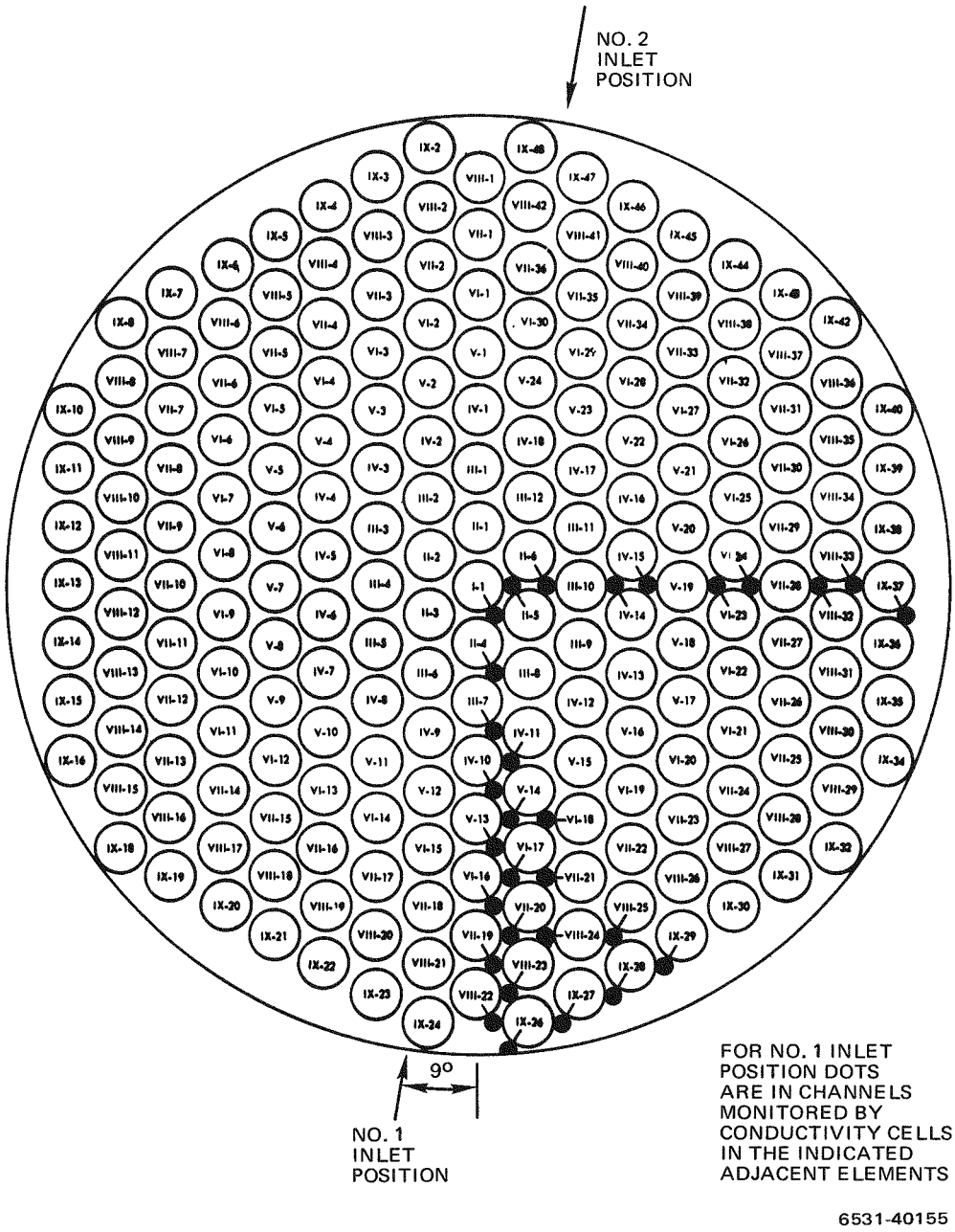

Figure 7. S8DR Cone Configuration Indicating Instrumentation Orientation and Flow Channels Monitored

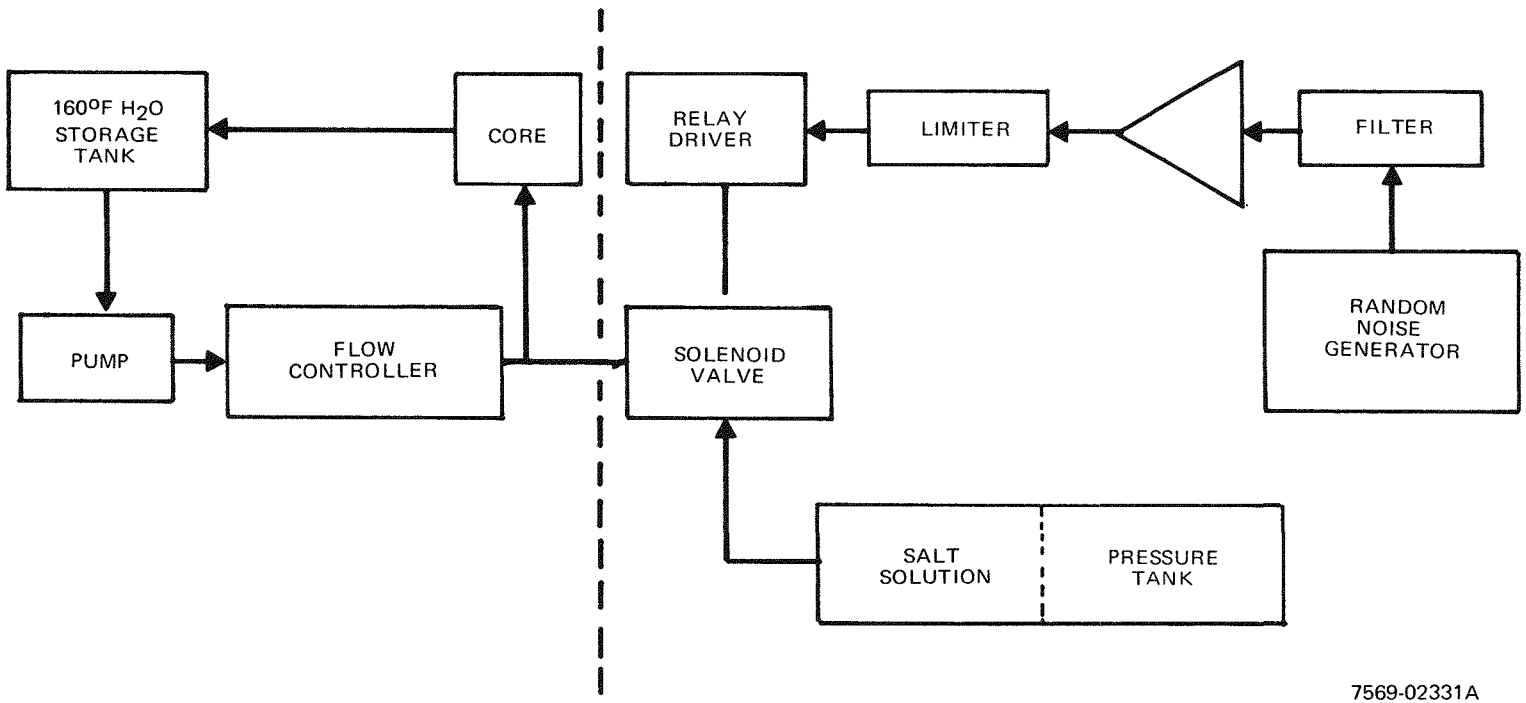

Figure 8. Salt Injection System Block Diagram

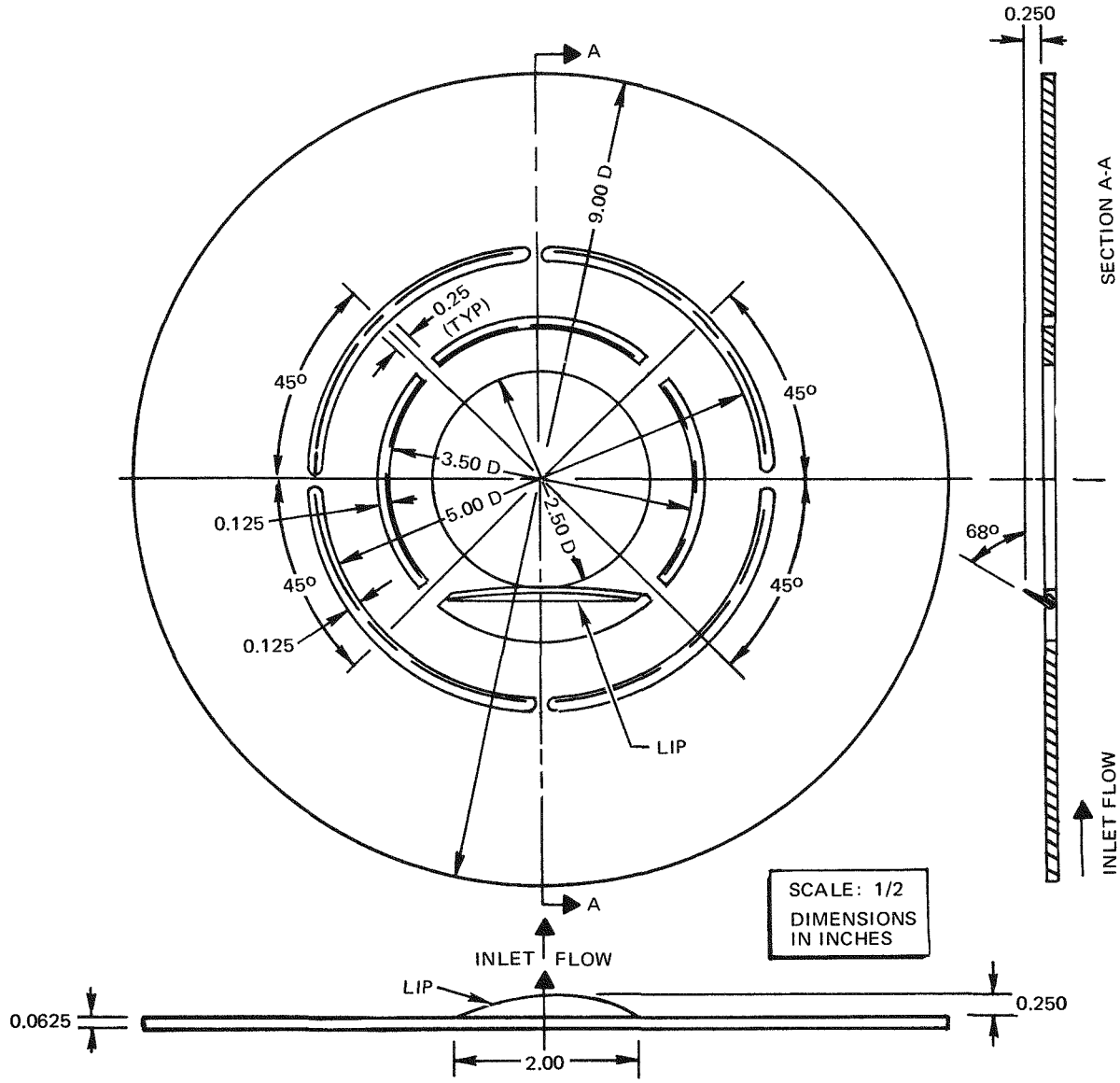

PLENUM CHAMBER ID = 9.214 in.

EFFECTIVE DIAMETER OF BAFFLE = 9.214 in.

AREA OF CENTRAL HOLE = 4.91 $in.^2$

AREA OF THREE INNER ARC SLOTS = 0.937 $in.^2$

AREA OF OPENING WITH LIP = 0.750 $in.^2$

AREA OF FOUR OUTER ARC SLOTS = 1.875 $in.^2$

TOTAL FLOW AREA = 8.47 $in.^2$

DISTANCE BETWEEN TOP SURFACE OF BAFFLE AND BOTTOM SURFACE OF BOTTOM GRID PLATE = 0.4375 in. (BOTTOM SURFACE OF BAFFLE FLUSH WITH TOP EDGE OF SIDE INLET PORT IN BOTTOM PLENUM)

6531-40156

Figure 9. Sketch of S8ER Baffle No. 27

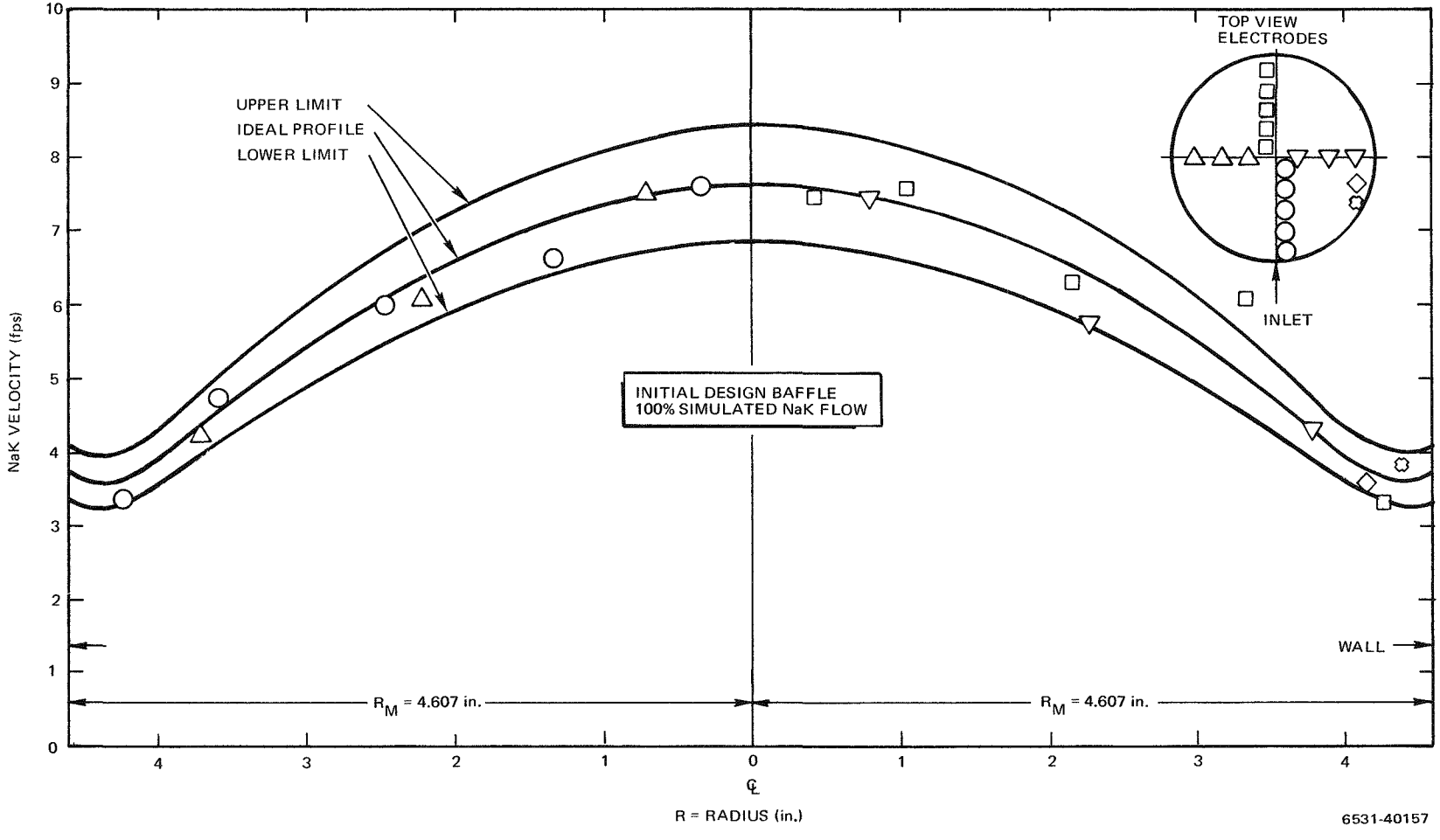

Figure 10. S8ER Predicted NaK Velocity Profile for Selected Baffle No. 27 at 100% Flow

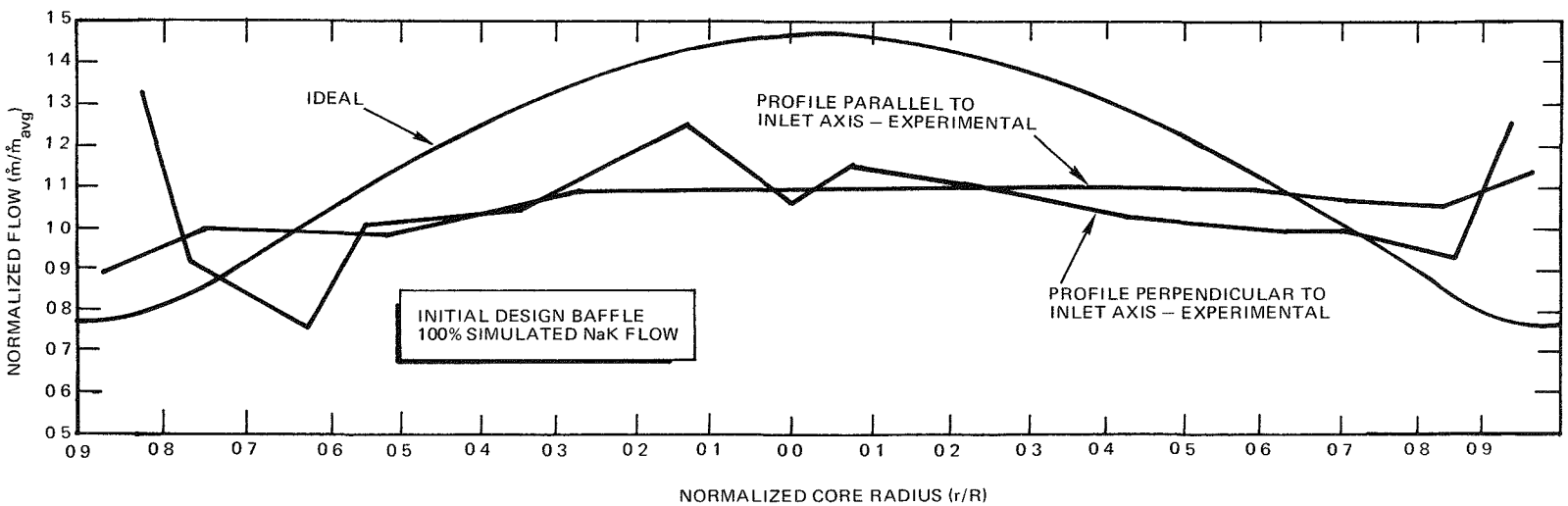

Figure 11. Exit-Plane Mass Flow Profile for S8ER

Water pressure-drop measurements were also made across the core model and converted to equivalent NaK pressure-drop values using Reynolds number similarity relations. These measurements provided the operating characteristics of the selected baffle configuration over a major portion of the expected operating range.

A subsequent study of the results of these initial salt velocity studies showed the data had poor reproducibility. The mass sampling technique was therefore used to measure the channel exit flowrates from the inverted core model. Results of these tests, presented as flow channel mass flowrate ratios, $\dot{m}/\dot{m}_{avg}$, versus non-dimensional radius r/R, showed significant variance from the desired theoretical profile (Figure 11).

The disagreement of the profiles measured by the salt velocity technique with those measured by the mass capture technique is probably due more to the measurement methods than to data reproducibility. The salt velocity technique measured an average velocity through the core to determine channel flow while the mass capture technique determined the actual flow through the outlet grid plate for each flow channel sampled. Subsequent tests showed that the initial high flow velocities in the core center gradually decreased as flow passed through the core (Figure 12). Thus the salt velocity measurements would have been biased toward higher center channel velocities because they were average velocity measurements rather than those determined from the outlet grid plate exit flowrate measurements.

The initial S8ER baffle was designed with various hole patterns to obtain the desired flow profile. Subsequently, the design objective was to shape the core flow by controlling the radial flow of coolant between the baffle and grid plate. The basic baffle configuration had a central hole surrounded by four concentric rings extending from the baffle toward the inlet grid plate. Initial tests with all rings of the same height and a 2-in. center hole, produced excessive core center flow and high core pressure drop. A series of tests was conducted in which the center hole was modified, the ring heights varied, and the effects of concentric rings of holes determined. From this succession of tests, a baffle configuration (Figure 13) was determined which gave an acceptable flow profile (Figure 14) and a minimum pressure drop.

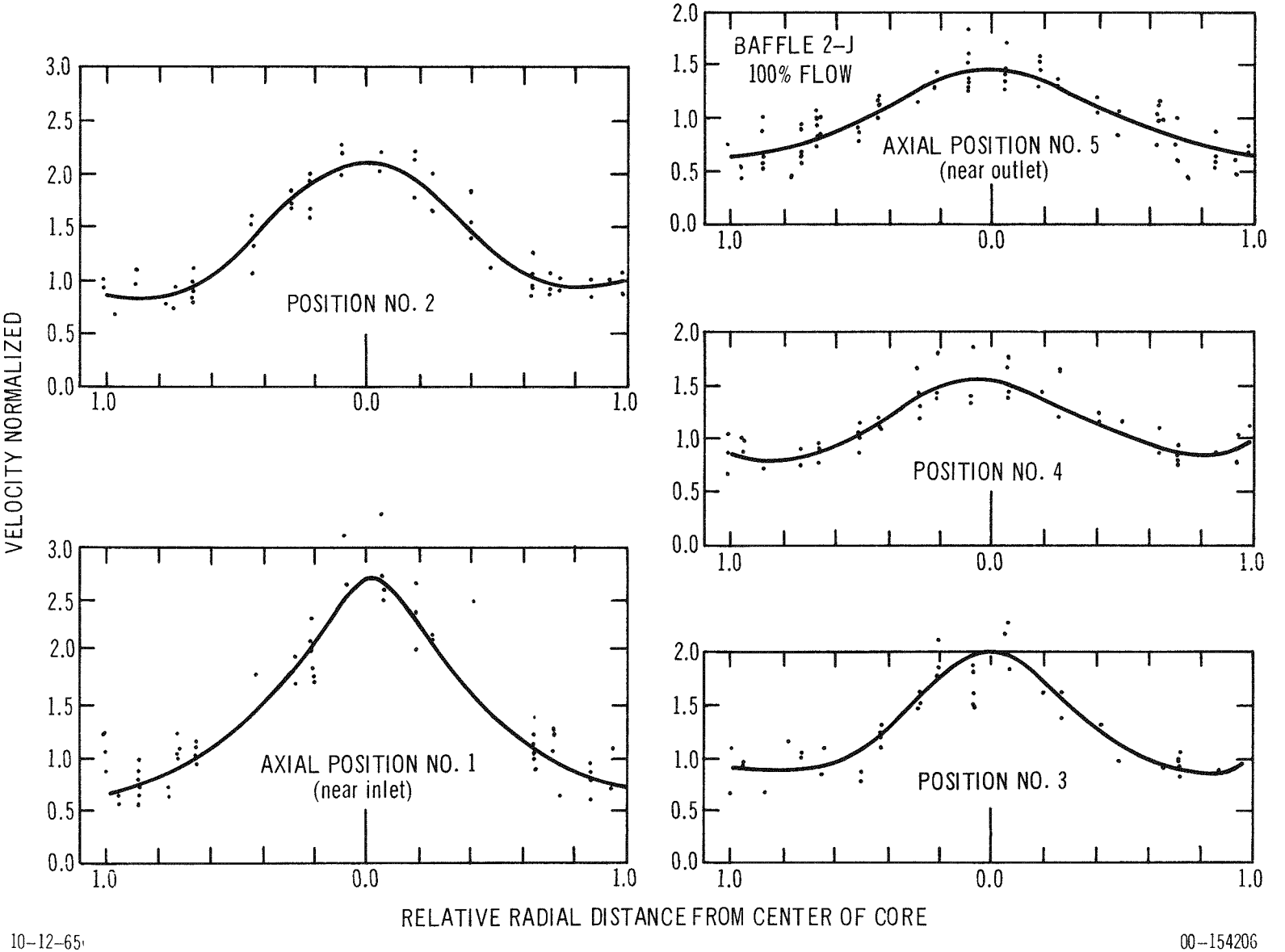

Figure 12. S8DS Flow Profiles at Various Cone Axial Stations for Design Baffle 2J

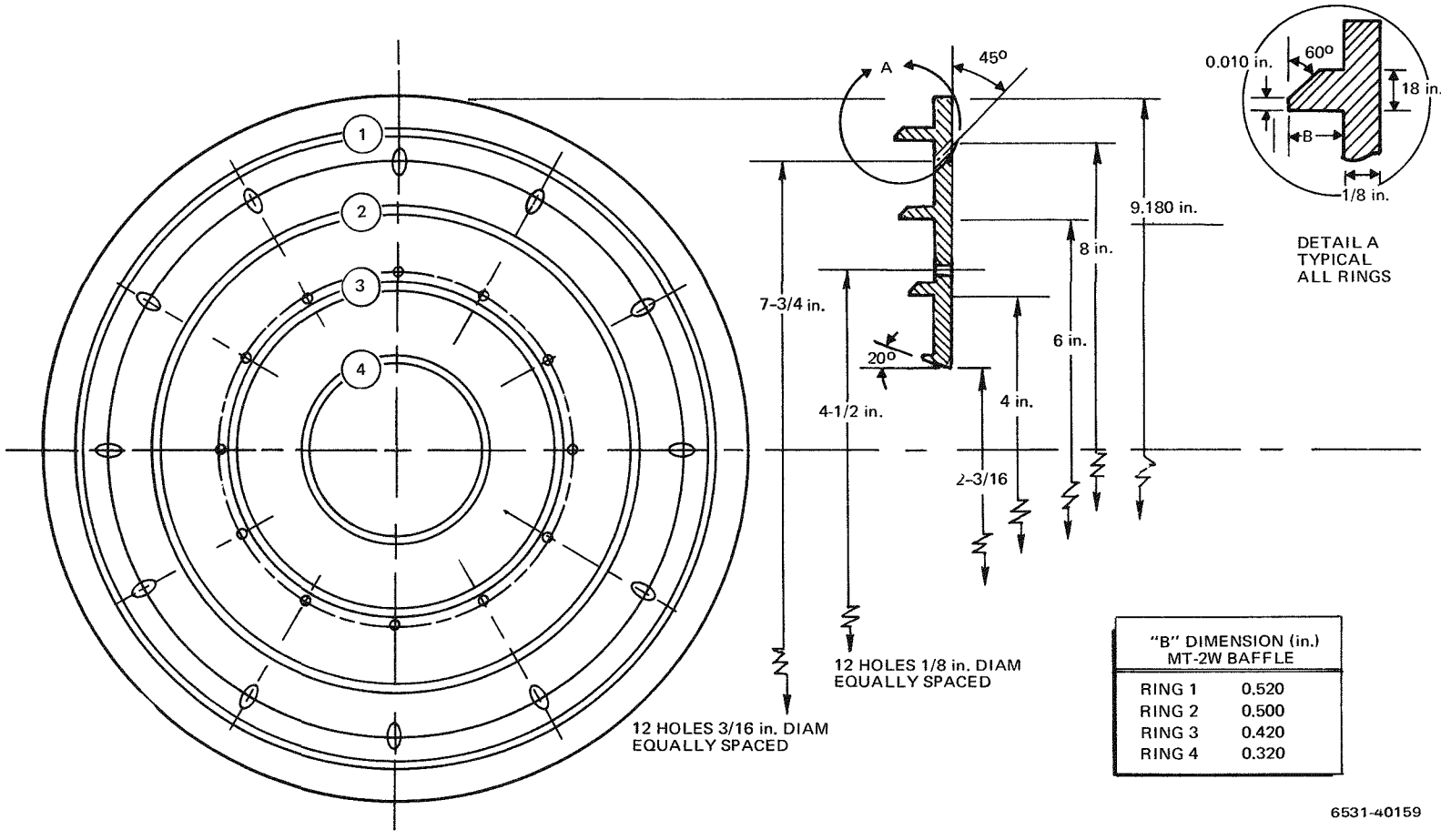

Figure 13. Sketch of Final Selected S8ER Baffle MT-2W

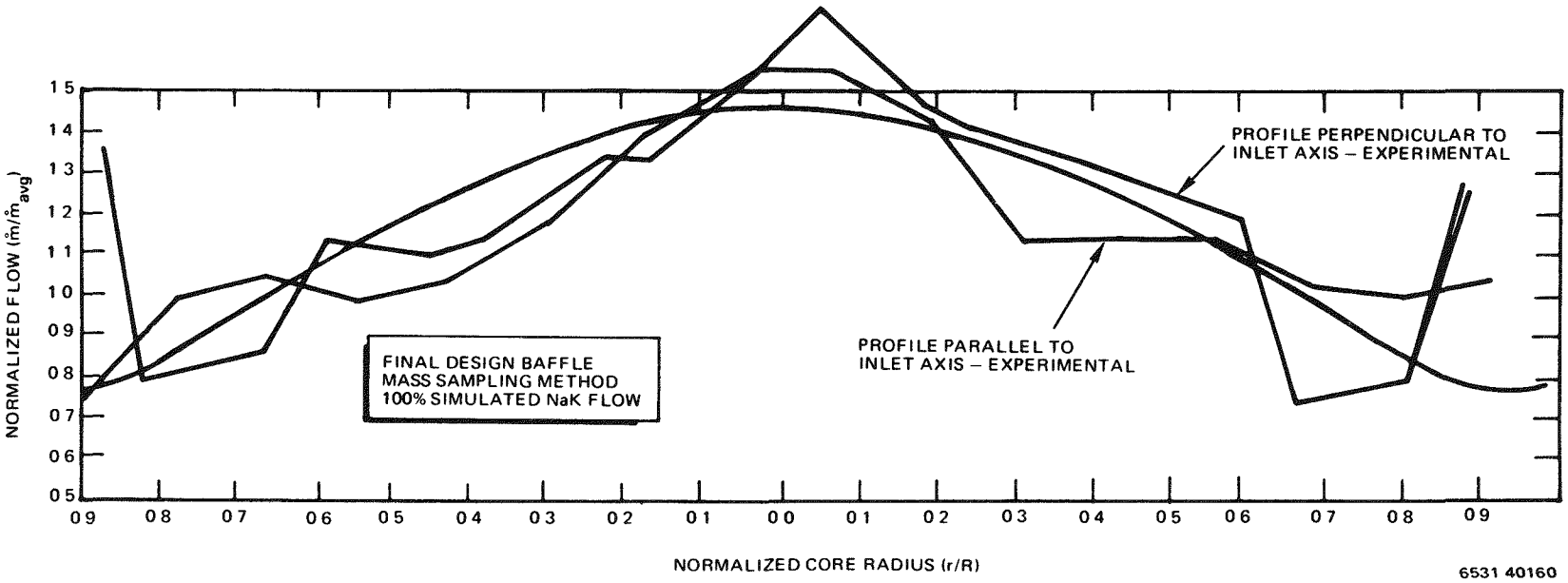

Figure 14. Comparison of Design and Experimental S8ER Exit Plane Flow Profile at Simulated 100% NaK Flow with Baffle MT-2W Installed

2. SNAP 8 Developmental Reactor

For the S8DR, additional tests were conducted to develop a solid baffle plate having a simpler design than the S8ER baffle. The noise analysis method of interpreting conductivity changes from in-core sensors as channel flow velocities was also developed during these tests.

As in the S8ER, the baffle was designed to constrict the coolant flow radially with a small clearance between the baffle and the lower grid plate. Data were presented as plots of $\dot{m}/\dot{m}_{avg}$ versus r/R as determined from the transit time between instrumented element sensors 3 and 5 (Figure 5). Effectiveness of baffle configurations was determined by comparing the measured core flow profile with the desired profile at Z/L = 0.8, a point located at 0.8 of the distance between the inlet and outlet grid plates. (This location, Z/L = 0.8, was the expected location of the maximum fuel temperature.) The core flow profile measured at Z/L = 0.8 was shaped by successive baffle modifications. The center hole diameter was changed, the shape of the center hole edge was modified, and the clearances between the baffle plate and lower grid plate were varied. The main objective was to produce an ideal core profile with a minimum core pressure drop; however, difficulties were encountered because quite often a change which improved one parameter had an adverse effect on the other.

Subsequently, the design approach was modified to utilize the inlet baffle only to distribute the flow from the small radial inlet uniformly over the core diameter. A secondary multi-orificed plate was used to control the flow to individual flow channel inlet orifices in the inlet grid plate. The selected design of the basket-type flow distribution baffle (Figure 15) and the flow-control orifice plate, (Figure 16) provided acceptable flow characteristics as shown in Figure 17. The predicted core pressure loss at the design NaK flow was 4.6 psi.

The occurrence of cracked fuel elements during the operation of the S8DR prompted a post-operation analysis effort. A series of hydraulic tests was performed to support this analysis effort. Of particular interest in these tests was the determination of the effect entrained gas in the coolant would have on coolant flow through the core.

The test approach used at AI was to construct a full-scale model of the S8DR core flow region and test this model at water flowrates duplicating the range of

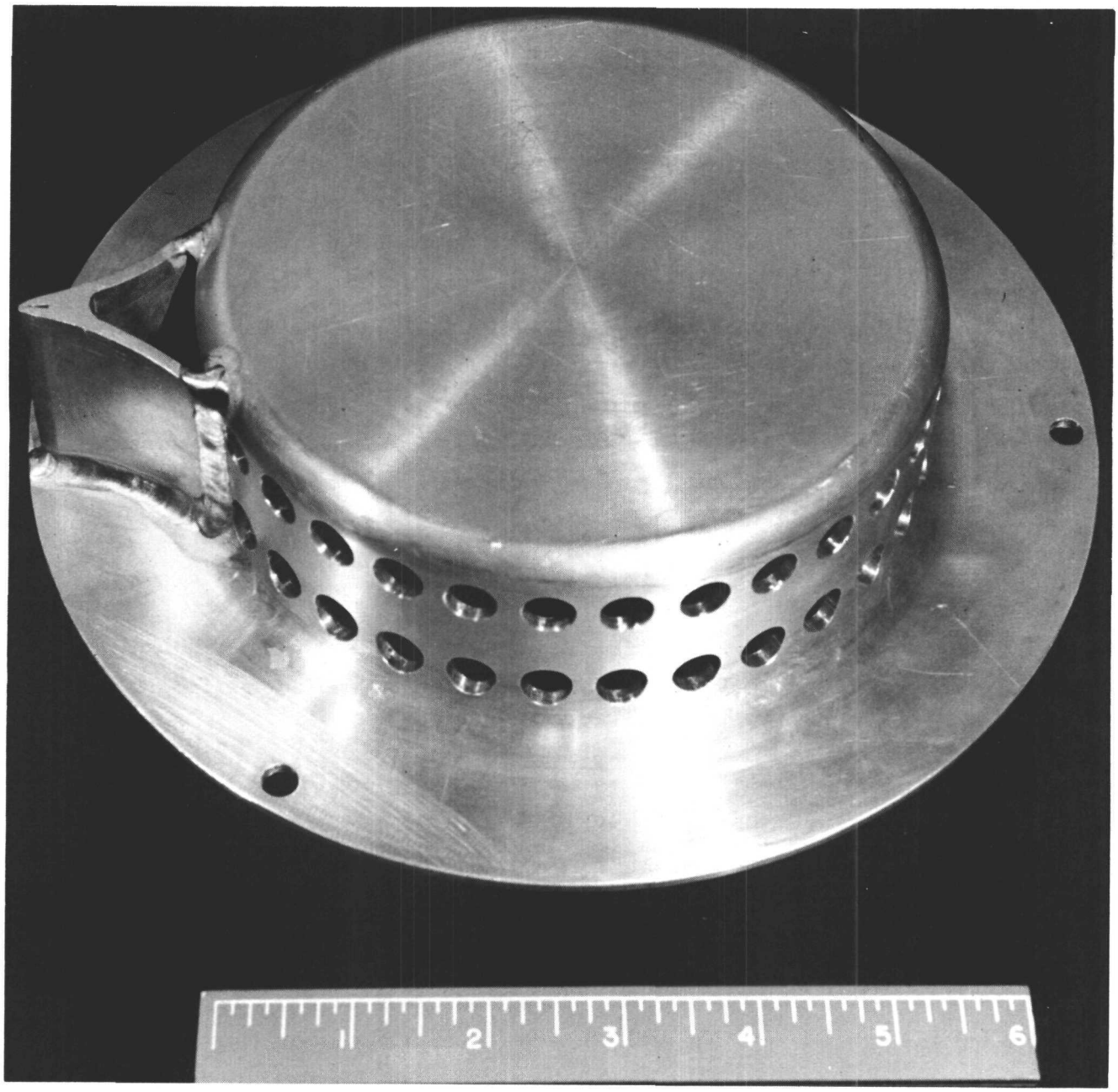

4-14-67

7695-5404

Figure 15. S8DR Flow Distributor

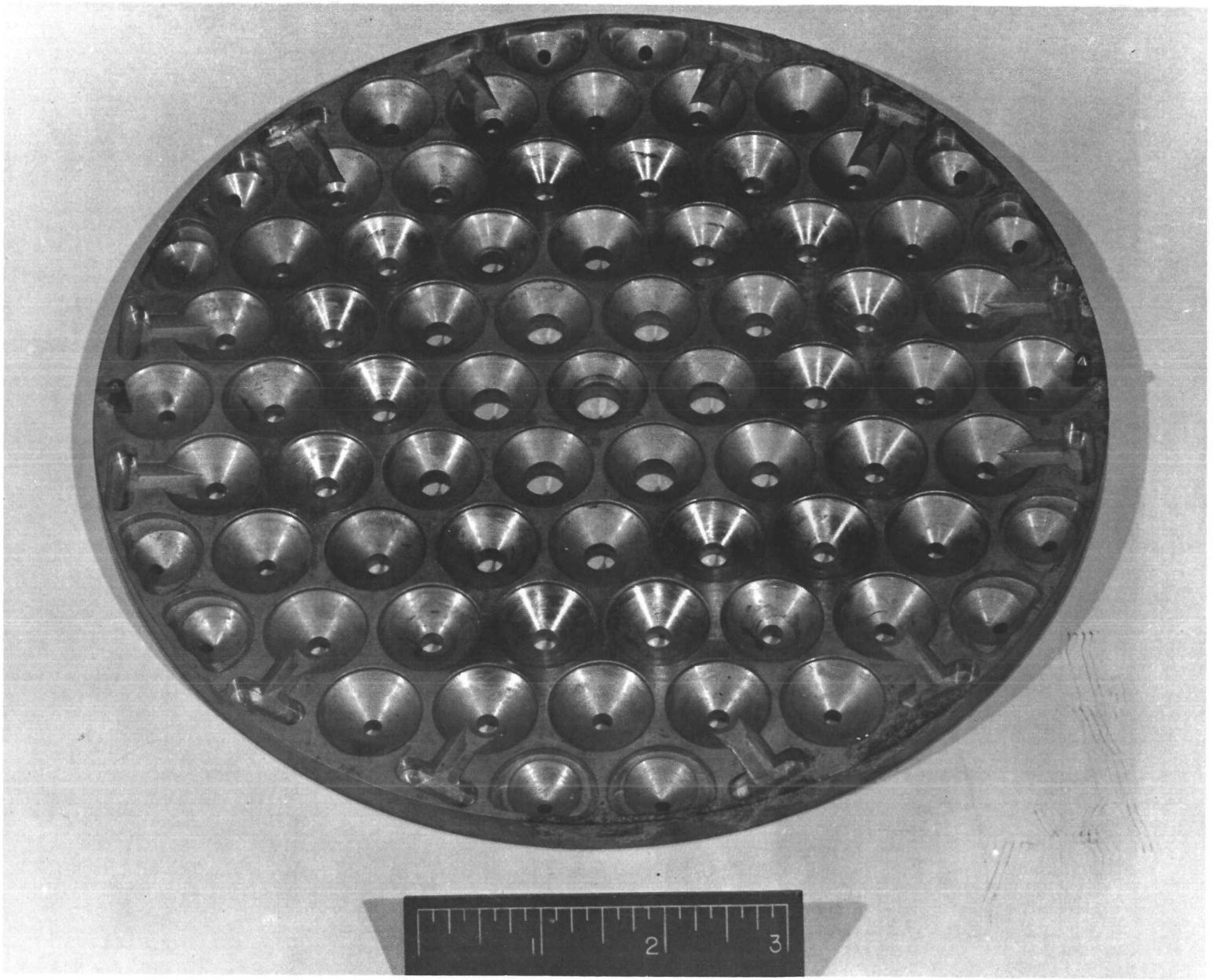

9-12-67

7695-5211

Figure 16. S8DR Orifice Plate 4M

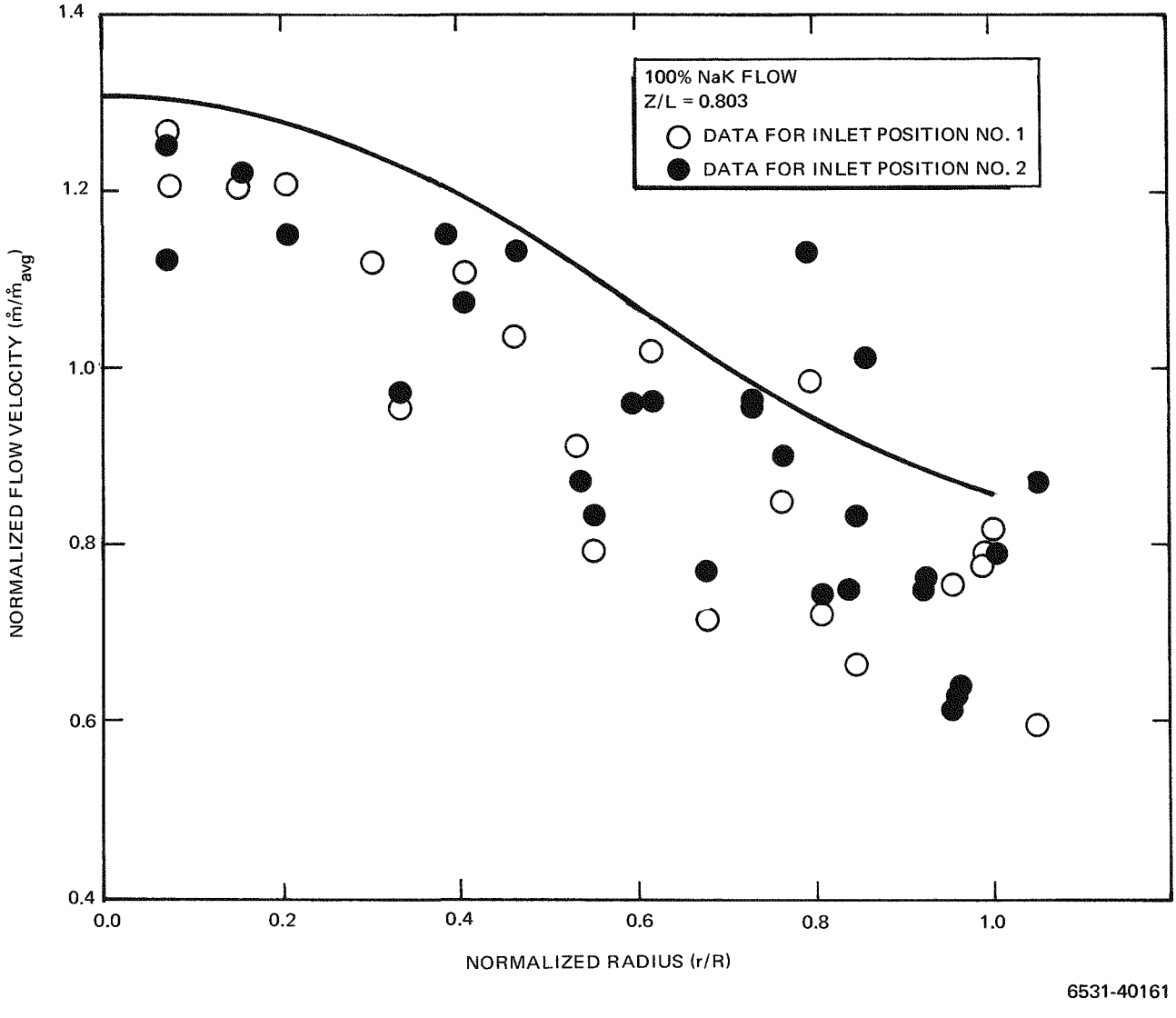

Figure 17. S8DR Core Flow Profile

NaK flows used in the S8DR operation. The core model consisted of simulations of the inlet plenum, core assembly and outlet plenum regions of the S8DR. As much of the structure as possible was fabricated from transparent acrylic plastic (see Figure 18) to allow visual and photographic observations of flow behavior. The flow system (Figure 19) for the test provided 100° F water flows of 50, 70, 130 and 170 gpm, corresponding to prototype design flowrates of ~40%, ~55%, 100% and 130% respectively. The flow system used for these tests included a gas injection system which provided a metered supply of helium gas. This gas was used for both flow visualization and observation of entrained gas effects at gas volume flowrates of 0.05 to 6% of the system water flowrates.

A pressure-measuring system was used to detect inlet plenum static and total pressures at selected orifice plate inlet holes. This system consisted of static and impact pressure probes (Figure 20) extending out of the upstream ends of selected mockup fuel elements. Pressures from these probes were measured using a manometer system.

In addition to the tests conducted at AI, another series of tests was conducted by the University of California Los Alamos Scientific Laboratory. A simplified two-dimensional model of the inlet plenum, flow distributor and orifice plate (Figure 21) was used. Flow experiments were conducted using this model on a free-surface water table with flows of~6 gpm. The effects of the position of the components of the S8DR inlet plenum on the flow patterns and pressure distribution upstream of the orifice were investigated.

Both the full core tests and the two-dimensional water tests provided similar results. The flow in the S8DR inlet plenum had two swirls or vortexes which existed inside the flow distributor (Figure 22). Full core flow visualization tests using gas injection showed that these low pressure areas generally fed the orifices providing flow to channels adjacent to four particular fuel elements. The two-dimensional tests showed not only the low pressure swirls or vortexes, but regions of high pressure in the inlet plenum. The regions of high pressure tended to coincide with areas of fuel element survival, while the vortex locations roughly coincided with regions of fuel element failure.

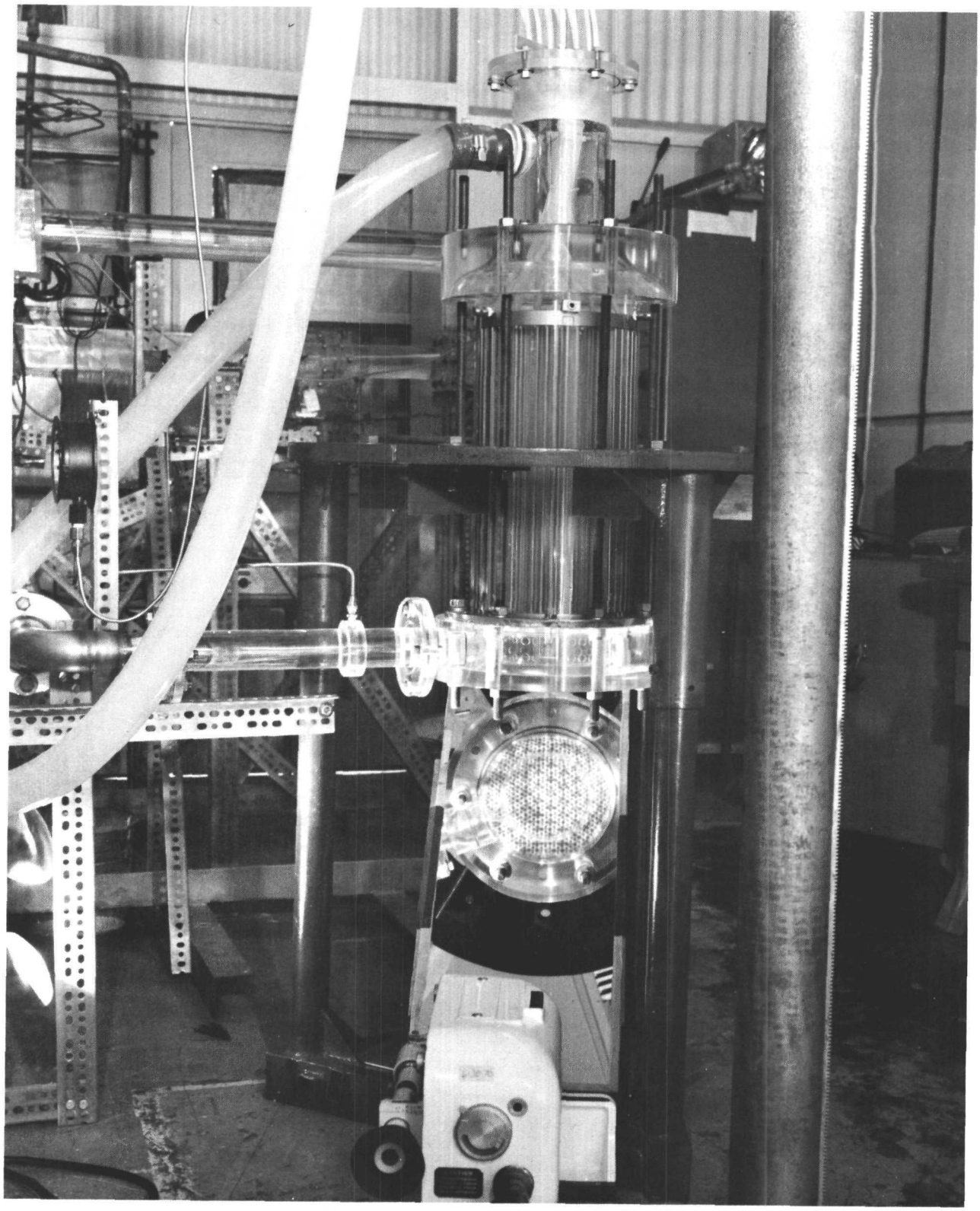

7-17-70

7759-40607

Figure 18. S8DR Model for Post-Operation Studies

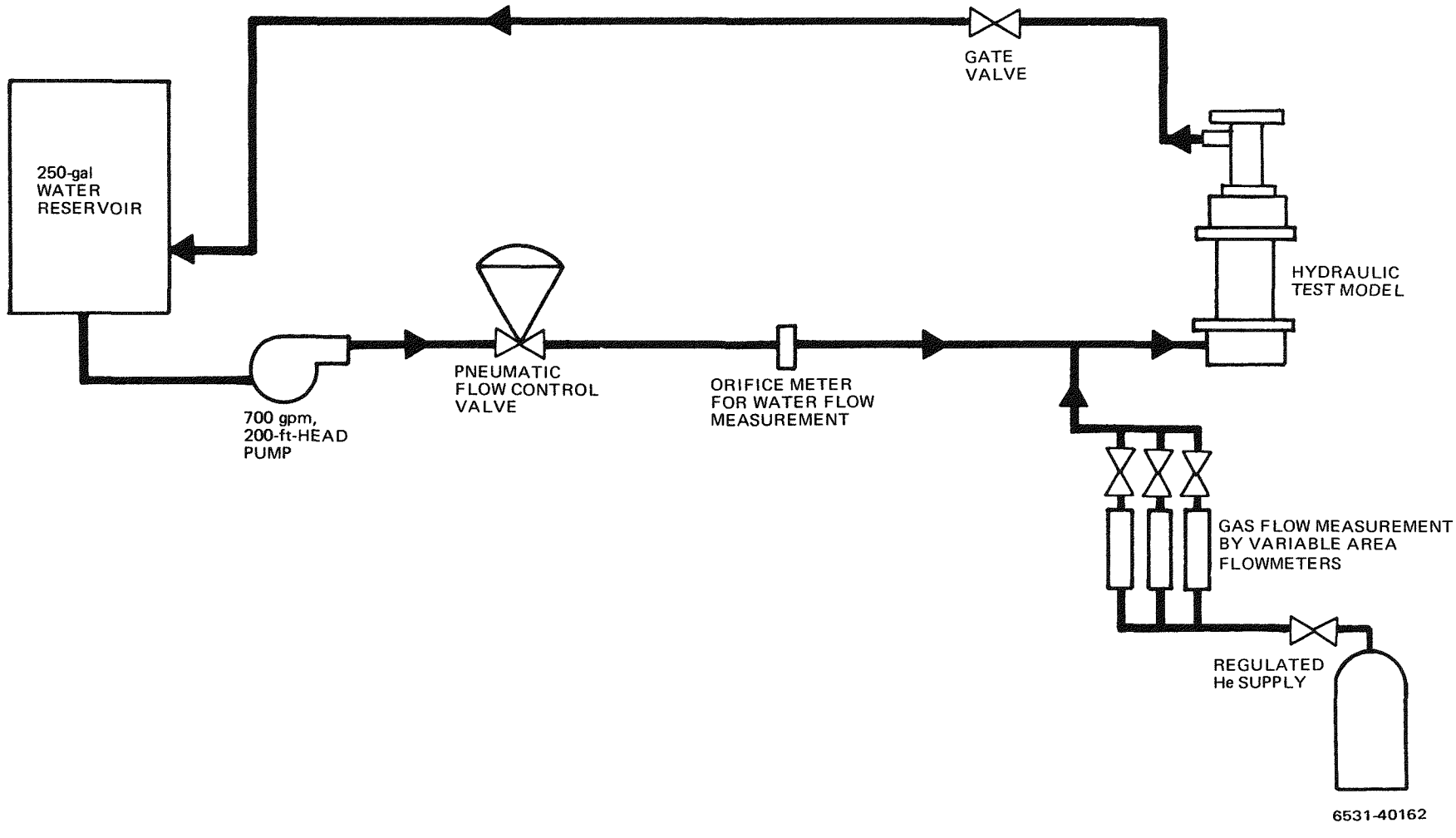

Figure 19. Flow System for S8DR Post-Operational Tests

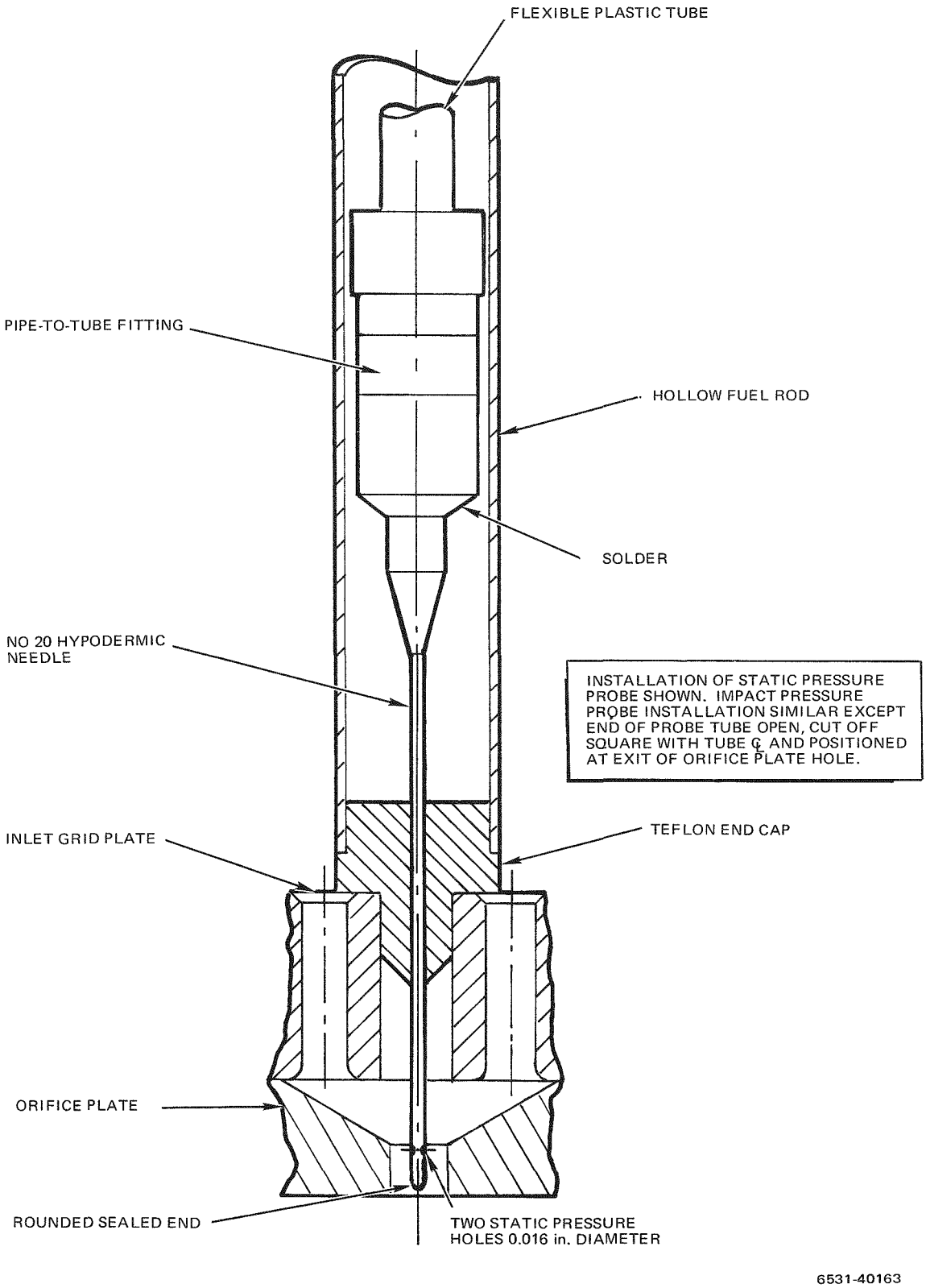

Figure 20. Detail of Orifice Plate Pressure Probe Installation

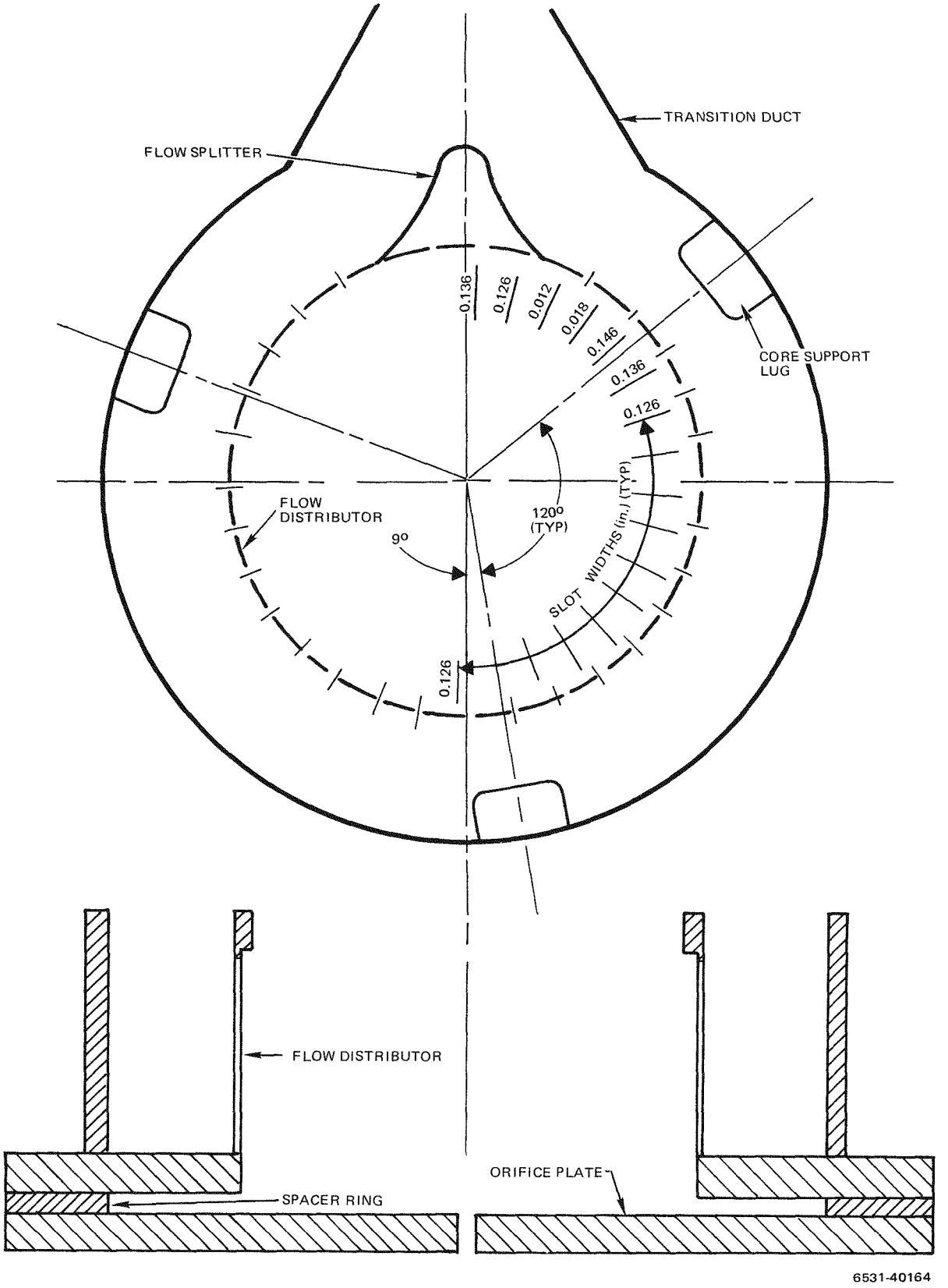

Figure 21. Two-Dimensional Water Table Model

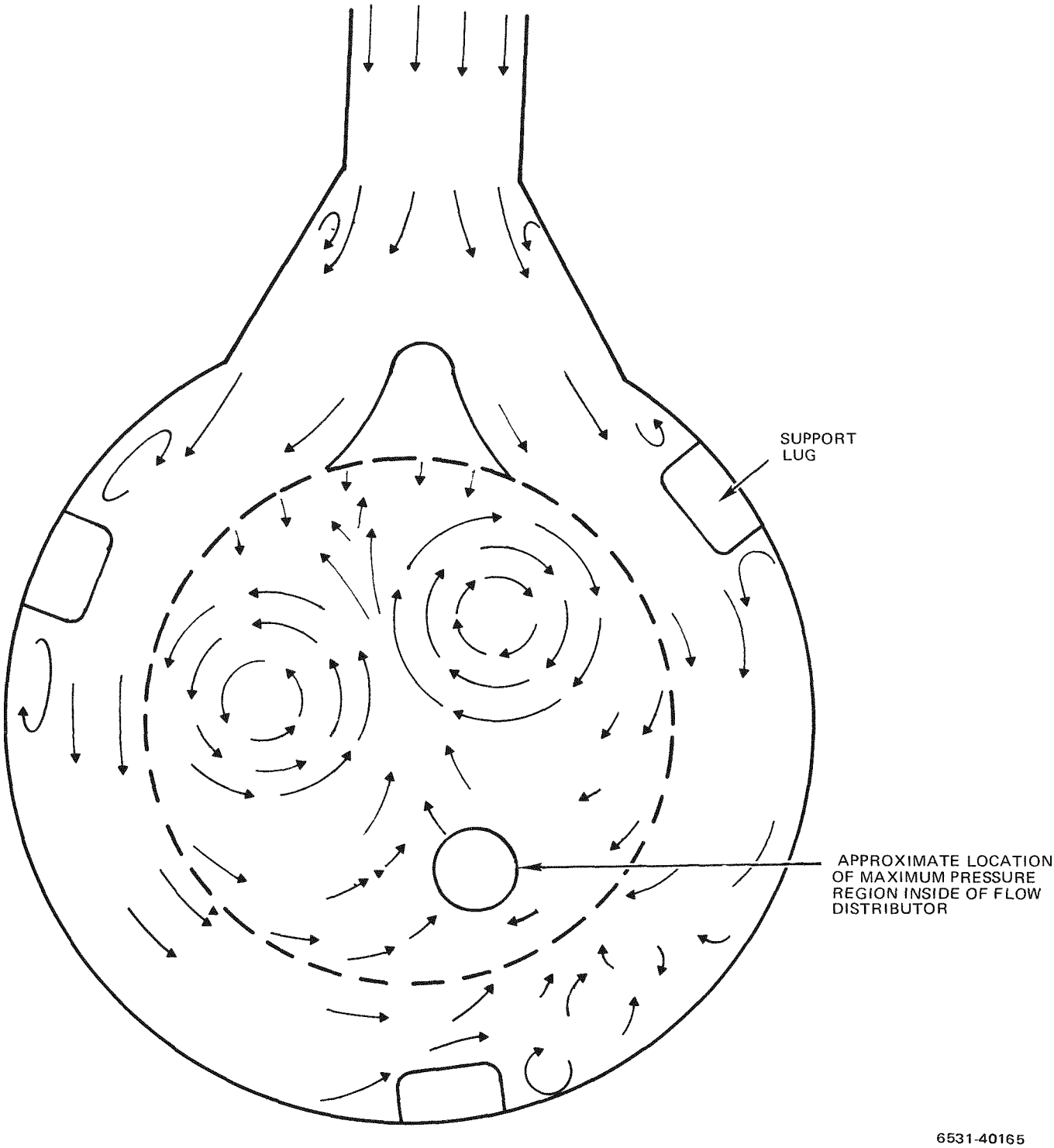

Figure 22. Sketch of Flow Patterns in Water Table Model

Considerable study of the behavior of entrained gas was done. Motion picture and still photography records were made of the gas behavior, not only in the inlet plenum, but in the core and at the exit of the outlet grid plate. These records showed that the vortexes in the inlet plenum would accumulate incoming gas and randomly feed it into one or another of the adjacent orifice plate holes. The gas fed into an orifice plate hole passed up the flow channels fed by that hole without much dispersion and passed through the outlet grid plate with a sort of "puffing" action because of the intermittent gas feed. Pressure measurements used to calculate orifice hole flowrates showed no significant effect for gas injection rates up to 6% by volume.

The two-dimensional water table tests provided some insight into the effect of various parts of the inlet plenum assembly on the inlet plenum flow pattern. Inserting core support lug mockups in the model indicated that these lugs probably had a strong effect on the inlet plenum flow behavior (compare Figures 22 and 23). This strong support lug effect, coupled with the effect of the orifice plate orientation, was also indicated in tests where the lugs and orifice plate were rotated 18 degrees clockwise from their normal positions to provide both complete and partial mirror- image plenum configurations. Rotation of either the support lug pattern or the orifice plate pattern caused the inlet plenum flow pattern to move proportionally.

The results of both these tests show a certain amount of coincidence between failed element locations and the location of the plenum vortexes, and between element survival locations and apparent regions of plenum high pressure. However, the complex mechanical, thermal, and hydraulic phenomena which existed in the S8DR core make it unlikely that one set of phenomena was responsible for the fuel element failures. Thus, the unfavorable flow characteristics of the inlet plenum with its high and low pressure regions and possible preferential gas collection, probably only reinforced other factors contributing to fuel element failure.

C. SPF REACTOR

The SPF ZrH reactor design had 199 fuel elements, an inlet grid plate design using various diameter flow channel holes, and an inlet plenum fed by four inlets 90 degrees apart. The desired inlet plenum flow conditions were

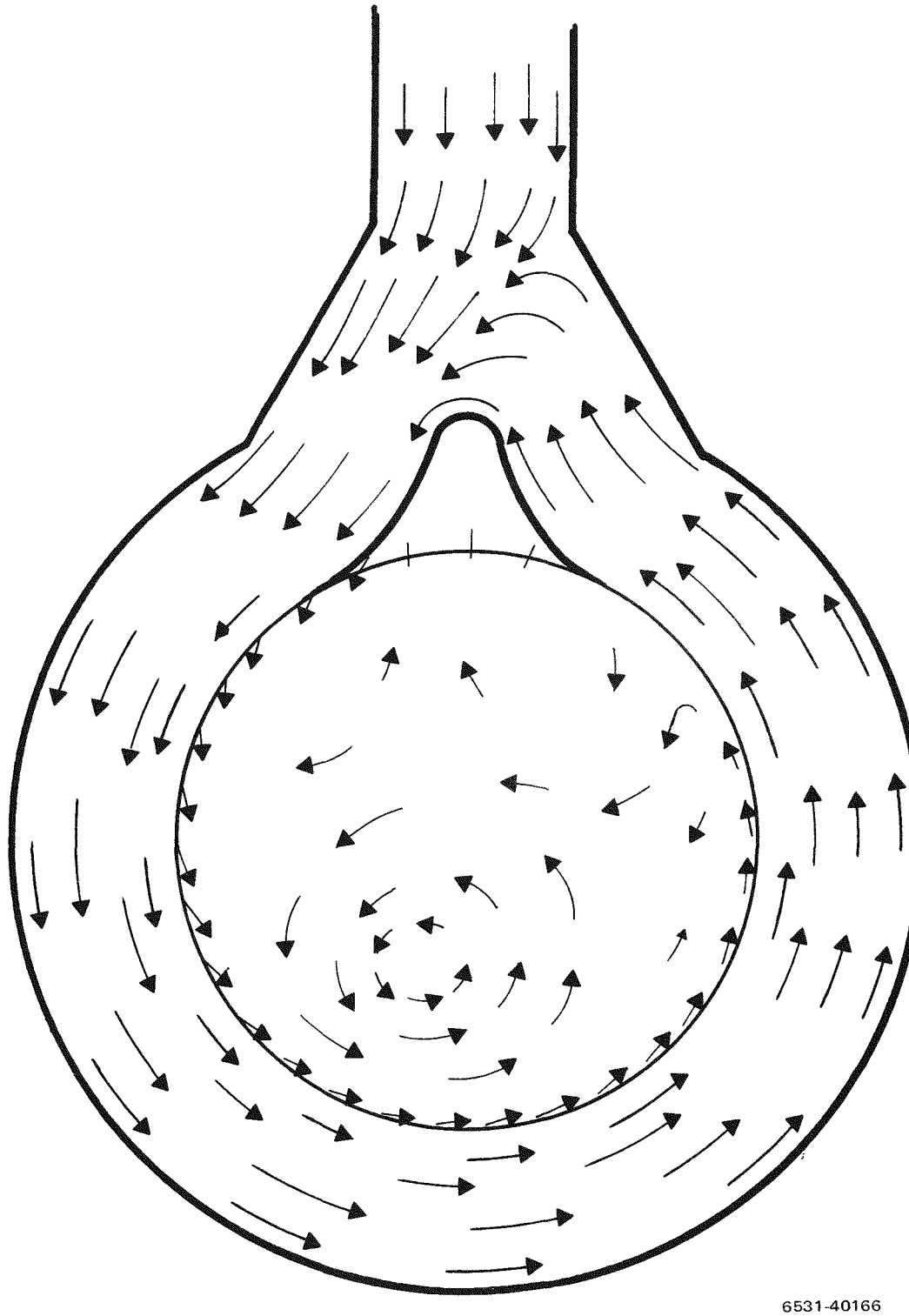

Figure 23. Two Dimensional Model Flow Pattern Without Support Lugs

a uniform pressure at the grid plate surface and the absence of vortexes. The success of the water table model in duplicating the vortex patterns observed in the S8DR model, and the ease with which configuration changes could be made in this type of model, suggested that this experimental approach be used to determine the SPF preliminary inlet plenum geometry.

1. Test Description

The preliminary SPF inlet plenum configuration was evaluated with an approximately full-scale, open-channel model (Figure 24). This model simulated the inlet piping and plenum. The inlet lines were simulated by open, half-round channels with a 4-in. wall height and the lower contour of a 2-in. diameter tube. These inlet lines were inserted through contoured holes in the plenum model shell. The inlet plenum was simulated by the stainless steel shell and a coaxially mounted, axially positionable grid plate (see Figure 25).

The flow system for the model supplied de-ionized water and was assembled from noncorroding components to avoid water discoloration from rust. Two interconnected stainless-steel reservoir tanks supplied water to the model through four individually valved supply lines. The model was mounted at the top of a 55-gal. sump tank which collected the model exit flow. The sump tank was drained using a 150-gpm pump to return water to the reservoir tanks through a pneumatically operated flow control valve.

Instrumentation for these experiments consisted of flow- and pressure-measuring devices. Pitot tubes were mounted in each open channel inlet line and calibrated, using a variable area flowmeter, so the pressure measurement from these tubes could be related to water flowrates in the range of 5 to 30 gpm. Additional flow direction measurements were made in the plenum model for certain tests using white teflon streamers supported from masts mounted on the inlet grid plate. Pressure instrumentation consisted of pressure taps, on the surface of the inlet grid plate, connected to atmospheric reference pressure water manometers. These manometers were constructed by connecting lengths of transparent plastic tubing to the grid plate pressure-tap stubs and supporting the tubing opposite ends on vertical boards with 1/2 cm grid lines.

Test procedures consisted of removing air from the manometer lines, checking manometer zeroes, installing the plenum configuration of interest,

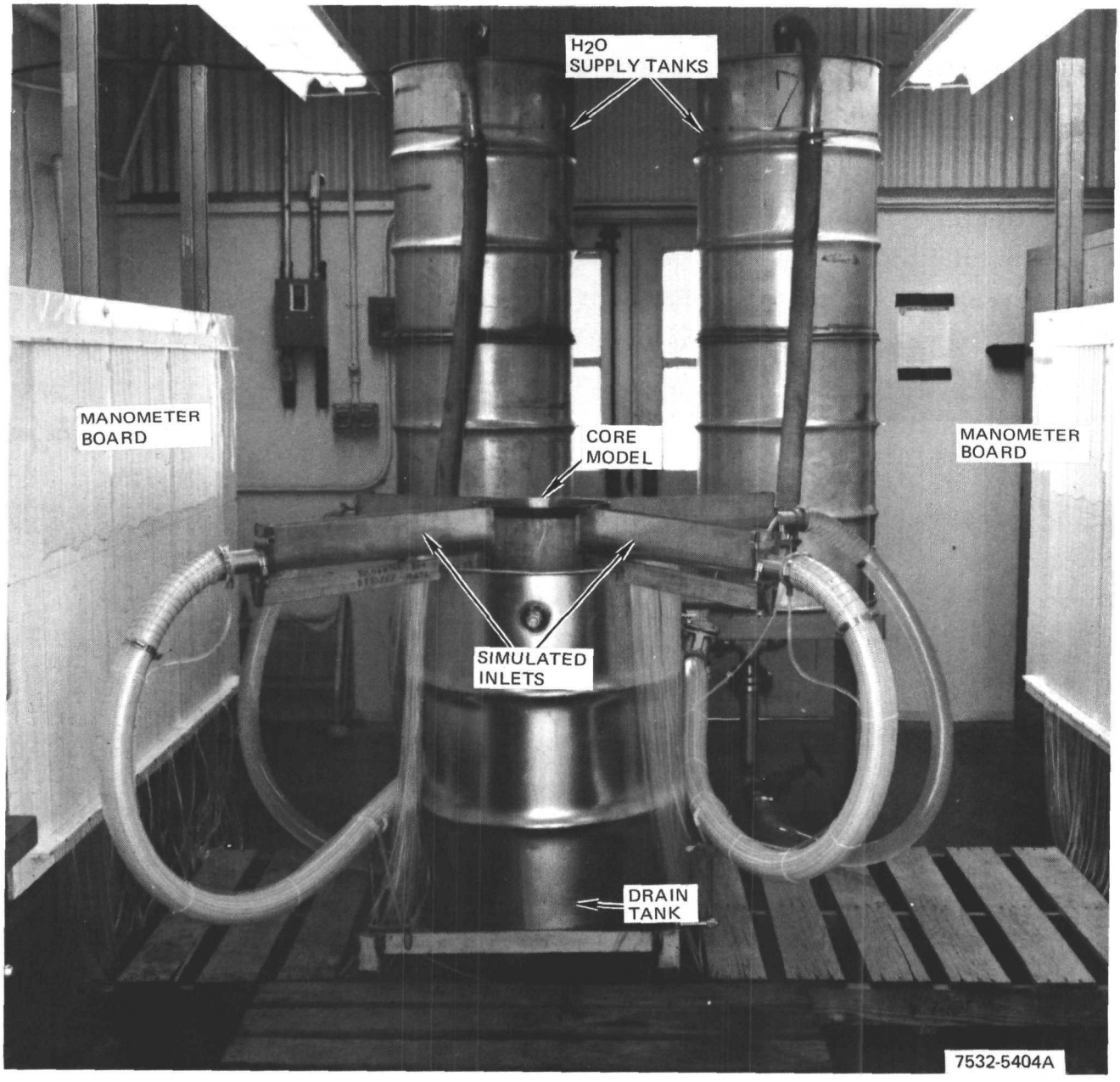

Figure 24. SPF Open-Channel Plenum Flow Model

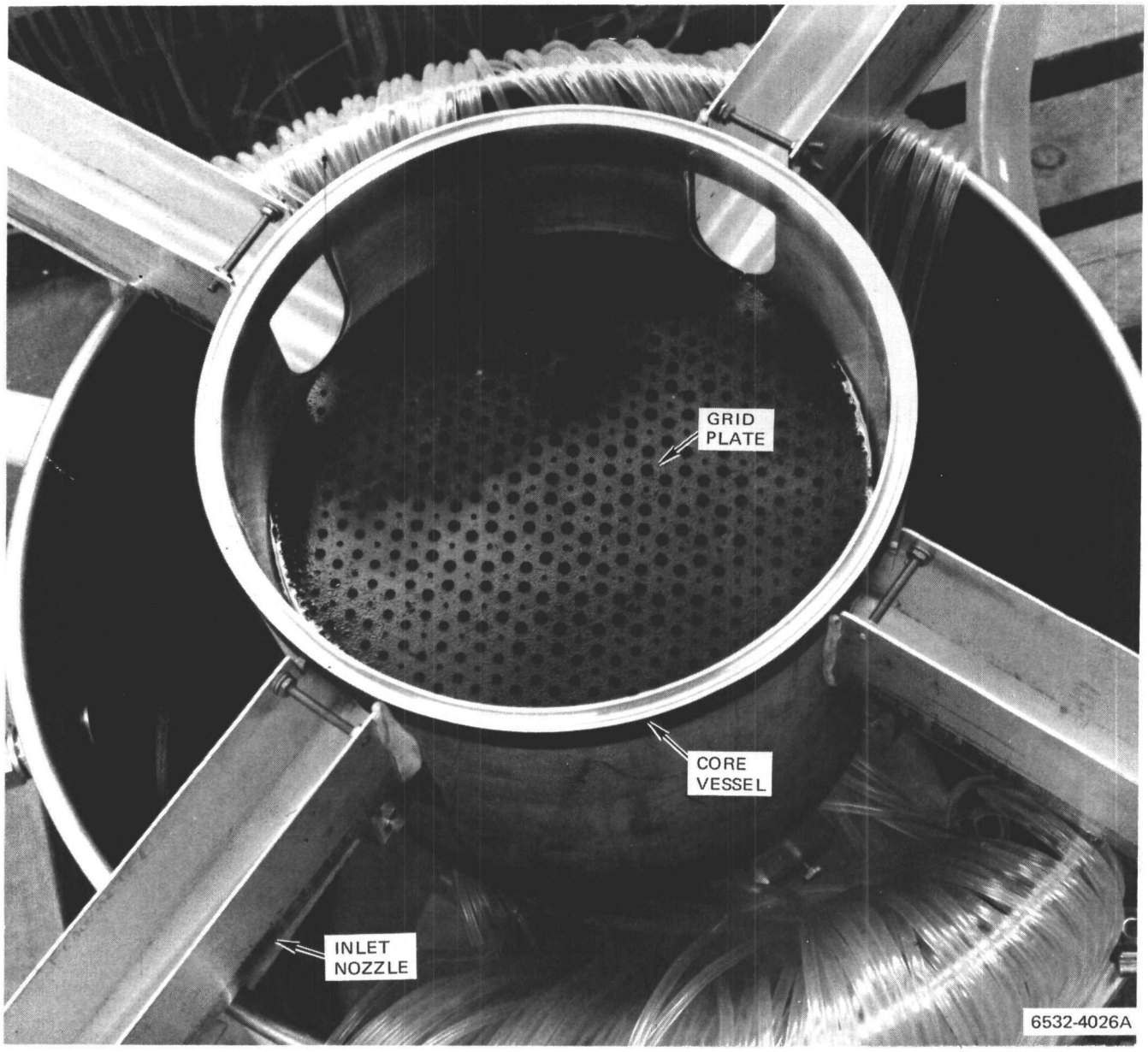

Figure 25. Top View of SPF Open-Channel Plenum Model

Figure 26. SPF Model with Straight Flared Inlet

and performing a flow test to determine configuration flow characteristics. Air was removed from the manometer lines with water flowing through the model. The open end of each manometer tube was pressurized to force any air in the lines into the flow stream and, when pressurization was removed, allow tubes to fill with water from the model flow. When the flow was stopped, the water in the manometer tubes returned to the level of the grid plate upper surface and thereby established a reference level on the manometer board so that pressure at the grid plate surface could be read directly in centimeters of water for any configuration tested. Most initial tests were performed at flows of 25 gpm/inlet; but eventually, for the more promising configuration, a flow range of 15 to 30 gpm/inlet was used.

Data from tests consisted of manually recorded pressure data and written descriptions of visual flow observations. These records were supplemented, as needed, by photographs of the flow behavior and of manometer board fluid heights. To improve the visibility of manometer fluid column heights for both manual and photographic recording, a small, dark, unity specific gravity plastic bead was floated on the water meniscus in each manometer tube.

The SPF preconceptual-design inlet plenum configurations was tested in two phases. Initial tests were conducted with straight inlet lines (see Figure 25). Subsequently, the inlet openings in the plenum shell were enlarged and 4-in square, 3-in. -high open boxes installed between the 2-in. , half-round inlet lines and the model plenum. This allowed flared inlet geometries to be tested (see Figure 26).

The plenum flow-control devices investigated in these tests consisted of antiswirl plates and flow diffusers. The antiswirl devices fit into the plenum model above the grid plate and consisted of two plates joined at their centers to form a cross with an angle of 90° between each arm of the cross. The flow diffusers consisted of groups of vertical plates inserted into the plenum inlets and diverging at various angles in a downstream direction (Figure 26).

2. Test Results

The first series of tests with the straight inlet lines were run to determine the flow characteristics of the model inlet plenum without flow-control devices. The flow patterns observed (Figure 27) reflect the high velocity of the inlet flow across the grid plate. The excess velocity in the impingement zone of the four

Figure 27. SPF Model Flow Conditions without Baffles or Diffusers

inlets was converted from a dynamic head to a potential head and resulted in a non-uniform pressure distribution. Thus, it became apparent that the probable method of obtaining a uniform, i. e. , flat, pressure distribution was to dissipate the inlet velocity as efficiently as possible. Subsequent tests involving the anti-swirl devices, which obviously only compounded the dissipation problem, were undertaken to confirm this preliminary conclusion. With the nonperforated anti-swirl baffle dividing the plenum into quadrants, each fed by a single inlet, the resulting pressure profiles only departed further from the desired flatness. Some improvement was obtained by placing the antiswirl baffle so as to split the inlet line flows, but this resulted in a tangential flow pattern with two vortexes in each quadrant. The use of a perforated antiswirl baffle was also ineffective.

An analytical study of flow profiles in the reactor inlet plenum indicated that diffusers might be effective in spreading the inlet flow and dissipating the inlet velocity. The designs for the three-and four-vane diffusers (Figure 28) were based on a best fairing to obtain uniform flow impedance (equal flow areas). The five-vane diffuser was based on a design developed in an analytical study.

The three diffuser types were tested simultaneously using the nonperforated antiswirl baffle to minimize the interacting effects of adjacent diffusers. The antiswirl baffle, however, appeared to have a definite influence on the pressure profiles for the individual diffusers and was removed, therefore, and additional data obtained. Also, the inlet line without a diffuser was temporarily provided with a screen to minimize its influence on the flow field of adjacent diffusers and yet still retain comparable water levels in the plenum. This arrangement provided the best results in the multiple diffuser tests.

The flow patterns of all three diffusers were characterized, to different degrees, by surface vortexes (eddies) in the region adjacent to the plenum wall. The four-vane and five-vane diffusers produced comparable degrees of surface turbulence in this region. The two outer vanes of the five-vane diffusers were modified, therefore, to allow them to be moved while the diffuser was in place and thus attempt to eliminate or lessen surface turbulence. This approach was not successful: moving a vane closer to the plenum wall, even though it decreased the turbulence in the flow channel there, caused turbulence to develop in the adjacent interior flow channel.

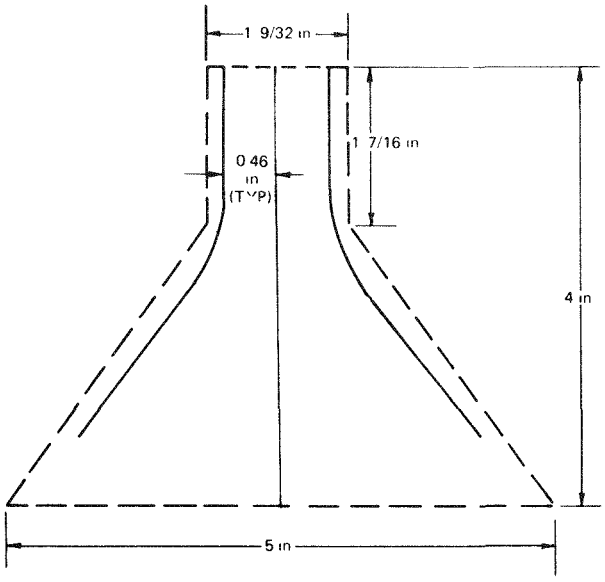

a. Three-Vane Diffuser

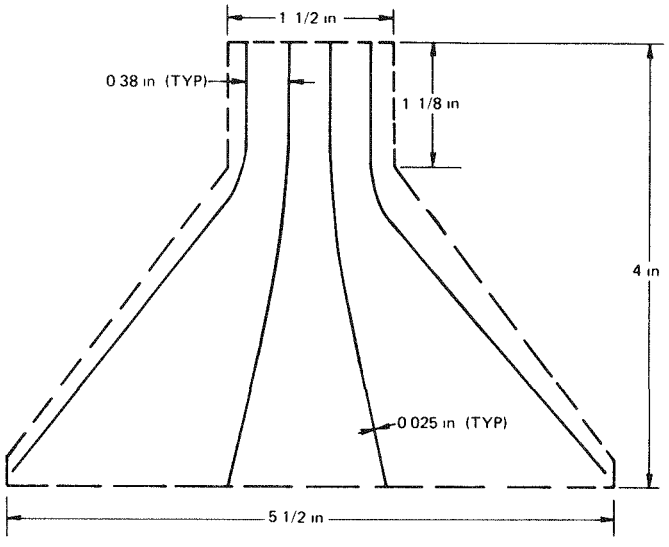

b. Four-Vane Diffuser

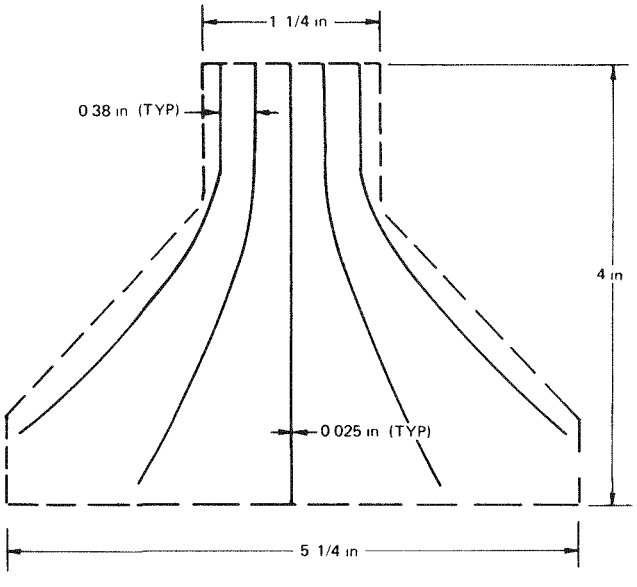

6531-40167

c. Five-Vane Diffuser

Figure 28. SPF Diffusers

Based on overall performance, the four-vane diffuser was the best of the designs tested. Three additional diffusers were fabricated, therefore, and a configuration with a four-vane diffuser in each inlet was tested over a flow range of 15 to 25 gpm/inlet. Satisfactory pressure profiles were obtained at both 15 and 20 gpm/inlet. Except for a few pressure measurements at 15 gpm, the only points indicating pressure deviations greater than ±0.01 psi were in the diffusers themselves. Greater pressure deviations were observed at 25 gpm, but it is believed these deviations resulted from the diffusers being totally under the water level in the plenum. At low flows the surface was smooth (Figure 29), but for the higher flow conditions, above what is presumed to be the critical Froude number, the water surface was striated with what appeared to be refracted waves of very small amplitude. Associated with this was a noticable increase in sound level, giving an impression of an increase in water velocity out of proportion to the slight change in flowrate. Because of the uncertainty as to the applicability of the model under these conditions, no pressure data were obtained with the four-vane diffusers in this flow regime.

For the four-vane diffusers installation, the grid plate pressure profiles were also determined for unequal inlet flows. The individual inlet flows for this test ranged from 15 to 19.5 gpm; this was a larger range than was anticipated for the prototype. The multiplicity of flow paths evidently provided sufficient compensating effect to make the unbalanced inlet flows a second-order influence, and the grid plate pressure profiles were only slightly worse than those for equal inlet flows.

The results of the straight inlet tests were used to design tests for flared inlet nozzles (Figure 30). Use of the four-vane diffusers from the straight inlet tests resulted in acceptable pressure profiles for 2-by 3-by 3-in. straight-flared inlets (all 199 pressure measurements were within a ±0.015-psi band and only five measurements were outside a ±0.010-psi band). Consequently, testing was directed toward obtaining comparable performance from either four-vane or five-vane diffusers specifically designed for use in straight-flared inlets. Pairs of like diffusers were tested as both opposed and adjacent pairs to allow simultaneous evaluation of the four-vane and five-vane configurations with interaction effects minimized. Two vane lengths were tested; the results indicating that the five-vane diffuser was the better design.

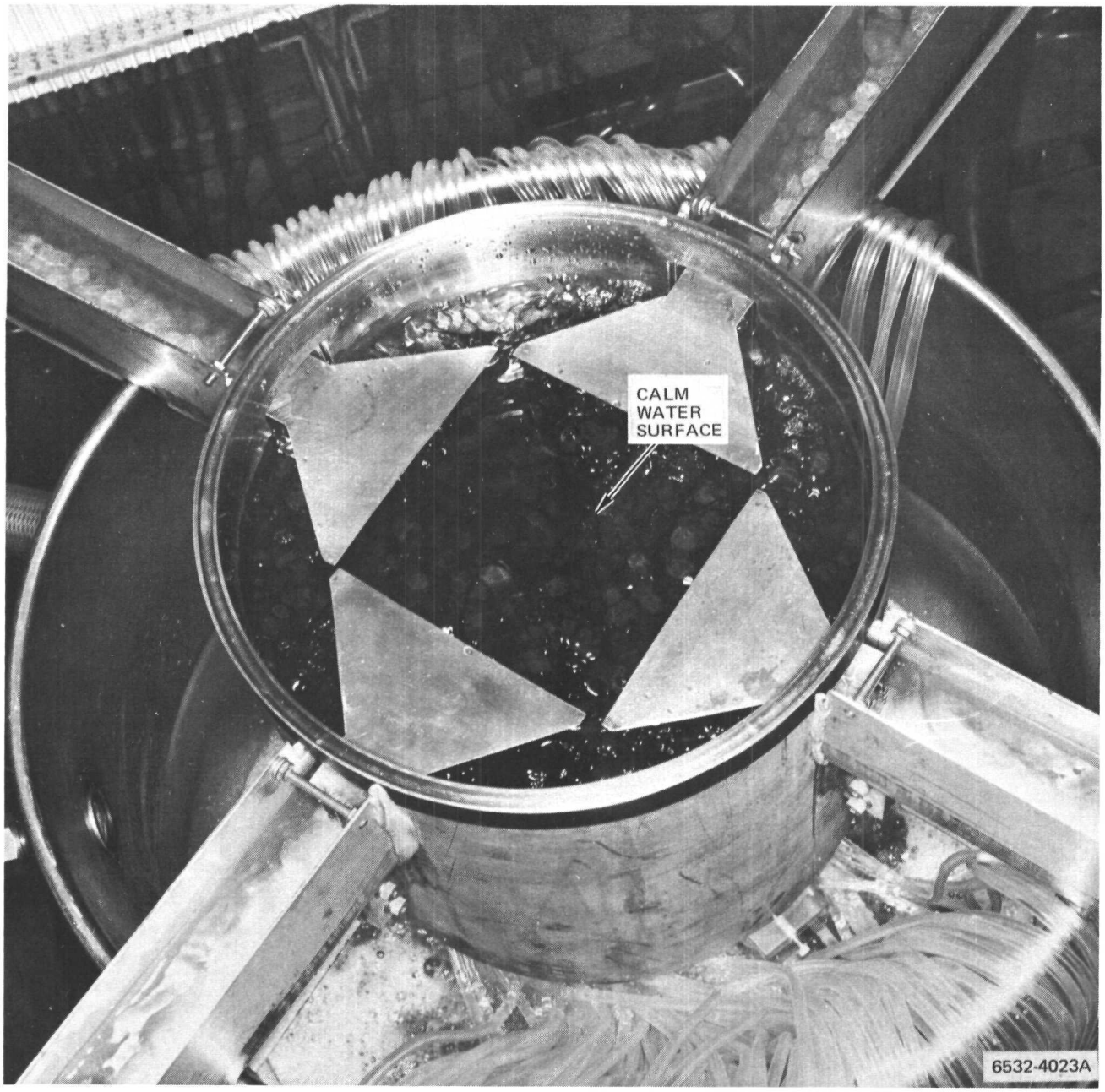

Figure 29. SPF Model Flow Conditions with Four-Vane Diffusers in Each Inlet

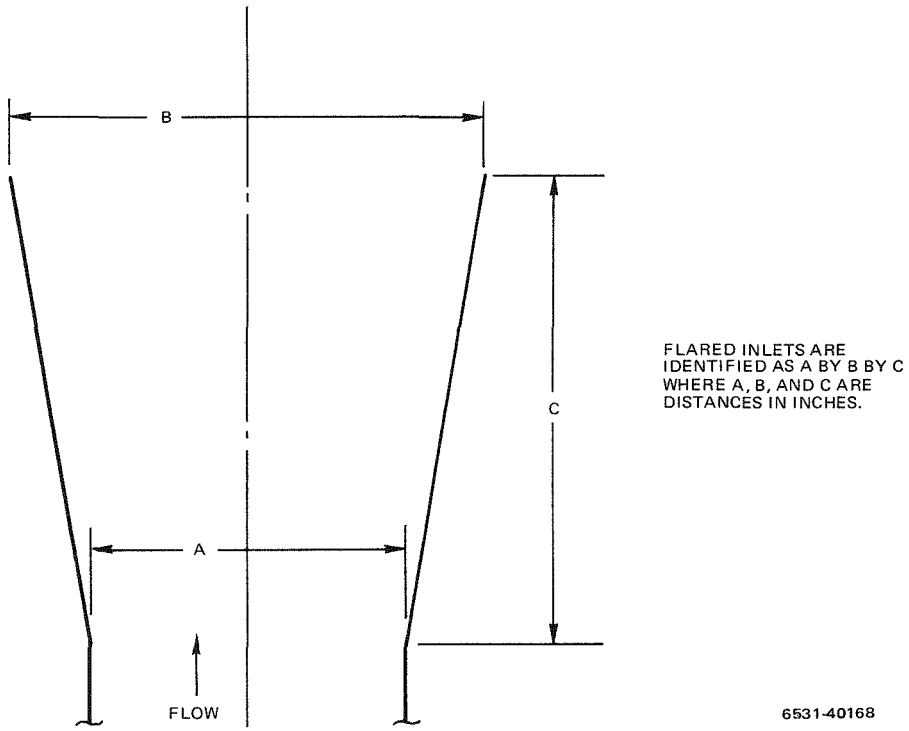

Figure 30. Flared Inlet Nomenclature

Four five-vane diffusers were subsequently fabricated to allow testing with five-vane diffusers in all four inlets. These diffusers were 5-1/2 in. long with a vane height increased from 2-1/4 in. to 2.95 in. to allow greater flows without submerging the diffuser support structure (top plate). Tests of these diffusers were conducted in which the lengths of the diffuser vanes were modified and the diffuser position in the straight-flared inlet changed. The final five-vane diffuser configuration had 4-in. long vanes and was recessed 0.45 in. into the inlet.

This final five-vane configuration was used in the evaluation tests of two additional inlet configurations: a 2-by 3- by 3-in. curved-flared inlet and a 2-by 4-by 3-in. straight-flared inlet. In each case, the five-vane diffusers were installed in these inlets and then the diffuser position in the inlet was changed in an attempt to obtain the flattest pressure profile. The curved-flared inlets were inferior in performance to both straight-flared inlets, and the 2-by 4- by 3-in. straight-flared inlets produced a flow condition slightly improved over that obtained with the 2-by 3-by 3-in., straight-flared inlets.

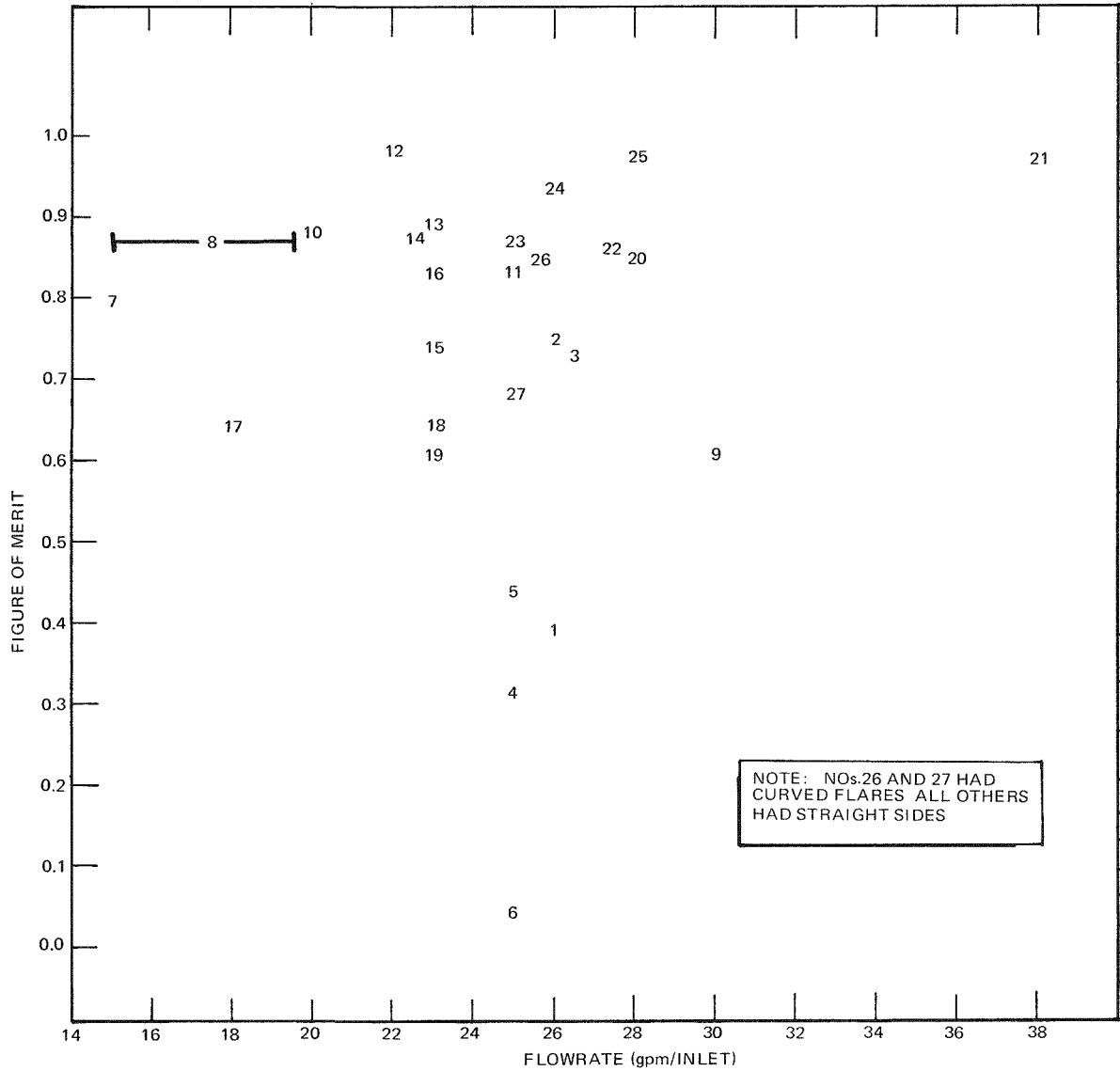

	INLET NOZZLE CONFIG-URATION	NUMBER OF DIFFUSERS IN PLENUM	NUMBER OF VANES IN EACH DIFFUSER	ANTI-SWIRL BAFFLE
1	2 x 2	1	3	YES
2	2 x 2	1	4	YES
3	2 x 2	1	5	YES
4	2 x 2	1	3	YES
5	2 x 2	1	4	YES
6	2 x 2	1	5	YES
7	2 x 2	4	4	NO
8	2 x 2	4	4	NO
9	2 x 2	4	4	YES
10	2 x 2	4	4	NO
11	2 x 2	4	4	NO
12	2 x 3	4	4	NO
13	2 x 3	2 2	4 5	NO
14	2 x 3	2 2	4 5	NO
15	2 x 3	2 2	4 5	NO
16	2 x 3	2 2	4 5	NO
17	2 x 3	2 2	4 5	NO
18	2 x 3	2 2	4 5	NO
19	2 x 3	2 2	4 5	NO
20	2 x 3	4	5	NO
21	2 x 3	4	5	NO
22	2 x 3	4	5	NO
23	2 x 3	4	5	NO
24	2 x 4	4	5	NO
25	2 x 4	4	5	NO
26	2 x 3	4	5	NO
27	2 x 3	4	5	NO

6531-40169

Figure 31. Comparison of SPF Inlet Plenum Configurations by Figure of Merit

The effect of the five-vane diffusers on the plenum flow was demonstrated by operating the plenum model with the diffusers removed. For this case, flow conditions in the plenum were noticeably unstable. Random occurrences of a large vortex which cleared an approximately 1-in.-diameter circle on the grid plate alternated with periods of calm flow with no vortex present. When the flow was calm, the pressure profiles were quite flat and comparable to those obtained with the diffusers in place.

3. Conclusions and Design Selection

The multiplicity of geometries studies, as well as the simultaneous testing of differing configurations, prompted the search for some compatible basis for evaluating the results of the entire test series. The basis finally adopted weighs both the number of pressure measurements which fall outside the specified ± 0.01-psi limits, and the magnitude of the deviation from the average pressure in the form of a Figure of Merit (FM) as follows:

$$FM = \left[1 - (n/m)\,\overline{P - P_a}\right]$$

where

n = number of pressure measurements outside the established limits

m = total number of pressure measurements

$\overline{P - P_a}$ = the average magnitude of the difference between a local pressure exceeding the established limits and the average pressure at the grid plate surface (expressed in manometer scale divisions)

A plot of the FM values as a function of flowrate per inlet (see Figure 31) allows comparison of the configurations tested. This comparison clearly shows the superiority of the straight-flared inlet over the curved-flared and straight inlets. The comparison also shows that although the highest FM value was obtained when the straight-inlet, four-vane diffusers were installed in the 2- by 3- by 3-in., straight-flared inlets, almost comparable FM values were obtained for the five-vane diffusers in the 2-by 3- by 3-in. and 2-by 4-by 3-in., straight-flared inlets. The above results, coupled with the easier fabricability of the five-vane diffuser, prompted the recommendation that the five-vane diffuser in the 2- by 3-by 3-in., straight flared inlet be adopted as the SPF plenum reference design.

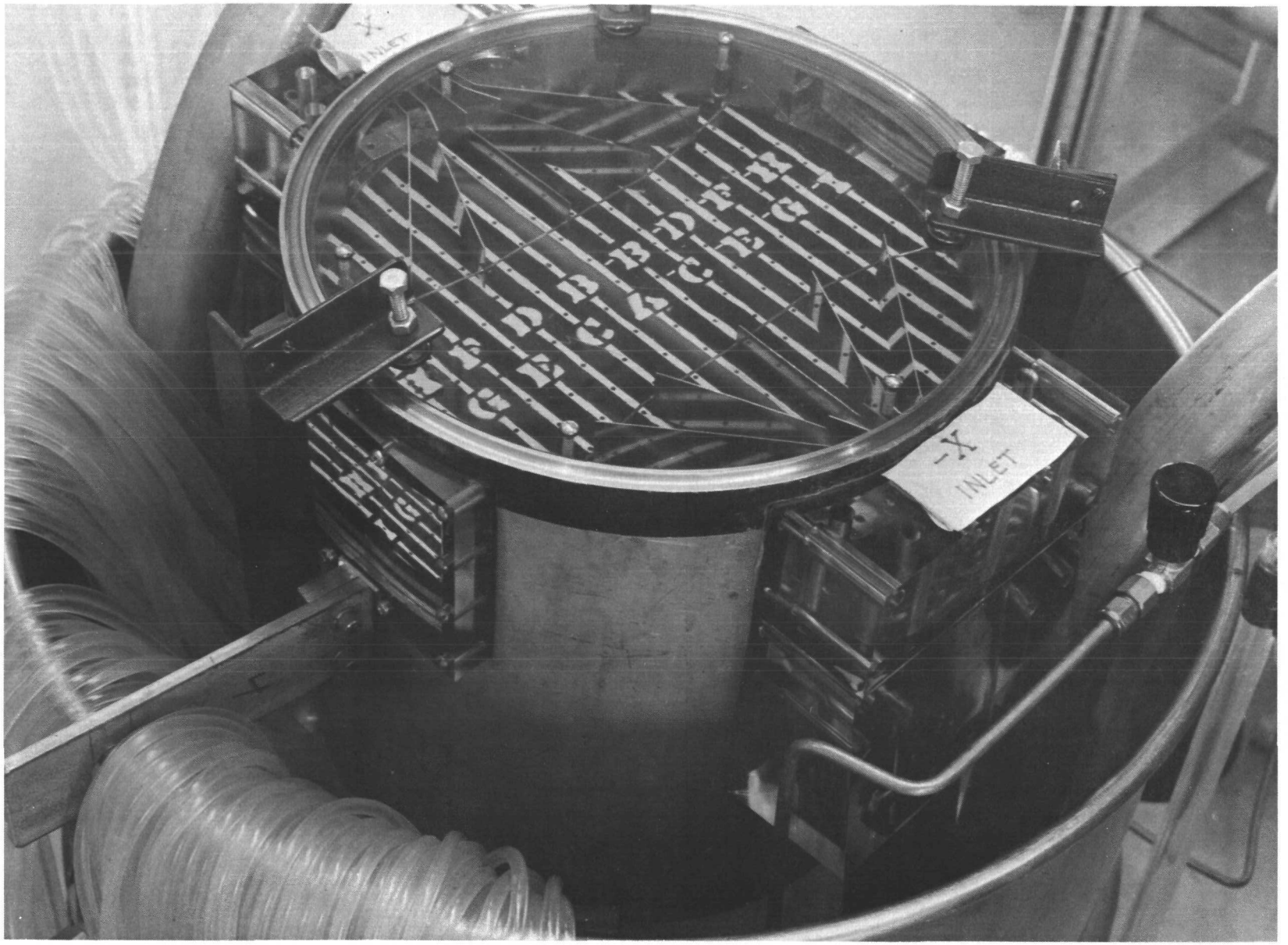

6531-4047

Figure 32. 5-kwe Inlet Plenum Model with Configuration E Installed

D. 5-kwe SYSTEM REACTOR

The 5-kwe reactor design used the same approach to core temperature control as the SPF reactor. The fuel element array would have finned and unfinned elements arranged to provide in-core mixing of the coolant. Thus the 5-kwe reactor had the same inlet plenum flow requirements as the SPF reactor: uniform grid plate pressure with no flow vortexing. However, as the 5-kwe reactor concept had only two plenum inlets instead of the four inlets of the SPF reactor, additional hydraulic tests were required.

1. Test Description - Preliminary Inlet Plenum Configuration

The similarity of the 5-kwe reactor flow requirements and envelope geometry to that of the SPF reactor suggested that SPF open-channel test components and test results might be useful in determining the optimum 5-kwe reactor inlet plenum configuration. Accordingly, the SPF plenum model was modified to approximate the 5-kwe reactor configuration and the flow system was modified to be compatible with this new model. One of the proposed flow-shaping configurations to be evaluated in this model was a vane configuration similar to that found to be satisfactory in the SPF reactor tests.

a. Test Model

The 5-kwe reactor model was to be a three-dimensional (i. e. , closed) model approximating the inlet line and inlet plenum configurations of the proposed reactor. Transparent plastic parts were to be used, where practicable, to allow visual observation and photographic recording of flow behavior. The model, and its inlet lines, was to be compatible with the supply lines and sump tank of the flow system used for the SPF open-channel tests.

A model installation was designed which met these requirements (see Figure 32). The model inlet lines were immersed in the sump tank and rose to meet simulated plenum inlet lines at the approximate prototype angle. These inlet lines fed the water flow into the modified SPF model through machined plastic blocks which simulated the two inlet line-to-plenum transitions of the proposed 5-kwe reactor.

The SPF model components were modified to provide a slightly oversize model (1.13 scale) of the 5-kwe configuration. The grid plate was changed by

reducing the number of grid plate flow holes and enlarging them to a uniform size. The two unused inlet holes in the shell were plugged with machined, transparent plastic blocks. Machined circular plates of transparent plastic were mounted inside the plenum shell above the inlets to simulate various prototype plenum closure shapes.

b. Flow and Measurement Systems

The water flow system used for the 5-kwe plenum tests was nearly identical to the SPF flow system, except for minor changes. Two of the four supply lines were not connected. The height of the storage tank support stand was increased to provide more head and allow flows of more than 50 gpm/inlet. The pitot tubes for flow measurement in the open-channel model were not usable so pitot static tube assemblies were installed in each inlet line and calibrated using variable area flowmeters. Flow temperature was measured by a mercury-in-glass thermometer in the sump tank.

As in the SPF system, the measurements of primary importance in evaluating the performance of plenum flow-shaping devices were those of grid plate pressure. The connection method and identification scheme for the grid plate pressure taps were identical to those used in the SPF reactor tests except for the addition of painted letters and stripes on the grid plate surface to identify the rows of "Y" pressure taps. The pressures sensed by the grid plate pressure taps were measured using open tube (atmospheric reference pressure) manometer boards with tubes from the "Y" pressure tap rows grouped together. These manometer boards were those from the SPF tests mounted at an increased height above the grid plate surface to prevent the increased plenum pressure from forcing water out of the open tube end. A pressurized nitrogen gas bottle was connected to both inlet lines and used to inject gas bubbles into the water flow for flow visualization. Initially, the pressure drop was determined by measuring the inlet line static pressure from the pitot-static tube. Later, a static pressure tap was installed in each inlet line just upstream of the inlet line-to-plenum transition to allow pressure drop determination from measurements there.

c. Plenum Flow Shaping Configurations

The various inlet plenum configurations tested are listed in Table 1. The horizontal baffles, located just below the inlet nozzles, partially divided the plenum near the nozzle in two regions. The upper region between the baffles and the head was designed to diffuse the high velocity inlet flow without disturbing the flow near the grid plate region below. Multivane diffusers, similar to the SPF configuration, were intended to distribute the flow over the grid plate.

When these devices alone failed to produce the desired flow characteristics, they were combined (Figure 33). Various modifications of the baffles, diffuser, head contours and plenum heights were made during the successive tests. Other series of tests with a multi-holed orifice plate replacing the horizontal baffles, with and without the multi-vane diffuser above it, were also conducted.

2. Test Results and Conclusions

A total of 16 plenum configurations were evaluated to select an optimum configuration on the basis of grid plate pressure variation, flow pattern as observed with N_2 bubble injections, and pressure drop. For a prototype NaK flow at an inlet line Reynolds number of 1.85×10^5 the optimum configuration should have a predicted NaK-flow grid plate pressure variation about the average of less than $\pm$ 0.008 psi (i.e., maximum pressure difference less than 0.016 psi). In addition, this configuration should not produce any major vortexes in the plenum and should not cause excessive pressure drop in the flow through the plenum.

The limitations of using water as a modeling fluid and the flow capability of the test system required that both modeling techniques and data extrapolation be used in comparing configurations. Grid plate pressure differences measured in the water system were converted to equivalent NaK pressure differences at the same inlet line Reynolds number using Reynolds number-dependent relations. Also, although the water flow system could provide flow at twice the NaK design flowrate it could not duplicate the prototype NaK Reynolds number of 1.85×10^5. Data for each configuration, therefore, were taken at several inlet line Reynolds numbers. This allowed determination of the estimated prototype NaK grid plate pressure variation at operating conditions by straight line extrapolation (on

TABLE 1

SUMMARY OF 5-kwe PLENUM CONFIGURATIONS TESTED

Configuration	Description	Components*		
		Closure	Baffle	Vanes
A	Basic plenum	1	None	None
B	Horizontal baffles	1	1	None
C	Equal inlet area vanes	1	None	1
D	10-10-30 vanes	1	None	2
E	10-10-30 vanes, flat head	2	None	2
F	Horizontal baffles, vanes, flat head	2	1	3
G	Horizontal baffles, vanes, convex head	1	1	3
H	Horizontal baffles, vanes, concave head	3	1	3
I	Contoured baffles, vanes, concave head	4	2	4
J	Slotted baffle, vanes, concave head	4	3	4
K	Slotted baffle, shaved vanes, concave head	4	3	5
L	Baffle-grid plate separation increased 0.15 in.	3	3	5
M	Configuration L, but with plenum closure mismatch	4	3	5
O	199-hole orifice plate	3	4	None
P	591-hole orifice plate	3	5	None
R	591-hole orifice with vanes	3	5	5

* Codes used to identify configuration components are as follows:

Plenum Closure

1 – Basic Convex Head
2 – Flat head
3 – Concave head
4 – Concave head positioned with 0.05 in. mismatch to edges of inlet line-to-plenum transitions because of vane interference.

Baffles

1 – Two flat, semicircular baffles mounting on the plenum inlet blocks.
2– Horizontal baffle with 4-1/2-in.-wide slot and semicircular ends.
3 – Horizontal baffle with slot continued to edge.
4 – 1/2-in.-thick orifice plate with 199 holes - 1/8 in. diameter.
5 – 1/2-in.-thick orifice plate with 591 holes - 1/8-in. diameter

Vanes

1 – "Stepped" vanes providing approximate fit to the convex head, fitting above the grid plate and dividing the projected plenum inlet area into equal portions.
2 – Stepped vanes fitting above the grid plate, dividing half the projected plenum area into three sections having, from the centerline out, 10, 10, and 30% of the total inlet area.
3 – Stepped vanes fitting above the horizontal baffles, positioned in a modified 10-10-30 configuration
4 – Contoured vanes fitting snugly between the baffle plate and the concave plenum head and positioned in a modified 10-10-30 configuration.
5 – All vanes except center vane of contoured vanes (No. 4 above) cut down in height to give clearance between edge of vane and concave plenum closure.

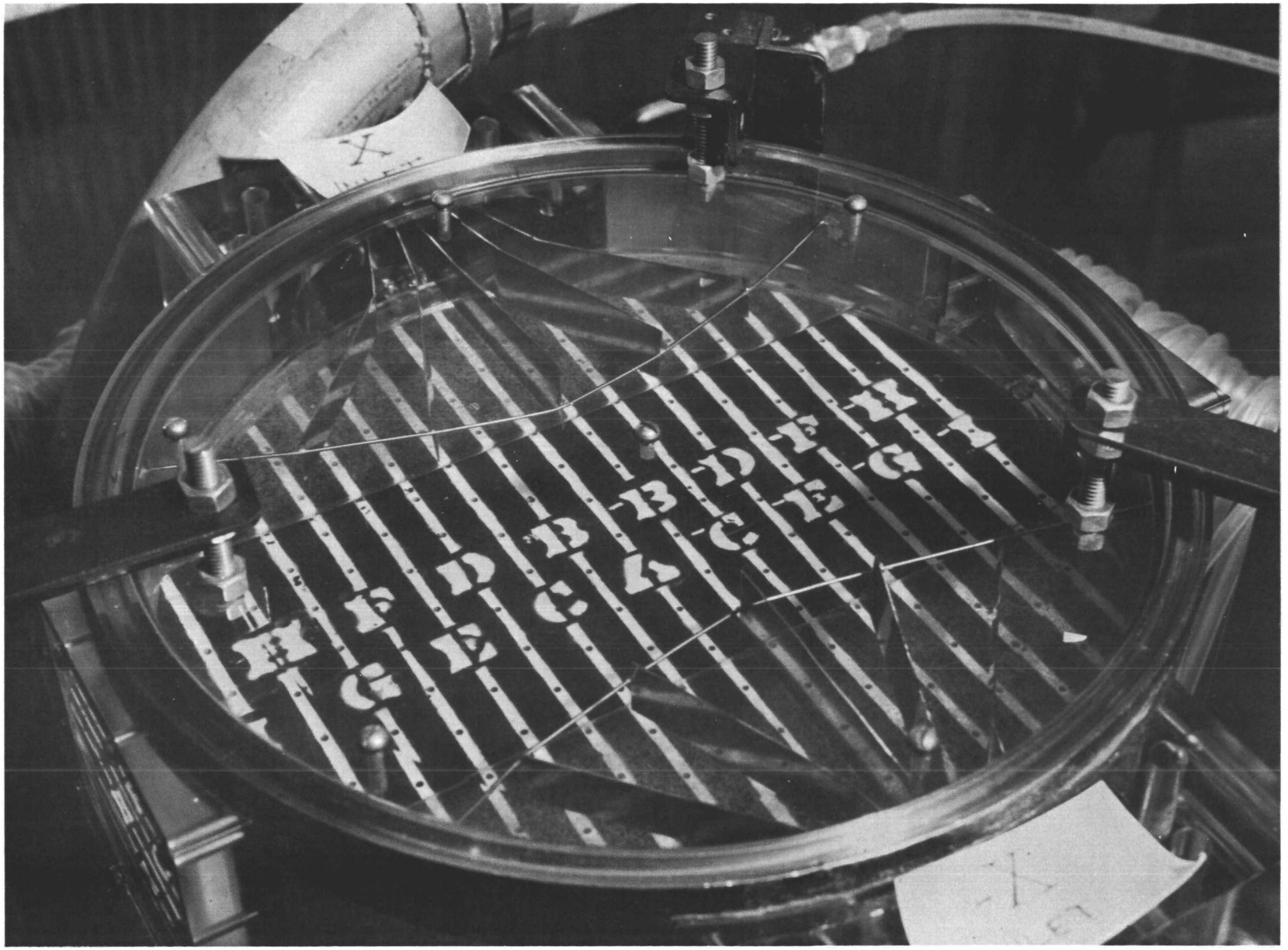

6531-4073

Figure 33. Inlet Plenum Configuration L

TABLE 2

SUMMARY OF REYNOLDS NUMBER EXPONENTS AND PREDICTED NaK ΔP's FOR 5-kwe REACTOR PLENUM CONFIGURATIONS

Configuration	Reynolds Number Exponent n (Slope of Experimental Data for $\Delta P = KRe^n$)	Predicted NaK ΔP at $Re = 1.85 \times 10^5$	
		Extrapolated Experimental Data	For $\Delta P = KRe^{1.815}$
A	2.074	0.051	0.039
B	2.051	0.043	0.034
C	1.958	0.044	0.039
D	1.795	0.030	0.031
E	1.577	0.023	0.028
F	0.908	0.007	0.013
G	1.833	0.019	0.019
H	1.618	0.007	0.008
I	2.418	0.033	0.020
J	1.672	0.012	0.013
K	1.593	0.010	0.012
L	1.581	0.006	0.008
M	1.733	0.009	0.009
O	1.881	0.083	0.078
P	1.990	0.019	0.016
R	2.008	0.015	0.012

log-log graph paper) to an inlet line Reynolds number of 1.85×10^5 as listed in Table 2. The straight line extrapolation was done for two slopes (i. e. , Reynolds number exponents) of the log ΔP versus log N_{Re} lines. It was expected that these slopes, for nonlaminar hydraulic data, would have values from 1.8 to 2.0; and, except for configuration F, the results did have slopes close to this range. Therefore, an average slope, 1.815, was determined from the data of the first 12 configurations. This average slope and the individual configuration correlation slopes were both used to determine the predicted NaK grid plate pressure variation at the operating Reynolds number and thus allow comparison of proposed plenum configurations.

Initial comparison of the maximum grid plate pressure variation (maximum ΔP) was made for the base case (Configuration A), with horizontal baffles (Configuration B), and with vanes at the inlets (Configuration C). Even though both the baffles and the vanes reduced the pressure variation to less than that for the base configuration, the variation for all three configurations exceeded the allowable 0.016 psi ΔP at the prototype Reynolds number.

A satisfactory grid plate ΔP was obtained by combining the horizontal baffles with a modified vane configuration and also changing the contour of the plenum head. The vanes were modified according to the results of potential flow calculations performed using a computer setup similar to that used for the 300-kwt SPF reactor program. Equipotential lines were determined for four layers in a plenum quarter section for both the basic plenum case and for the plenum with horizontal baffles. Velocity vectors were determined by taking the negative derivative of the potential function, and the configuration of the vanes was designed* to force the actual flow to follow these ideal frictionless streamlines.

A flat plenum head used with the modified vanes and horizontal baffles did provide additional improvements in grid plate ΔP but was unacceptable for structural reasons. Therefore, a concave (dished-out) head (Figure 34) was substituted for the original convex head and tested with the modified vanes and horizontal baffles (Configuration H). Experimental results indicated a predicted ΔP of 50% less than the maximum acceptable value of 0.016 psi (see Table 2).

*O. G. Feil, "Vane Systems for Very-Wide-Angle Subsonic Diffusers," J. Basic Eng., Vol 86, p. 759 (December 1964)

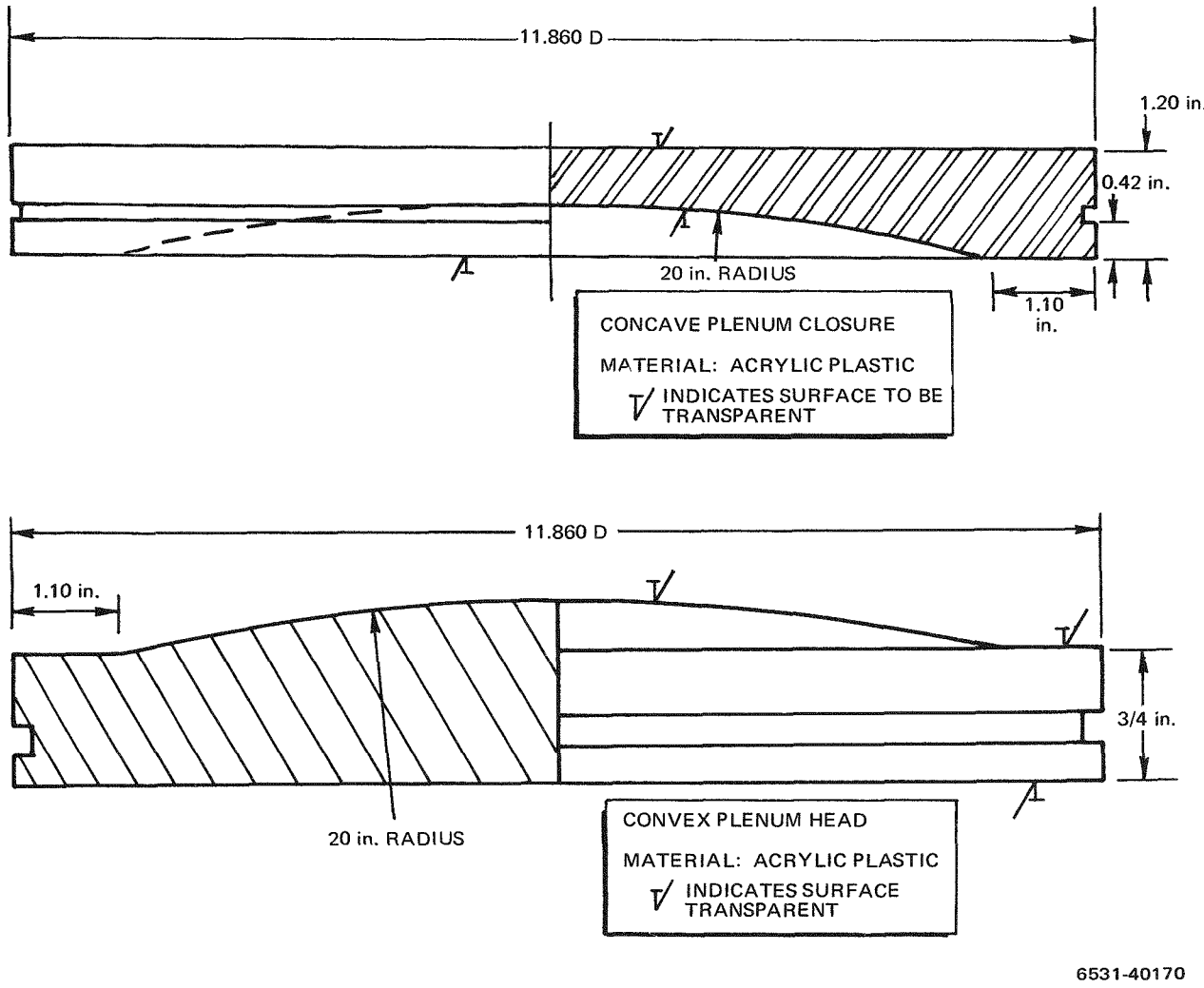

Figure 34. Plenum Head Configurations

Modifications were made to this ideal configuration to make it more compatible with the proposed reactor geometry and structural requirements. A new set of vanes was fabricated with contours to fit close to the concave head. The two horizontal baffles were combined into one baffle with a center slot which slipped into the plenum shell. Test results with these new components and concave head indicated an excessive prototype grid plate ΔP. The baffle was further slotted (Figure 35) and the two vanes on each side of the center vanes were cut down to allow flow over the top of these vanes. This configuration (K) provided an acceptable ΔP.

To further reduce ΔP variation, the effective plenum height was increased 0.15 in. by lowering the grid plate. This increased the distance between the baffle plate and grid plate to 1 in. In addition, the center vanes were trimmed to eliminate a 0.05-in. mismatch between plenum head and the roof of the plenum inlet. This adjustment provided a smooth surface transition between the inlet nozzle and the head. The configuration resulting from changing both the plenum depth and correcting the 0.05-in. head mismatch was designated as Configuration L. The configuration which resulted from changing the plenum depth only was designated Configuration M. Testing of these configurations indicated that the increase in plenum depth below the grid plate and the elimination of the 0.05-in. head mismatch each provided a small but measurable improvement in estimated grid plate ΔP.

Orifice plate configurations were also formulated to provide an alternate design approach to that of the baffle and vane combination. The orifice plate, used in the initial Configuration O apparently had fluid jets from the orifice plate holes which did not dissipate in the 1 in. settling distance between the orifice plate and grid plate. This produced locally high grid plate impact pressures and gave an unacceptable overall grid plate ΔP. Increasing the number of orifice holes for Configuration P resulted in a barely acceptable ΔP. This orifice plate was therefore combined (Figure 36) with the vanes of Configuration L to provide, as Configuration R, a sufficiently low grid plate ΔP with a grid plate pressure variation similar to that of Configuration L (see Figure 37).

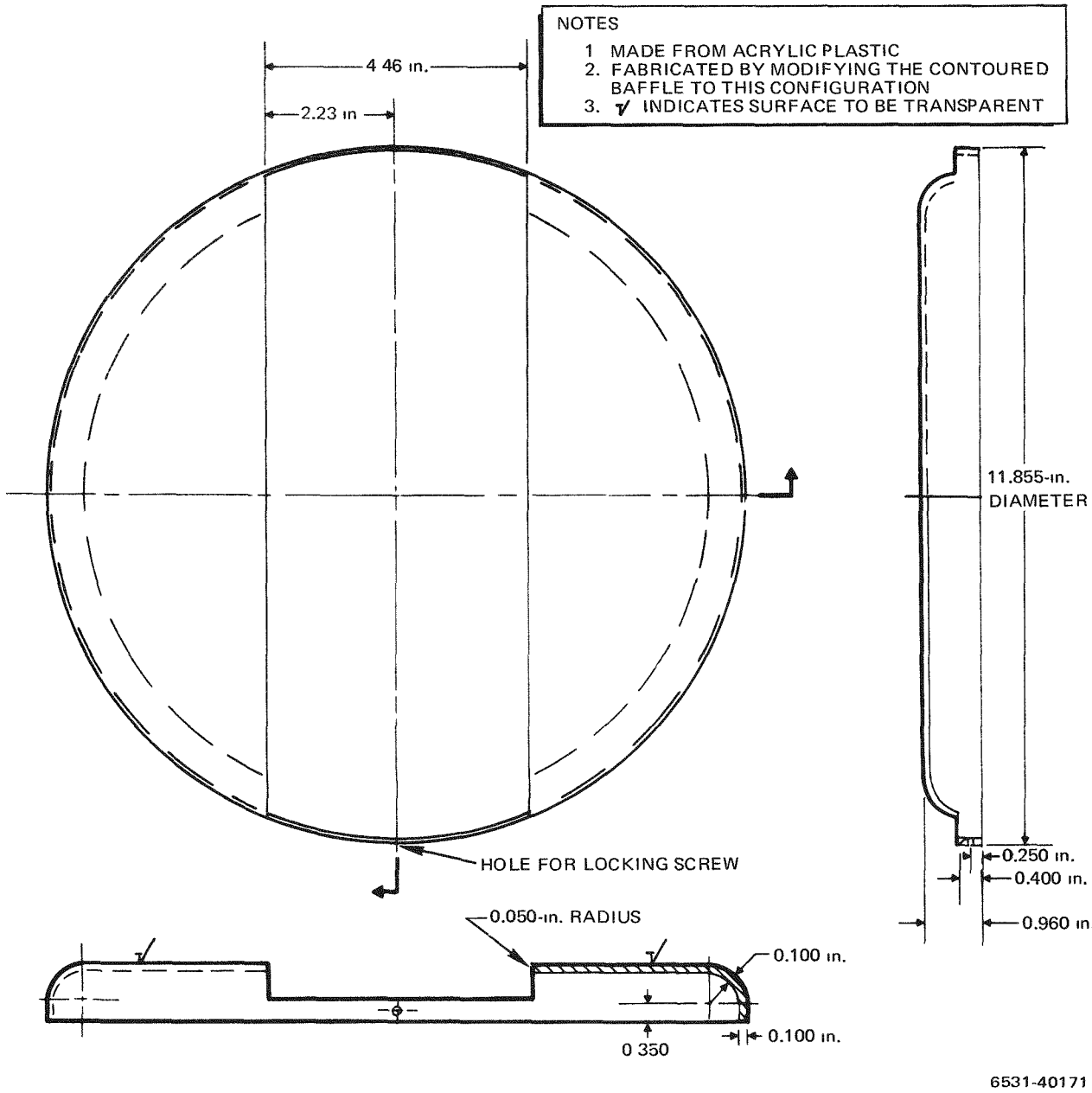

Figure 35. Joined Baffle Plates for Configurations J, K, L and M

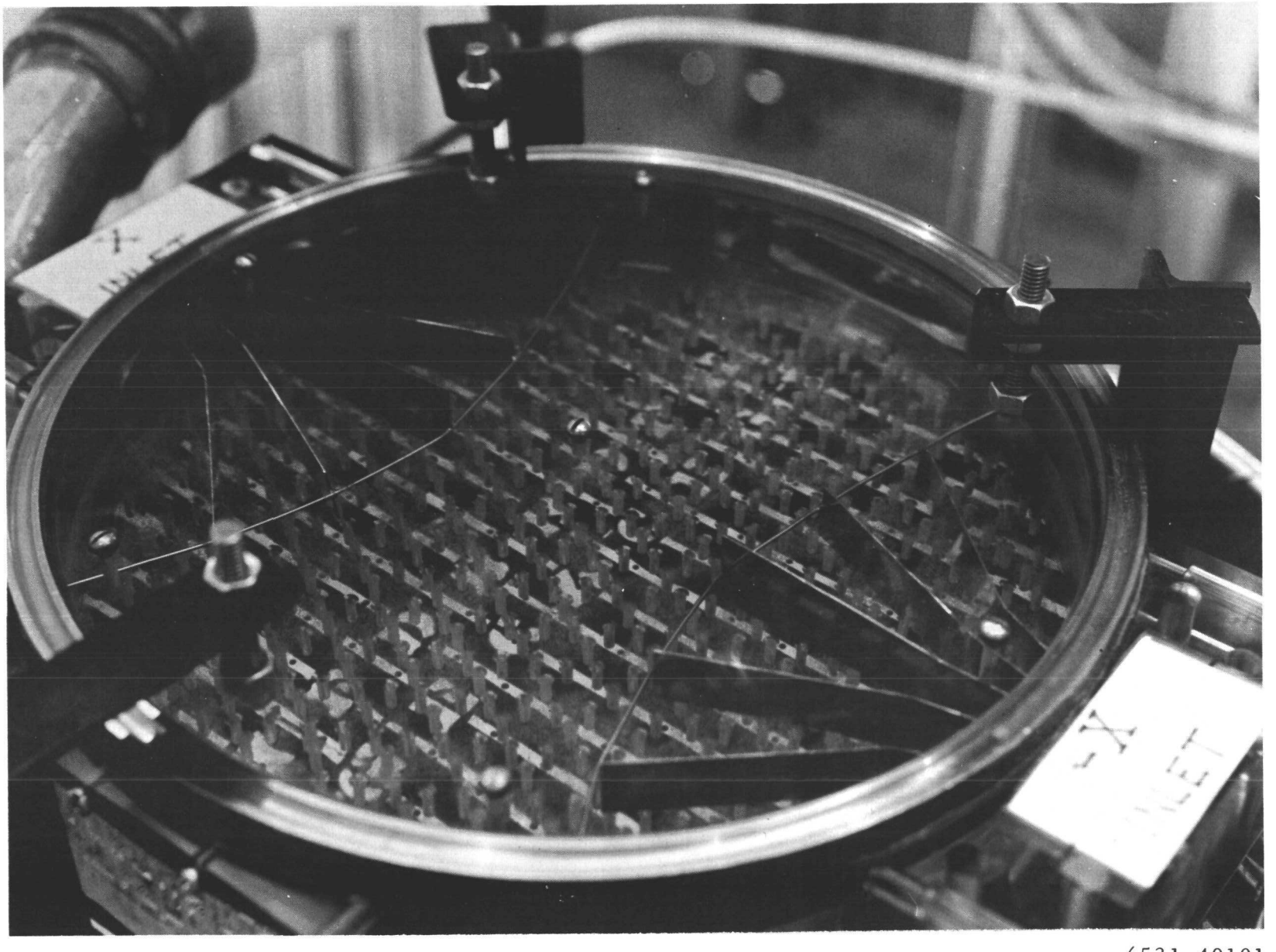

6531-40101

Figure 36. Configuration R: Orifice Plate, Vanes, and Concave Head

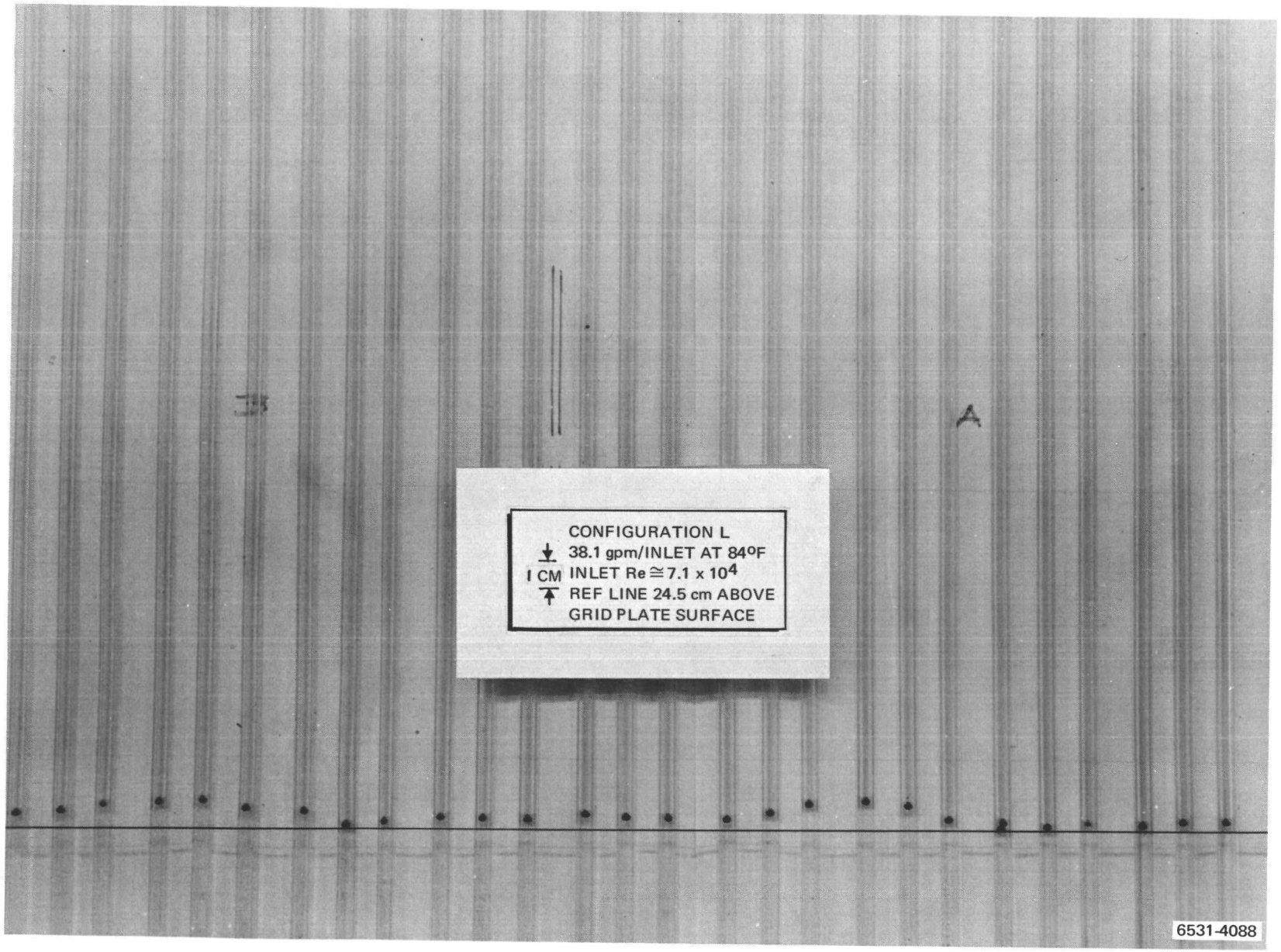

Figure 37. Typical Variation in Manometer Board Fluid Column Heights

Plenum flow patterns for the various plenum configurations were observed by injecting gas bubbles in the inlet lines as flow tracers. All configurations had a system of approximately four swirls, two on each side of the plenum, roughly 90 degrees from the inlets (Figure 38). These swirls continuously formed and disappeared and did not have sufficient strength to affect the pressure taps in that area. This was especially true for the orifice plate configurations where the swirls existed only between the closure and orifice plate, not between the orifice plate and grid plate. For those plenum configurations with horizontal baffles, additional swirls developed between the baffle and the grid plate in the region immediately in front of the inlets. However, only in the case of Configuration I did vortexes develop with sufficient strength to affect the pressure data.

Estimates of the effects of various plenum configurations on system pressure drop were made from inlet line pressure measurements. Comparison of measurements to those made for the basic plenum configuration showed no detectable change for the various vane and baffle configurations. The orifice plate configurations did increase the estimated NaK pressure drop: Configuration O produced an estimated increase of $\sim$0.3 psi, Configurations P and R produced an estimated increase of $\sim$0.03 psi.

3. Recommended Inlet Plenum Designs

Obviously, only one inlet plenum design was required. The results of these tests, however, indicated two designs would provide acceptable plenum flow characteristics (Figure 39). One design, Configuration L, had superior pressure characteristics but potentially poorer flow characteristics. The other design, Configuration R, had acceptable but slightly poorer pressure characteristics without, however, the potentially troublesome flow swirls near the grid plate. Configuration L was selected as the recommended design (Figure 40) and an additional series of tests proposed to verify its performance at the design Reynolds number. Configuration R was designated as an alternate configuration to be evaluated if Configuration L proved unsatisfactory.

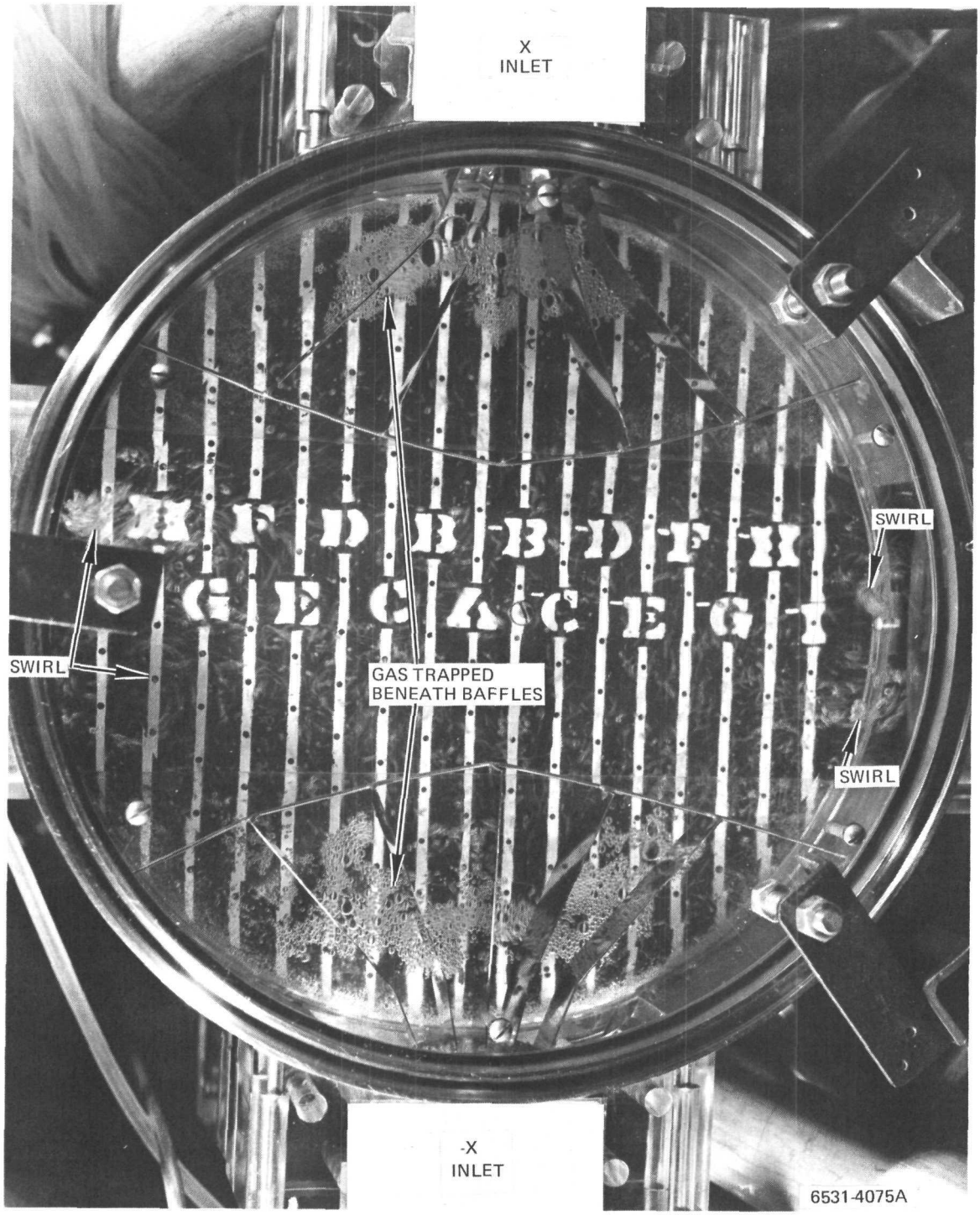

Figure 38. Typical Configuration L Flow Patterns as Indicated by Gas Injection

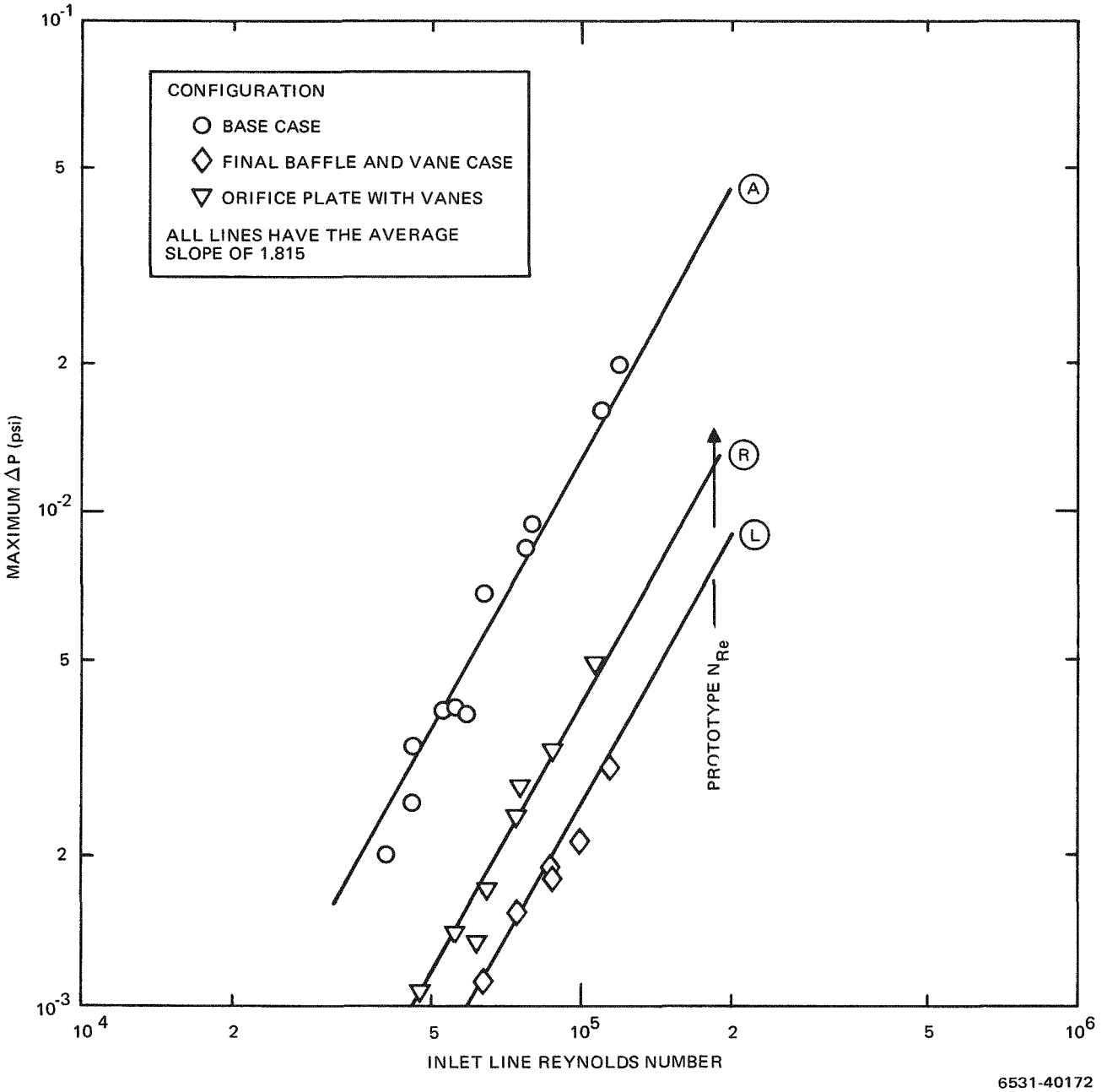

Figure 39. Comparison of Variation with Reynolds Number of Predicted Maximum Grid Plate Pressure Differences for Configurations A, L and R

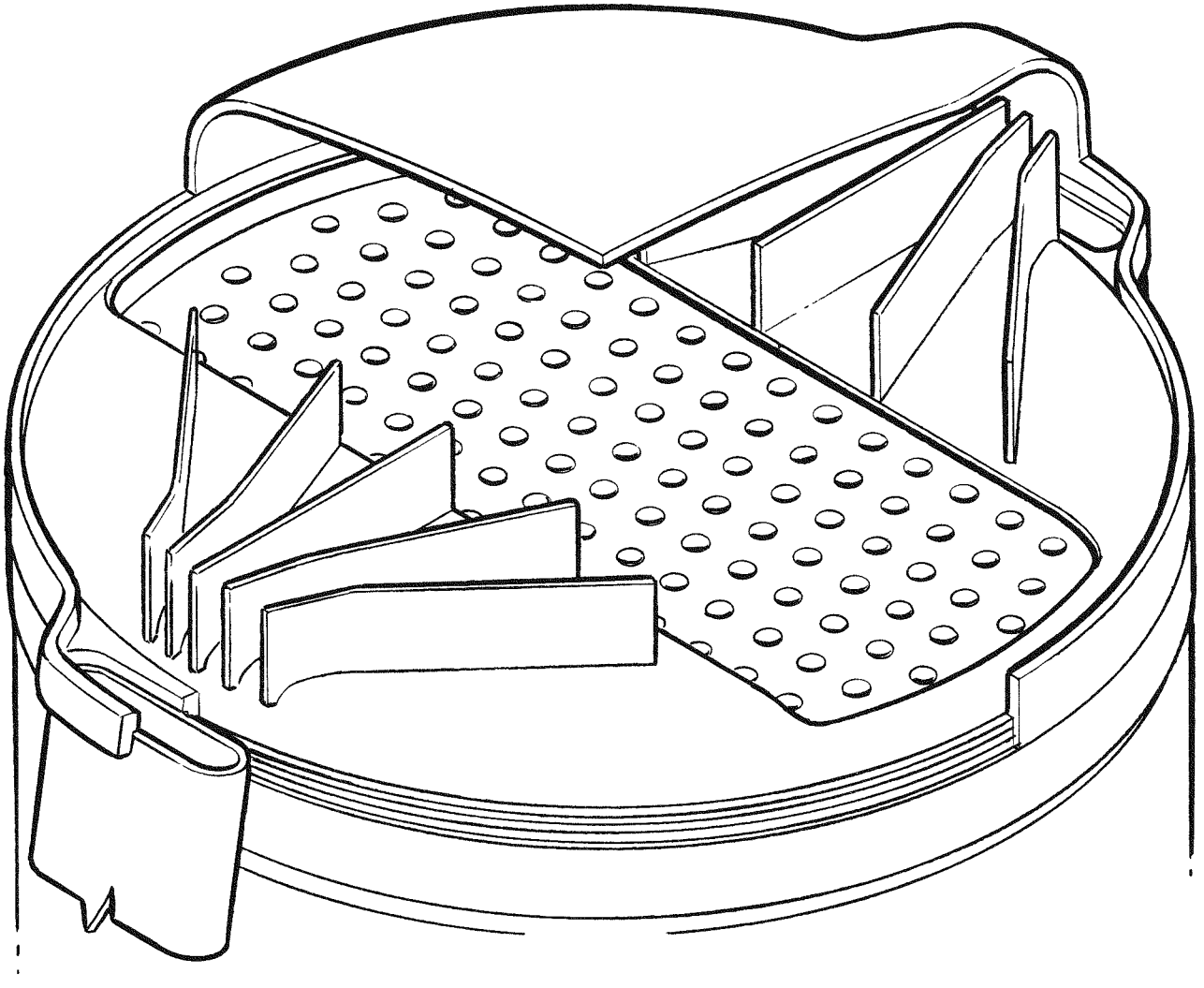

72-017-48-216

Figure 40. Cutaway View of Proposed 5-kwe Inlet Plenum Configuration

4. Design Verification Test, (Planned)

The additional tests proposed to evaluate the performance of Configuration L were to be performed in a flow system capable of higher flows and pressures. Also, the model required was to be a more accurate 1:1 representation of the recommended 5-kwe reactor inlet plenum configuration, with the capability of evaluating more than just inlet plenum hydraulics. Accordingly, a new hydraulic test model was designed to meet the proposed test requirements and be compatible with the higher capacity flow system.

The new model was designed to use the same type of assembly materials (stainless steel and acrylic plastic) and assembly scheme as that of the S8DR plenum model. The model would be designed to allow initial tests of the inlet plenum configuration with measurements of grid plate surface pressures in the inlet plenum. The model assembly was designed so that alternate plenum Configuration R could be tested if necessary. In addition, the design of this model would also allow a mockup of the entire finned-unfinned fuel element core array to be installed in place of the grid plate pressure instrumentation so that measurements could be made for the determination of core pressure drop and flow distribution. Program closeout, however, prevented the start of both the inlet plenum testing and design of the full-core tests.

III. INTRACORE MIXING STUDIES

A. BASIC APPROACH

A combined experimental and analytical effort was required for the evaluation of mixing in the proposed SNAP reactor configurations. Data available in the literature was primarily applicable to the configuration for which it was obtained. Correlations including all geometrical and flow aspects of the mixing configuration did not exist. A hydraulic test program was performed to provide the data necessary to support the analytical effort.

1. Test Model and Flow System

To evaluate the mixing of various proposed SNAP fuel element configurations, a series of hydraulic tests was designed and performed. These tests used de-ionized water to simulate the prototype NaK coolant, and were conducted using 19 simulated fuel elements arranged to provide full-scale simulations of the proposed reactor fuel element arrays. The water flow system (Figure 41) used for these tests is located at the Santa Susana Field Laboratory. For this series of tests, the flow system provided water flows to a maximum of approximately 70 gpm at temperatures of approximately 110° F. This allowed testing of fuel element arrays at Reynolds numbers up to 20,000.

The test models were fabricated of acrylic plastic and stainless steel. Two models were used in the test program. Both models were of the same general design: transparent acrylic plastic inlet and outlet plenums, inlet and outlet grid plates to support and position the 19 simulated fuel elements, and a transparent cylindrical plastic shell to provide the flow enclosure around the test element bundle (see Figure 42). The plenums provided inlet flow straightening, visual monitoring of salt injector location and exit ports in the outlet region for instrumentation leads. The cylindrical shell had partial elements attached around its inner circumference (Figure 43) to simulate elements in the prototype array which would be adjacent to the edge elements in the model.

The model used during the initial tests provided information for the selection of the optimum mixing configuration, and also was used in a series of tests resulting in an improvement of test operation and instrumentation technique. In general, this model used bare stainless steel rods to simulate the fuel elements. Various fin configurations were simulated by gluing plastic strips to the rod surface. Once the more successful type of mixing configuration had been

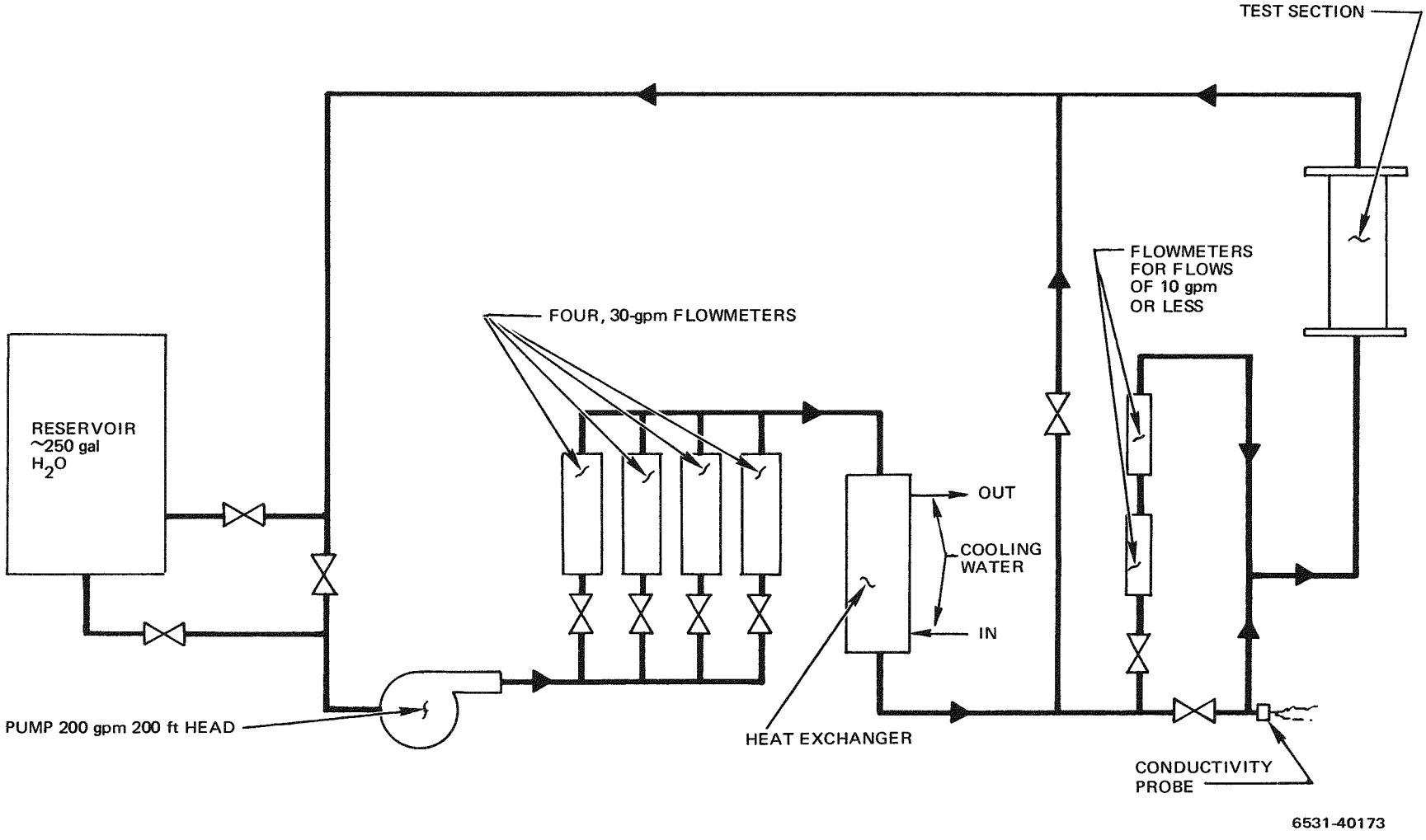

Figure 41. Schematic of Mixing Test Water Flow System

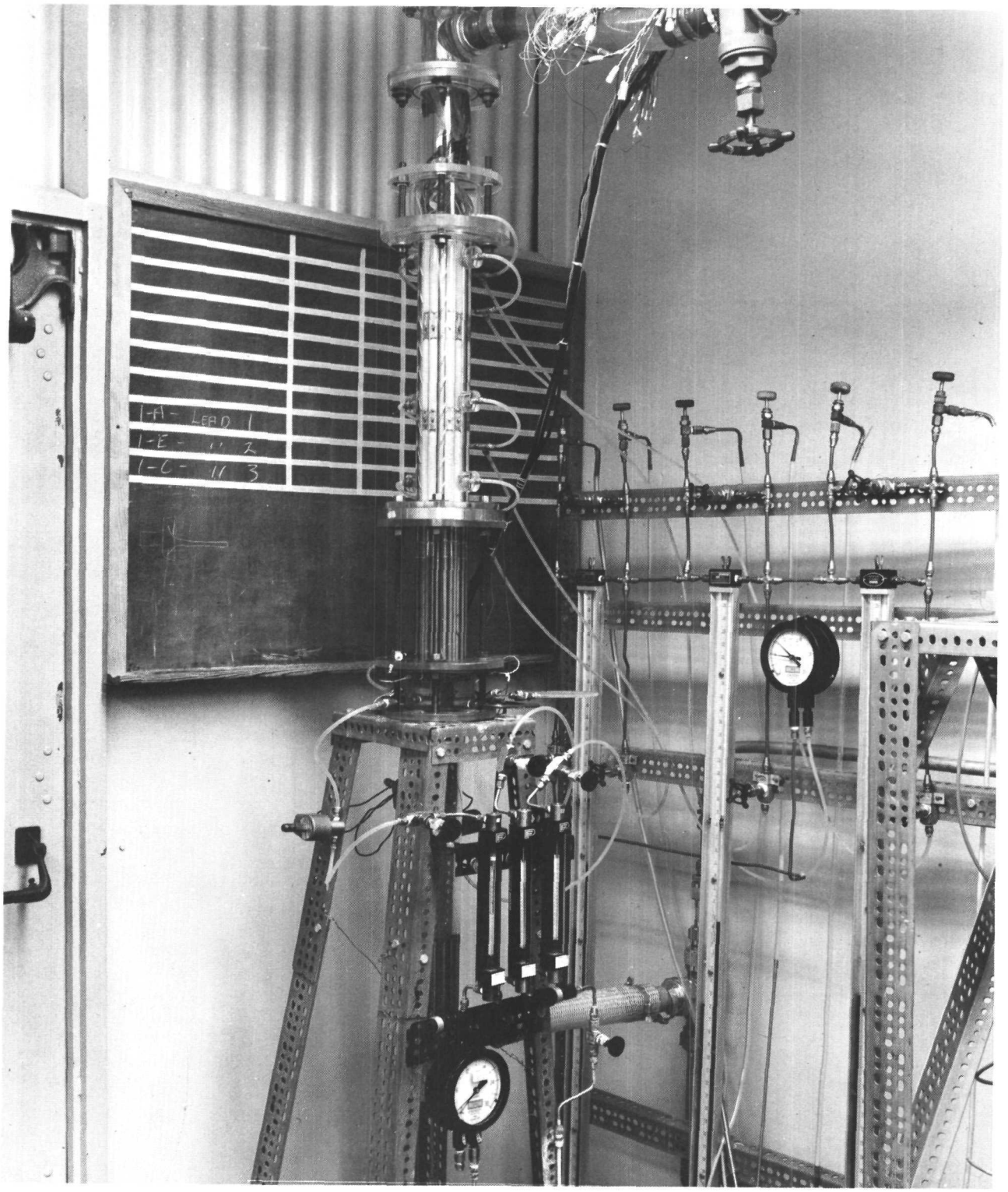

6532-4057

Figure 42. Typical Early Mixing Test Model Installation

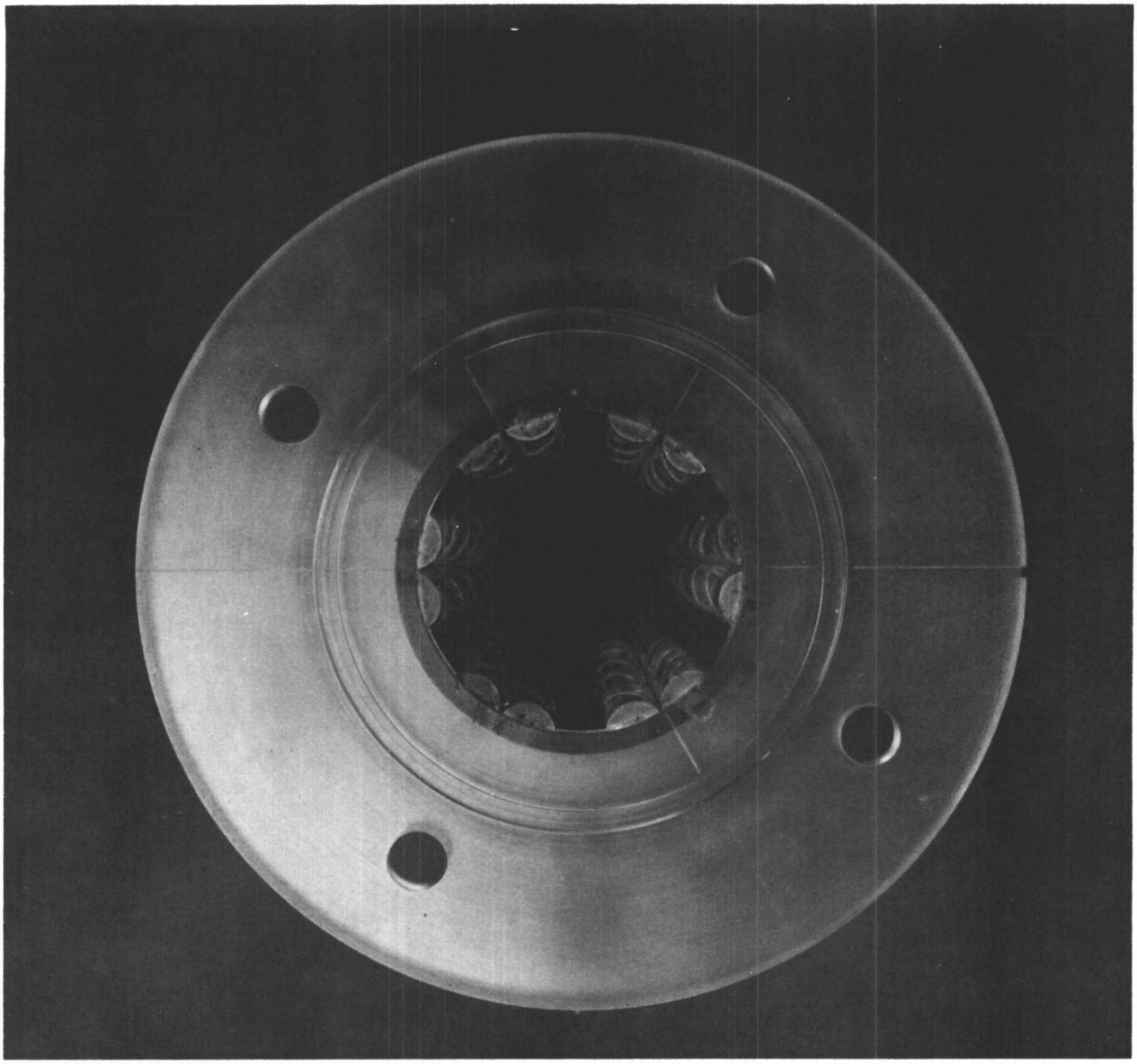

7759-40858

Figure 43. End View of Cylindric Shell Showing Partial Elements Attached for Configuration No. 7

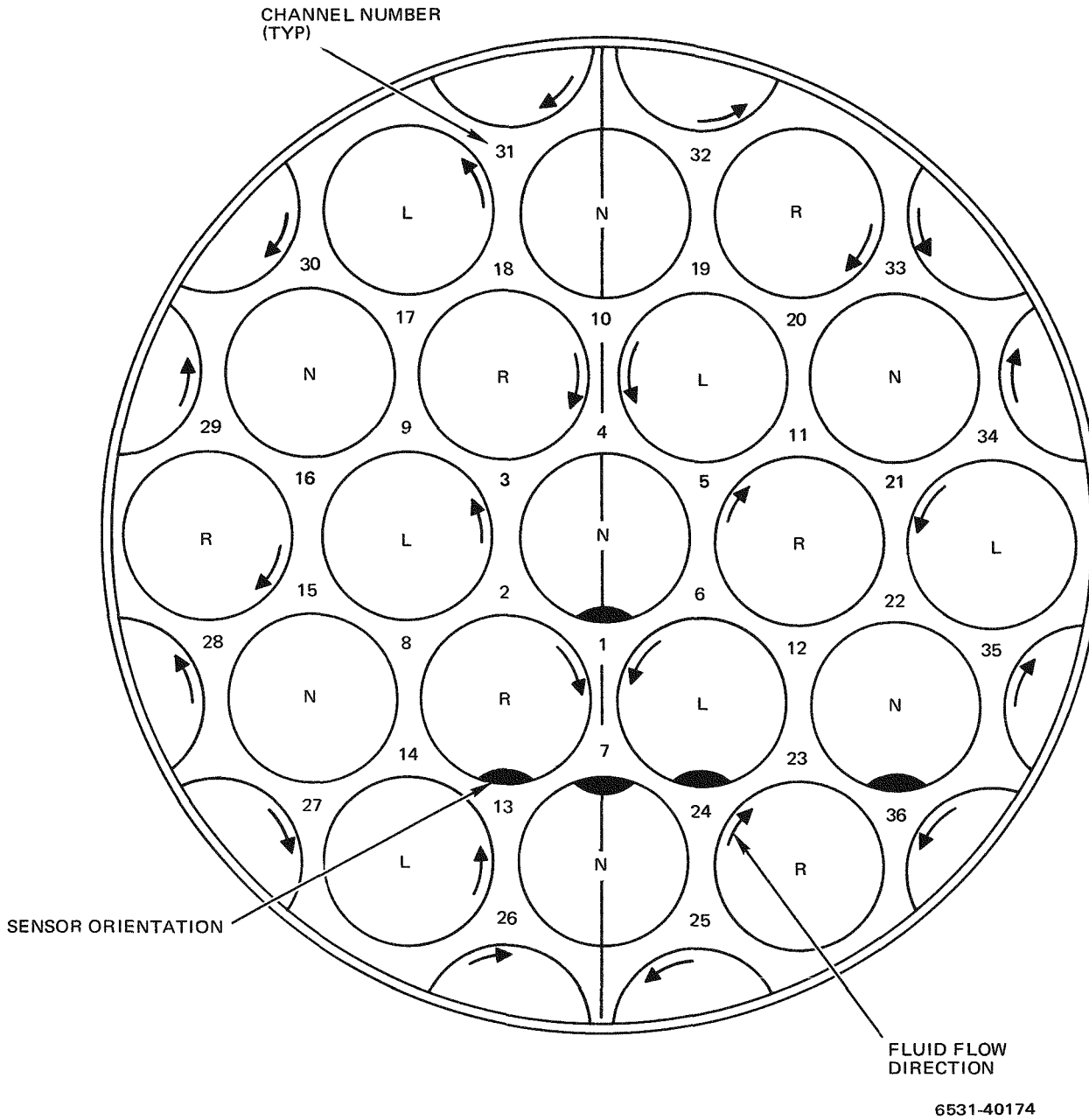

Figure 44. Orientation of Instrumented Elements for Tests of Configurations 1 through 8

selected, one of those configurations was assembled and a series of tests conducted to better understand the flow behavior in the test bundle and improve the bundle instrumentation.

The test bundle used for the final series of tests incorporated modifications based on the results of earlier tests and used components more similar to the prototype SPF reactor design. The simulated fuel elements were stainless steel rods with hobbed fins. The inlet grid plate had inlet tubes attached leading to each bundle flow channel entrance hole. These tubes helped the salt solution injected into selected channels to become well mixed with the flow-system water by the time the bulk flow reached intraelement flow channels.

2. Instrumentation

The experimental approach determined the test bundle interchannel mixing by measuring the amount of fluid moving between channels and then calculating the mixing fraction in %/in. necessary to cause this interchange. The basic instrumentation consisted of conductivity sensors mounted flush with the surface of the simulated fuel rods. The detection of fluid motion was accomplished by "tagging" the fluid entering one channel with an $NaNO_3$ solution to increase its conductivity over that of the normal water flow. Conductivity measurements at locations in the bundle could then be used to calculate how much of the fluid entering the "tagged" channel flow had moved to these locations.

The instrumentation systems required to gather data for interpretation of the mixing phenomena in the bundle were of three types. Instrumentation on the flow systems for both the total bundle flow and the injected channel $NaNO_3$ "tag" were conventional variable area flowmeters. A commercial conductivity probe and thermometer in the main flow system were used to determine the background $NaNO_3$ concentration in the main flow and to calibrate the test bundle sensors. The in-element conductivity sensors and their excitation instrumentation were used to measure intrachannel mixing. The instrumented fuel elements with conductivity sensors were similar to the instrumented elements described for the S8ER and S8DS plenum tests. These simulated fuel elements were installed in the test bundle with conductivity sensors facing the flow channels of interest (Figure 44). The excitation and indication circuitry for these conductivity sensors provided a common excitation voltage for all sensors being sampled and

produced a voltage output which, by calibration, could be related to the wt % of $NaNO_3$ at the sensor location.

In addition to the conductivity instrumentation used for detecting the mixing phenomena in the bundle, three additional conductivity sensors were installed in the final bundle assembly. These sensors were on the three tubes which were fed with the $NaNO_3$ tracer solution and were used to measure the mixed flow and tracer concentration before entry into the test bundle flow channels.

3. Experimental Procedure

Calibration data were required to relate the output voltages from the sensors in the mock-up fuel elements to the local $NaNO_3$ weight fraction. To accomplish this the commercial conductivity probe in the main flow system was initially calibrated in the Standards Laboratory using constant temperature (110° F) solutions of various $NaNO_3$ weight fractions to relate bridge conductivity measurement to the $NaNO_3$ weight fraction. The commercial probe was then installed in the flow system, flow was started, and the flow temperature stabilized at the calibration temperature. Sensor calibration was accomplished by incrementally increasing the whole flow system $NaNO_3$ concentration and recording sensor voltages at enough constant $NaNO_3$ concentration conditions to define the sensor calibrations over the range of test data.

Mixing data during test runs were recorded for constant flow conditions. Flowrate through the test bundle and flowrate from the $NaNO_3$ injection system were held constant. The temperature of the flow through the bundle was maintained at the conductivity probe calibration temperature. Thus, for the established constant flow, the voltage data from the sensors in the bundle could be interpreted to provide the amount of flow from the channel with the injected $NaNO_3$ solution to the channel region monitored by each sensor.

4. Data Recording and Reduction

Data recorded during the mixing tests consisted of flowrates, flow temperature, bundle pressures, initial system flow conductivity, and sensor output voltages. All data but the sensor output voltage data were obtained by manually recording a visual observation. The sensor output voltages from the modulator

detector circuit were amplified, filtered, and recorded using a data scanner system. This data scanner system sequentially sampled each sensor voltage and provided a printed digital record and/or a punched paper tape record. For some test sequences, an eight-channel, direct-writing oscillograph was also used to provide analog records of voltage variations from selected sensors.

The only data required for the element sensor calibration were the system flow temperature, conductivity reading, and the sensor voltage readings. Each calibration was, of course, conducted at a constant system conductivity (i. e., $NaNO_3$ concentration).

For analysis, each recorded sensor voltage was converted to the ratio $\Delta C / \Delta C_I$ (indicated salt wt % increment, ΔC, to the calculated injected salt wt % increment, ΔC_I). The salt increment ΔC was determined by first using the sensor calibration data to determine the $NaNO_3$ wt % equivalent to the sensor average voltage reading and then subtracting the initial or "background" wt % of the loop flow from this wt % value. The average sensor voltage was determined from those two or three "scan" voltage readings for which the background concentration of the flow entering the test bundle remained constant. The injected wt % increment was determined by calculating the ratio of total weight flow of $NaNO_3$ (background plus injected flowrates) to the total weight flowrate in the injected channel and subtracting the background weight fraction.

The terms in the $\Delta C / \Delta C_I$ ratio were calculated separately using the expressions: $\Delta C = C - C_o$, and

$$\Delta C_I = \left[\frac{\rho_o V_n Q_o + \rho_I V_I Q_I}{\rho_o V_n + V_I \rho_I} - Q_o \right] \times 100\%$$

where C = salt wt % read from individual electrode calibration curve at the average electrode voltage during the injection

C_o = wt % of salt flowing in solution before injection, determined from the commercial probe

ρ_o = density of salt before injection (1.0 gm/cc)

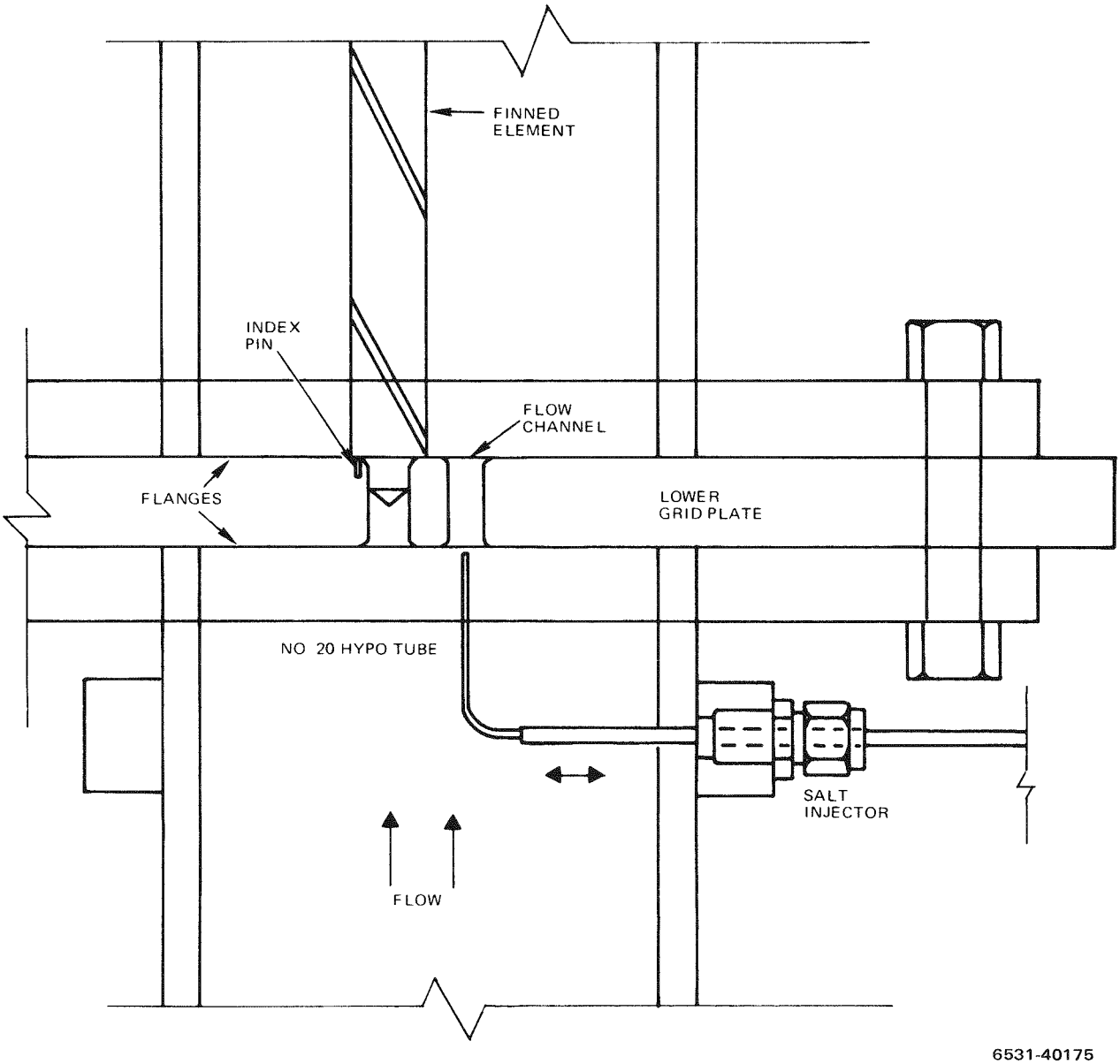

Figure 45. Sketch of Initial $NaNO_3$ Injection System

V_n = calculated flow in one bundle coolant channel (cc/min)

ρ_I = density of injected 20% x weight salt solution at 70°F (1.142 gm/cc)

Q_o = weight fraction of salt in solution prior to injection, $C_o/100$, determined from the commercial probe used for calibration

Q_I = weight fraction of salt injected (0.20)

V_I = measured flowrate at which 20% x weight salt solution was injected (cc/min).

These calculated ratios were then plotted versus the sensor position where data were measured to give the axial variation of concentration in a channel and, by inference, the amount of flow which had reached the sensor location from the injected channel.

5. Experimental Improvements

As the mixing test program progressed and better understanding of the test bundle flow was obtained, the experimental system was modified and improved. Changes were made in the $NaNO_3$ tracer injection system, in the instrumented mockup fuel element configuration, in the location and orientation of instrumented elements in the test bundle, and in the methods of recording and reducing the data. Specific improvements are discussed in the following subsections.

a. $NaNO_3$ Injection System

This injection system was to provide a mixed stream of inlet flow and $NaNO_3$ "tag" flow to the one bundle flow channel which was adjacent to a cluster of instrumented elements. Observations of data showed that the initial simple injection system was not providing a well-mixed, tagged inlet flow. Also, as investigation proceeded, it was learned that the readings of sensors in the bundle were sensitive to the $NaNO_3$ concentration near the element surface. The $NaNO_3$ injection system was modified to improve both these conditions.

The initial injection system consisted of a single hypodermic needle injecting into an inlet grid plate flow hole (Figure 45). This system evolved into that of three injection lines each with three slots for injecting tracer radially outward and located to allow tracer injection into three 11-in. long tubes, each soldered to the inlet grid plate coaxially with a flow hole. This modification allowed

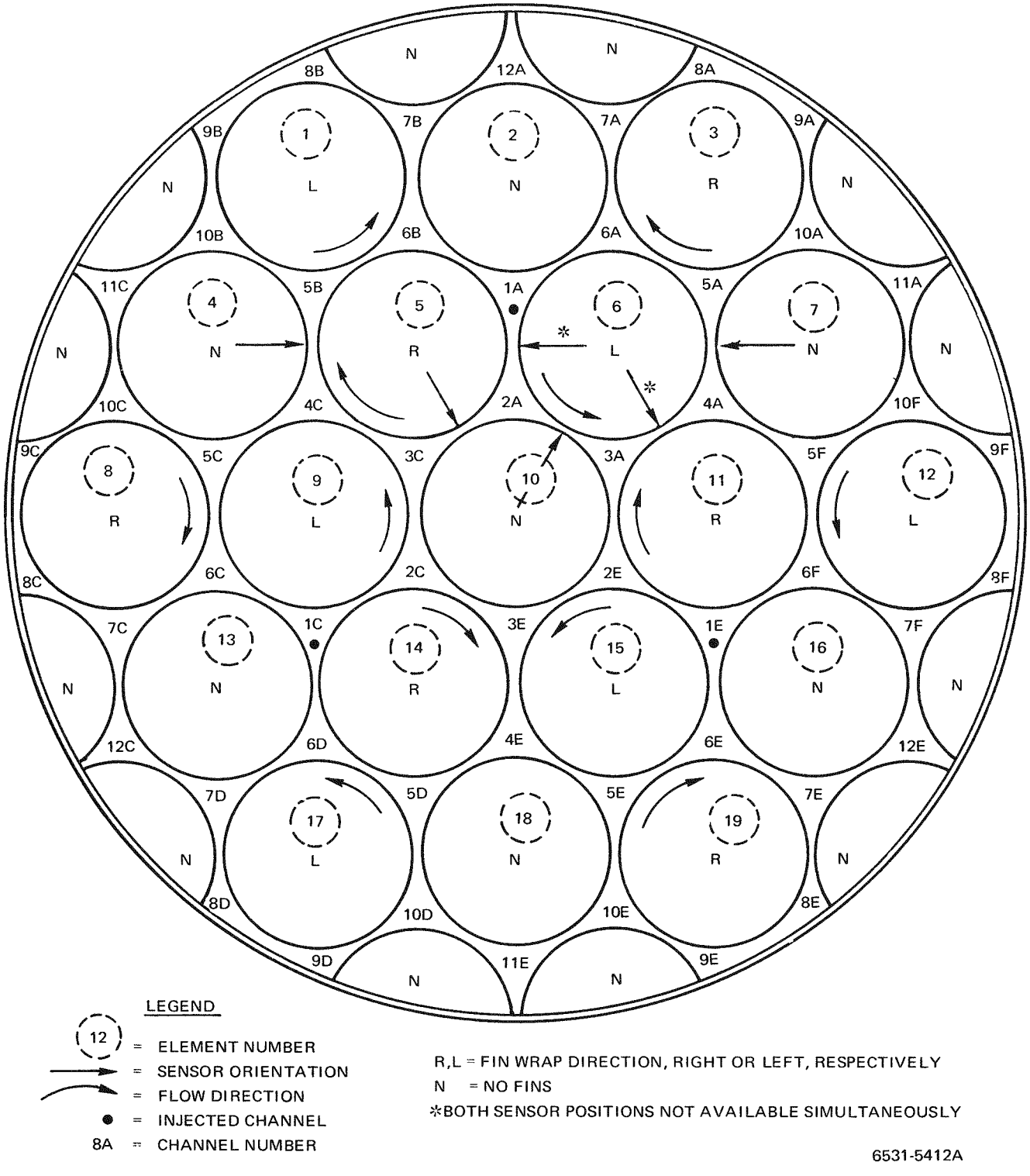

Figure 46. Typical Orientation of Instrumented Elements for Final Series of Mixing Tests

injection to be made far enough upstream to have the channel inlet flow and $NaNO_3$ "tag" well mixed. The tubes prevented any portion of the tagged mixture from entering any other flow channel inlet hole except that of the desired channel and also prevented dilution of the tagged flow.

The three shroud tubes fed by the injection lines were those which fed symmetrically located channels in the bundle (Figure 46). The flow of 20 wt % $NaNO_3$ tracer solution from the injection lines into the tubes could be individually metered and controlled. In general, all injection line flowrates were set at the same value. The use of equal injection flows into the three symmetrically located bundle flow channels made the $NaNO_3$ concentration more uniform both near and far from the element surface at the sensor location. This minimized any effect of local $NaNO_3$ concentration variation on the sensor reading.

b. Instrumented Elements

The instrumented elements were intended to provide flow conductivity readings at axial locations along the length of an adjacent flow channel. These readings were to be provided with minimum flow disturbance and at sufficiently small spacings to allow adequate definition of the tracer concentration variation along the flow channel. The instrumented element configuration used initially was similar to that used in the S8DR noise analysis tests. The sensor was a ceramic-insulated vacuum-feed-through soldered into the fuel element tube, then finished off to the tube OD. Experimental results indicated this initial element configuration was inadequate in two ways: (1) the amount, location and spacing of the sensors on the instrumented elements had to be changed; (2) the unshielded signal leads used in this configuration allowed signal interactions (crosstalk) to occur between individual sensor leads from the same instrumented element.

The final instrumented element configurations were determined from experimental results. In a series of tests with seven sensors per element, the definition of bundle flow characteristics was improved and the existence of the previously unsuspected signal crosstalk was demonstrated. Based on these test results, the finned and unfinned instrumented elements used in the final SPF test bundle were built with either 12 or 16 sensors spaced one-sixth of a fin pitch apart (see Figure 47). The axial location of the sensors, as well as their

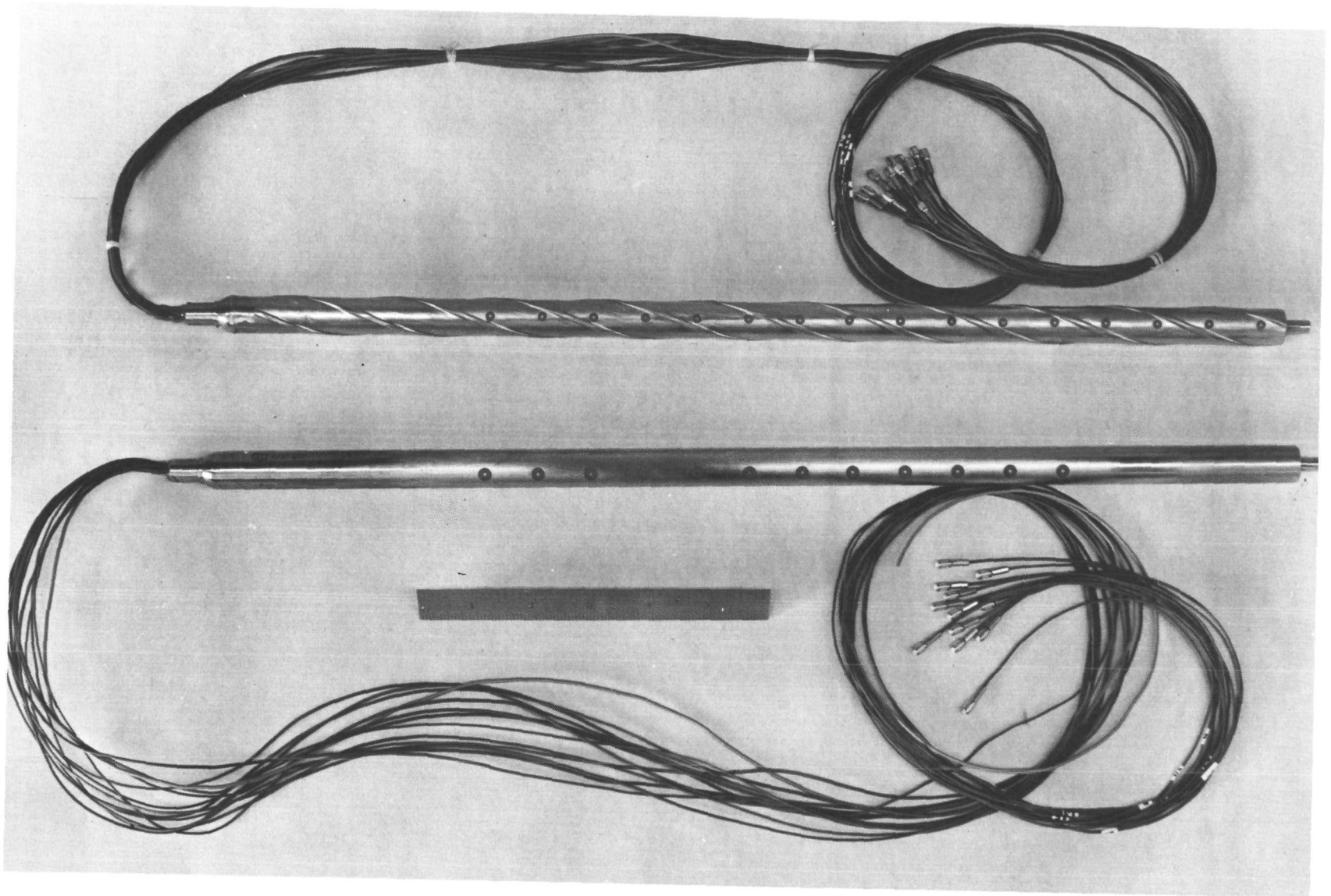

6532-4052

Figure 47. Typical Instrumented Element Configurations for Final SPF Test Series

number and spacing, were selected to provide the best definition of the maximum $NaNO_3$ concentration in the flow channel which was to be sampled by an instrumented element. To help minimize signal crosstalk, the leads for these sensors were fabricated from miniature shielded coaxial cable.

c. Location and Orientation of Instrumented Elements

The initial series of tests was performed with the instrumented elements oriented to sample channel flows in and adjacent to flow channels at the center of the bundle (Figure 44). Experimental results indicated that orientation of the sensors to the gaps between channels would give a better average concentration for flow out of a channel. As a result, the instrumented elements in the final SPF test sequence were oriented to sample across the channel exit gaps (Figure 46). Also, in this final configuration the location of the instrumented elements in the bundle was changed to provide monitoring of the correct flow channels for the three-channel symmetric $NaNO_3$ injection systems.

d. Data Recording and Reduction

Some of the equipment used for the initial series of tests was adapted from equipment used in the S8DR noise analysis tests. The number of sensors recorded was limited, therefore, to 14/run as that was the capacity of the available modular detector circuitry. The sensor calibration data were manually plotted and these plots used to determine local $NaNO_3$ concentrations for calculation of the $\Delta C/\Delta C_I$ ratios.

As the required number of sensors increased and the necessity of improving the data quality became apparent, both the recording system and the data reduction method were changed. To minimize signal crosstalk, shielded coaxial cable was used to connect instrumented element leads to a new modulator-detector unit. The new modulator-detector unit had a lower frequency (50 kHz) power supply to reduce signal crosstalk, and also had 28 signal channels. A punched-paper tape output section was put into operation to permit computer reduction of test data.

6. Development of the Analytical Model

The mixing occurring in the test bundles was evaluated by comparing the experimentally determined flow distribution ($NaNO_3$ concentration) to an analytical prediction. The analytical prediction methods used went through stages of

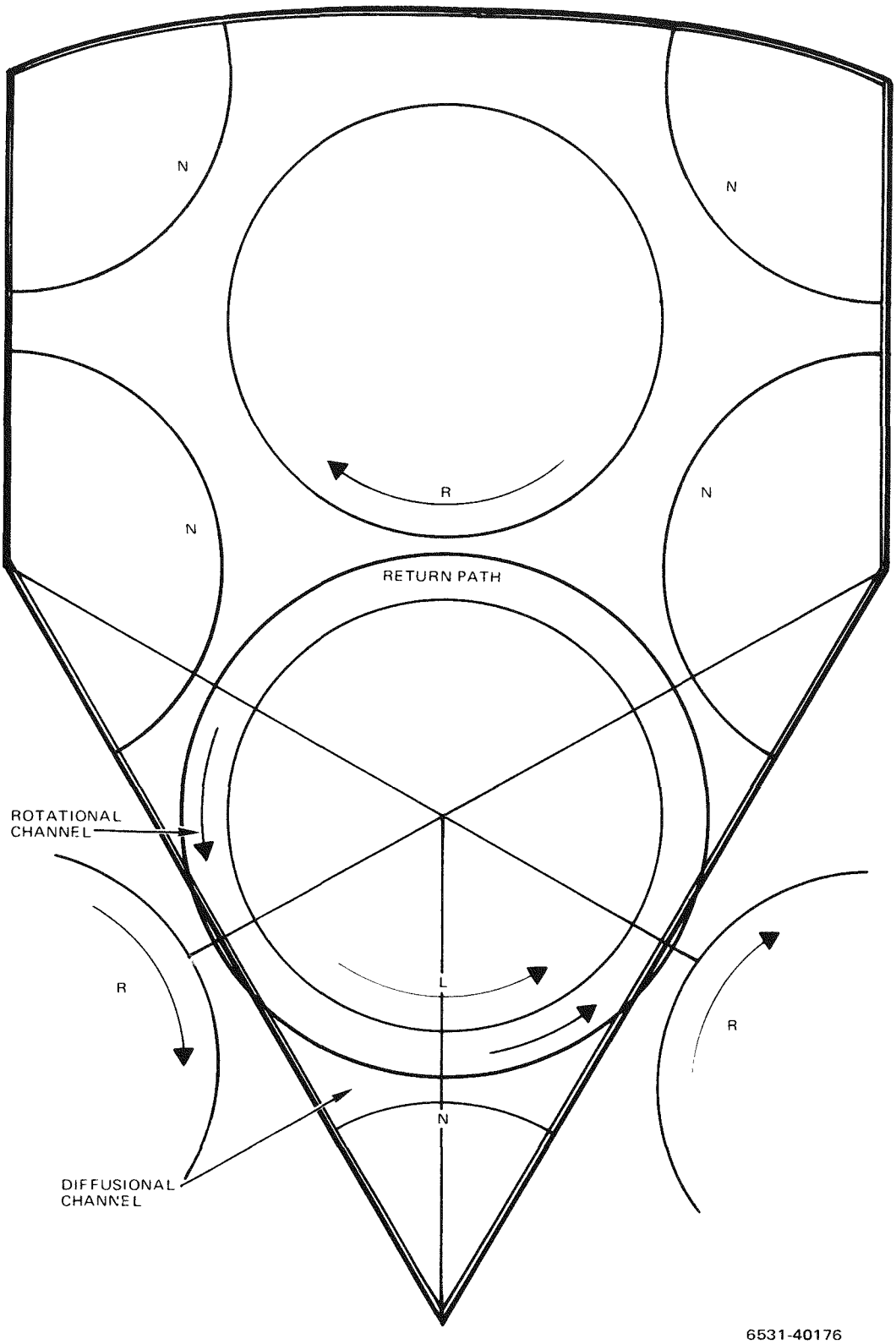

Figure 48. Basic Test Bundle Symmetry Group with Flow Around Finned Element Divided into Four Half-Tricusp Channels

development prompted by the inability of early models to match the results of the experimental efforts.

Early analytical efforts treated individual channels as entities (nodes) and assumed the mixing parameter, h, was constant down a channel. The mathematical model based on these assumptions of tricusp-to-tricusp channel mixing were unsuccessful in predicting $NaNO_3$ concentrations which correlated with the experimental data. Single channel crossflow calculations were thus used for the comparative mixing calculations and indicated the desirability of incorporating the right-left-neutral (R-L-N) finned element array in future reactor designs.

Further efforts, therefore, were directed toward determining interchannel mixing developed by the R-L-N element array. The tricusp-to-tricusp channel mixing model was improved and results from this model compared to the experimental results from an additional series of tests on an R-L-N array. These data confirmed the inapplicability of the analytical model to the experimental setup, as correspondence between the calculated and experimentally determined flow distributions ($\Delta C / \Delta C_I$ values) was very poor.

The data from the tests did, however, provide information on the complex flows occurring in the R-L-N mixing system. There were two types of flow in the R-L-N test bundles: rotational and axial. In addition, there was an entrance region in which rotational flow developed, and an established flow regime where rotational flow was constant.

An improved analytical model was developed to account for the effects of the flows in the bundle and relate the characteristics of these flows to the geometrical characteristics of a test bundle.

Analysis of mixing in the R-L-N test bundles was done with a basic group of channels subdivided into cells. The six-fold symmetry of the test bundle (Figure 46) allowed analysis of one basic group of four half-tricusp channels (Figure 48). These half-channels were adjacent to a finned element and were each subdivided into 30 radial sectors, 2 degrees wide (Figure 49). In general, these sectors were considered to have only spiral flow around the element in the general direction of the fin wrap. Some sectors, however, extended outside an effective fin height and were further subdivided into a rotational subchannel, with the fin-produced spiral flow, and a diffusion subchannel with an axial flow.

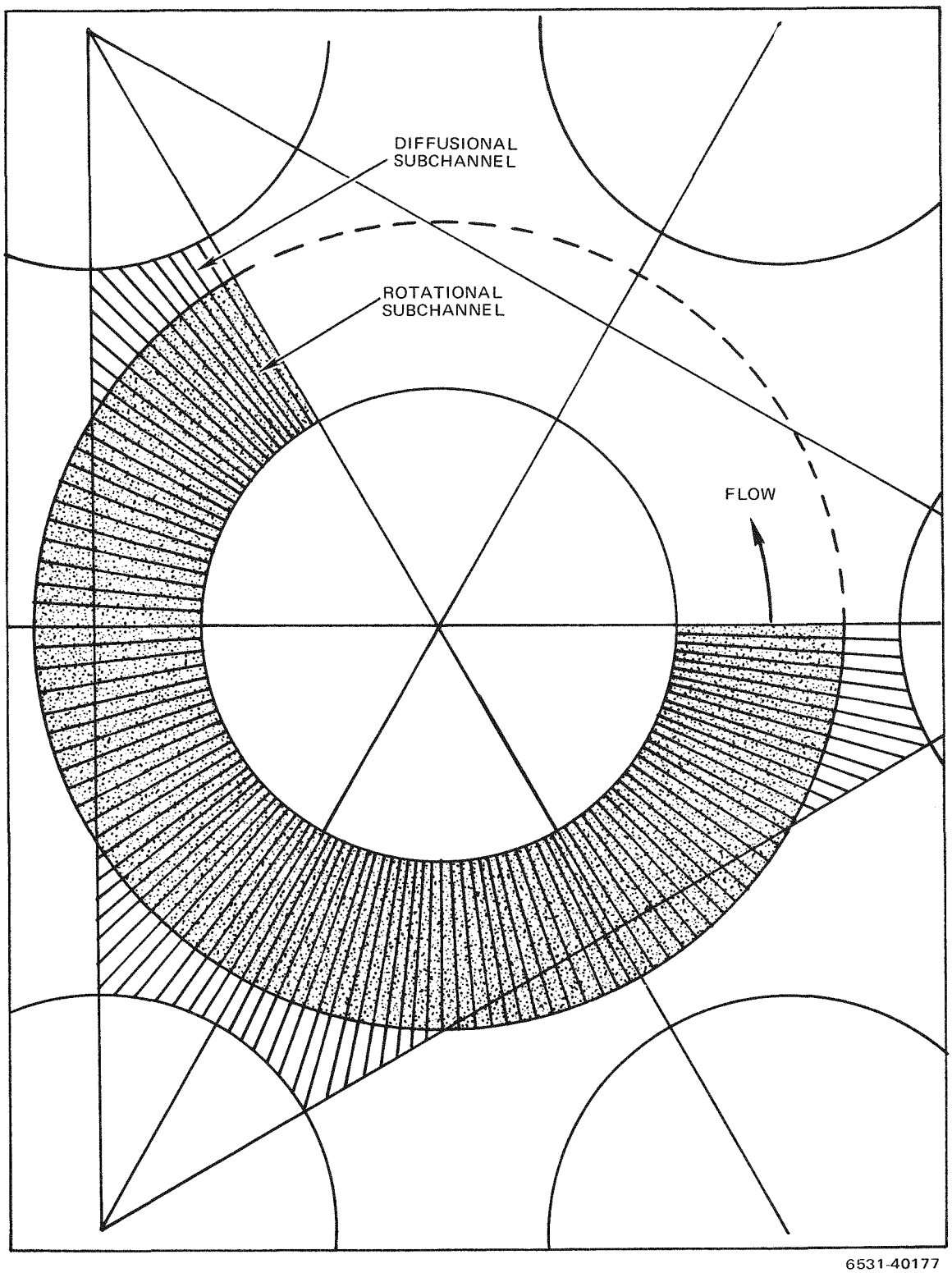

Figure 49. Subdivision of Channels into Radial Sectors

Because these subdivided flow channels approximated the general flow structure in the bundle, if the equations which described mass transfer in these channels reflected the actual flow conditions in a test bundle, then a reasonable prediction of mixing in the bundle should be possible. A set of generalized differential equations was written (Figure 50), as well as an equation for the tricusp-to-tricusp mixing rate (Figure 51). Both the generalized differential equations, which described the mass interchange between the rotational and diffusional subchannels, and the mixing rate equations, which could be solved for the mixing parameter, h, contained factors dependent on the test bundle geometry and flow behavior. Satisfactory mixing prediction was obtained by relating the factors describing the bundle flow behavior to the bundle geometry.

The important elements of flow structure which were defined were the development of the spiral flow in the entrance region, the effective thickness of the spiral flow on a finned element, and the diffusion coefficients for mass interchange between channels. The spiral flow development was modeled by having the flow pitch (the axial distance required for a particle travelling in a fixed spiral path to travel completely around an element) decrease exponentially, as a function of an entrance length, from an initial entrance value toward some final value (Figure 52). The thickness of the spiral flow and the diffusion coefficients were modeled, as were the spiral flow development parameters, by assuming a linear dependence on the bundle geometric constants.

The specific relationships between bundle flow parameters and bundle geometry were determined by using the differential equations solutions which "best fit" experimental data to determine the constants in these postulated relations:

1) The thickness of the fin envelope, t_{flow}, varies linearly with the averaged fin height, H_{fin}.
2) The normalized radial diffusion coefficient, D_R/V, and the normalized azimuthal diffusion coefficient, D_A/V, remain constant for an R-L-N finned bundle.

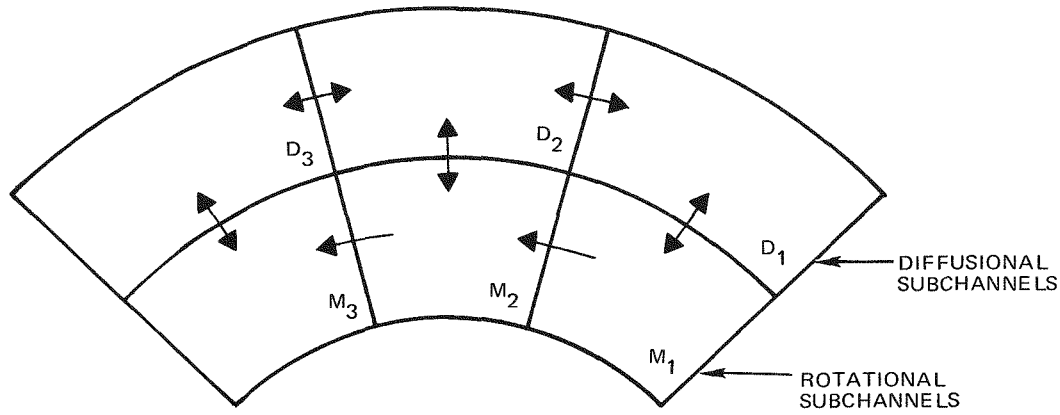

$$\frac{dC_{M_2}}{dZ} = \frac{1}{P_{flow/n}} (C_{M_1} - C_{M_2}) + \left(\frac{D_R}{V}\right) \left(\frac{L_{M_2 - D_2}}{A_{M_2}}\right) (C_{D_2} - C_{M_2})$$

$$\frac{dC_{D_2}}{dZ} = \left(\frac{D_R}{V}\right) \left(\frac{L_{M_2 - D_2}}{A_{D_2}}\right) (C_{M_2} - C_{D_2}) + \left(\frac{D_A}{V}\right) \left(\frac{L_{D_2 - D_3}}{A_{D_2}}\right) (C_{D_3} - C_{D_2}) + \left(\frac{D_A}{V}\right) \left(\frac{L_{D_2 - D_1}}{A_{D_2}}\right) (C_{D_1} - C_{D_2})$$

M_1, M_2, M_3	= ROTATIONAL SUBCHANNEL NOMENCLATURE
D_1, D_2, D_3	= DIFFUSIONAL SUBCHANNEL NOMENCLATURE
C_{M_i}	= SALINE CONCENTRATION IN SUBCHANNEL M_i
C_{D_i}	= SALINE CONCENTRATION IN SUBCHANNEL D_i
P_{flow}	= AXIAL FLOW PITCH
n	= NUMBER OF ROTATIONAL SUBCHANNELS/1/2-TRICUSP
D_R	= RADIAL DIFFUSION CONSTANT
V	= AXIAL AVERAGE VELOCITY
D_R/V	= NORMALIZED RADIAL DIFFUSION CONSTANT
D_A/V	= NORMALIZED AZIMUTHAL DIFFUSION CONSTANT
$L_{M_2 - D_2}$	= WIDTH OF BOUNDARY BETWEEN SUBCHANNELS M_2 AND D_2
A_{D_2}	= AREA OF SUBCHANNEL D_2
A_{M_2}	= AREA OF SUBCHANNEL M_2
$L_{D_2 - D_3}$	= WIDTH OF BOUNDARY BETWEEN SUBCHANNELS D_2 AND D_3

6531 40178

Figure 50. Typical Subchannel Arrangement and Applicable Differential Equations

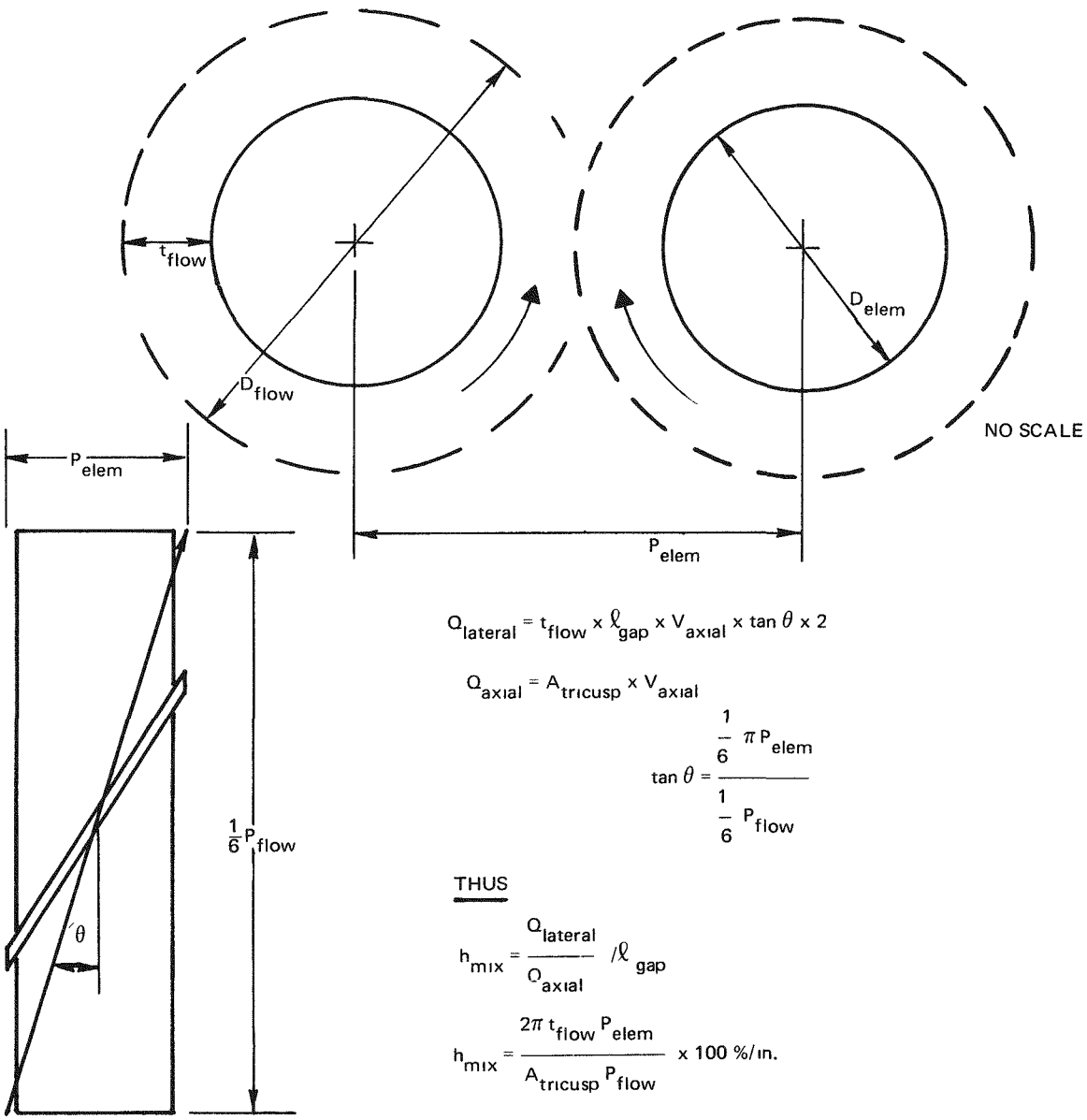

Figure 51. Tricusp-Tricusp Mixing Rate Model

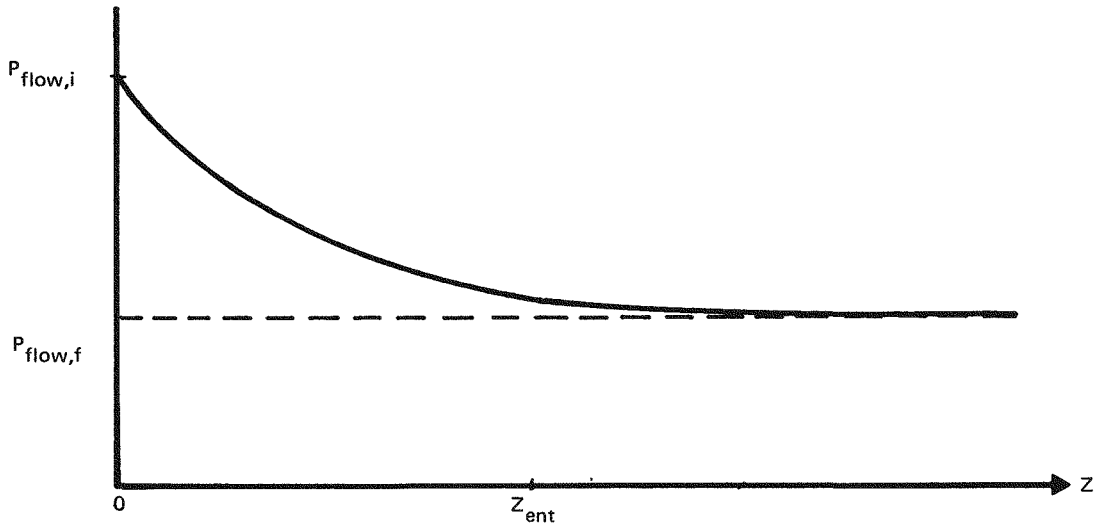

$$P_{flow} = P_{flow,f} + (P_{flow,i} - P_{flow,f}) \exp(-3z/Z_{ent})$$

WHERE:

P_{flow}	=	AXIAL FLOW PITCH
$P_{flow,i}$	=	INITIAL AXIAL FLOW PITCH (ON ENTRANCE TO BUNDLE)
$P_{flow,f}$	=	FINAL AXIAL FLOW PITCH (ASYMPTOTIC VALUE)
z	=	AXIAL DISTANCE INTO BUNDLE
Z_{ent}	=	EFFECTIVE ENTRANCE LENGTH

6531-40180

Figure 52. Axial Flow Pitch Entrance Effect Model

3) The effective flow development entrance length, z_{ent}, varies inversely to average fin height, H_{fin}.

4) Both the initial and final values of the axial flow pitch, $P_{flow,i}$, and $P_{flow,f}$, vary linearly with the axial pitch of the fins, P_{fin}.

The best-fit values of the flow parameters for the nominal 30-mil fin $\Delta C / \Delta C_I$ data were combined with the 30-mil fin test bundle dimensions to give the following empirical relations between flow parameters and bundle geometry:

$$t_{flow} = 0.717 \times H_{fin}$$

$$D_R/V = 3.50\%$$

$$D_A/V = 0$$

$$z_{ent} = 0.0663/H_{fin}$$

$$P_{flow,i} = 3.64 \times P_{fin}$$

$$P_{flow,f} = 1.91 \times P_{fin}$$

The true "uniqueness" of the best-fit input parameter set from the 30-mil data cannot be rigorously demonstrated. It is pertinent, however, that each parameter was varied about its best-fit value, with a resultant poorer-fit to the experimental data. Additional checks were made on those parameters which affected the mixing factor calculation. Pairs of these parameters were varied inversely about their best-fit values such that the mixing factor remained constant. Again, a poorer-fit to the experimental data resulted.

Calculation of the mixing parameter was done using the expression obtained by solving the equation for channel-to-channel mixing with the flow parameters expressed as functions of bundle geometry. The resulting expression for the mixing parameter is:

$$h_{mix} = \frac{236\ P_{elem}\ H_{fin}}{P_{fin}\ (0.433\ P^2_{elem} - 0.393\ D^2_{elem} - W_{fin} H_{fin})(1 + 0.91\ e^{-45.2\ H_{fin} z})}$$

where

P_{elem} = element-element separation (in.)

H_{fin} = average fin height (in.)

P_{fin} = axial pitch of fins (in.)

D_{elem} = element OD (in.)

W_{fin} = fin width, horizontal projection (in.)

z = axial distance into bundle (in.)

h_{mix} = mixing parameter (%/in.).

This expression was used to determine the variation of the mixing parameter through the R-L-N test bundles.

B. PRELIMINARY MIXING STUDIES

A series of mixing tests was conducted to determine the optimum core configuration to provide mixing in the ZrH reactor. Sufficient data analysis was done to allow selection of the configuration giving the greatest flow mixing.

In the initial series of tests, data were obtained to allow comparison of the effects on flow of various mixing-inducing devices (Configurations 1 through 5 in Table 3). Subsequently, tests were conducted to provide information on the effects of changes in geometry of the selected configuration (Configurations 6, 7 and 8 in Table 3).

Test data were recorded in general for three flow conditions for each configuration, using the printed paper tape output of the data scanner system. The general operating sequence was: (1) to calibrate the in-bundle sensors against the commercial probe, (2) replace the resulting high $NaNO_3$ concentration system water with fresh water, and (3) after warmup, record the mixing data.

With the exception of the basic configuration, two types of mixing configurations were tested. One used twisted stainless steel ribbon inserted in the flow channels; the other used plastic fins spirally glued to the unfinned stainless steel rods. Two basic types of finned rod configurations were simulated: a four-finned element configuration where all elements were wrapped in the same direction; and a three-finned, three-element configuration where two elements had opposite fin wraps and one element was unwrapped.

TABLE 3

PRELIMINARY MIXING TESTS

Config. No.	Number of Fins	Fin Pitch (in.)	Fin Wrap*	Fin Height (in.)	Fin Width (in.)	Element to Element Gap (in.)	Maximum Parameter h (%/in.)
1	4	4	R	0.020	50	0.044	3.0
2†	-	-	-	-	-	0.044	0.3
3	3	4	R-L-N	0.030	50	0.044	34.0
4	§	§	§	§	§	0.044	0.7
5	**	**	**	**	**	0.044	0.7
6	3	8	R-L-N	0.030	50	0.044	28.0
7	3	8	R-L-N	0.018	50	0.024	22.0
8	3	4	R-L-N	0.018	50	0.024	33.0

*Fin wraps designated as:
R - Right-hand wrap
R-L-N - Wrap for basic three-element array: one element right-hand wrapped, one element left-hand wrapped, and one element not wrapped.
§ Flat stainless steel ribbons twisted with 2-in. pitch inserted in flow channels with left-hand and right-hand twist in alternate channels.
† Basic test bundle with no mixing devices.
** Flat stainless steel ribbon twisted in a left hand manner with a 2-in. pitch and inserted in alternate flow channels.

Data from these configurations were analyzed to evaluate the mixing occurring in the flow through each configuration. All analysis techniques treated channels as individual entities (nodes). The data from the series of tests used for selecting the optimum mixing configuration was analyzed using the simpler techniques of curve fit or slope comparison. The data from the series of tests where various parameters of the optimum configuration were evaluated used analysis plots derived from more rigorous solutions of the channel mixing equations.

The test results (Table 3) indicated that the finned element configuration with the two oppositely wrapped elements and one unfinned element, the R-L-N configuration, provided a high degree of mixing and was, therefore, selected

as the reference configuration for the ZrH reactor design. Further tests of this configuration, with fin pitches of 4 in. and 8 in. and fin heights of 0.018 in. and 0.030 in., showed that the highest mixing was obtained with the 4-in. pitch and 0.030-in.-high fins (Configuration 3 of Table 3).

Analysis of the results of these tests also indicated that improvements were required in the experimental approaches. Difficulties in analyzing the experimental data showed that more than four sensors per channel were required to define the concentration variations. The number of sensors per channel was increased, therefore, from four to seven prior to running the R-L-N parameter tests.

Subsequent tests with the sensors closer to the inlet grid plate indicated that the 20 wt% $NaNO_3$ tracer solution might not be completely mixed with the flow in the injected channel. Therefore, prior to testing configurations 7 and 8, the $NaNO_3$ injection system was modified by changing the injection line configuration and moving it away from the inlet grid plate. This required that shroud tubes be attached to the inlet grid plate coaxially with injected channel flow holes. These tubes contained the tagged flow and allowed sufficient mixing to occur upstream of the grid plate so that a mixed stream entered the test bundle.

Although these experimental changes improved the data quality and improved the analytical results, they were not completely satisfactory. Inspection of the reduced data indicated that the relative mixing occurring in the bundle was consistent with the relative magnitude of mixing determined from the analytical models. However, the analytical models failed to adequately correlate with the experimentally measured $\Delta C / \Delta C_I$ variation in a flow channel. This meant that even though the relative values of mixing parameters were correct for the various configurations, the accuracy of the values calculated could be improved if an analytical model providing better correlation could be developed.

The conclusions reached from this series of tests were:

1) The R-L-N finned element configuration would be the ZrH reactor reference configuration.

2) Both fin pitch and height (element spacing) affected mixing, with fin pitch having a stronger effect.

3) The analytical model used did not accurately represent the flow in an R-L-N bundle.

To improve the understanding of the flow in an R-L-N test bundle, two additional series of tests were run to study the flow in R-L-N finned element configurations (Table 4). One series of tests used the Configuration 8 setup from the evaluation and parametric test series. The other series of tests used a 19 element bundle built to simulate the element configuration proposed for the SPF reactor. The initial series of tests determined the instrumentation and installation modifications required so that the data from the second series of tests would be adequate for determination and verification of an analytical mixing model.

TABLE 4

CHARACTERISTICS OF TEST BUNDLES FOR R-L-N FLOW STUDIES

Characteristics	Test Bundle Nominal Fin Height		
	30-mil Fins	15-mil Fins	20-mil Fins
Fin Type	Hobbed	Hobbed	Plastic Tape
Number of fins	Three	Three	Three
Element OD (in.)	0.642	0.657	0.560
Element-Element Separation (in.)	0.670	0.670	0.584
Actual fin height (in.)	0.0265	0.0115	0.0180
Fin width (in.)	0.070	0.070	0.050
Axial fin pitch (in.)	5.50	5.50	4.00
Finned length (in.)	16.0	16.0	16.0

Both series of R-L-N studies used the same flow system, with modifications as required to accommodate specific installations. The data-recording sequence was modified from previous tests by combining the recording of calibration data and mixing data. This was done by using the constant concentration data prior to each injection as both calibration and background data for the run. At the conclusion of testing, the calibration data range was extended in the normal way by incrementally adding salt solution until the range of electrode voltages recorded in the data runs had been covered.

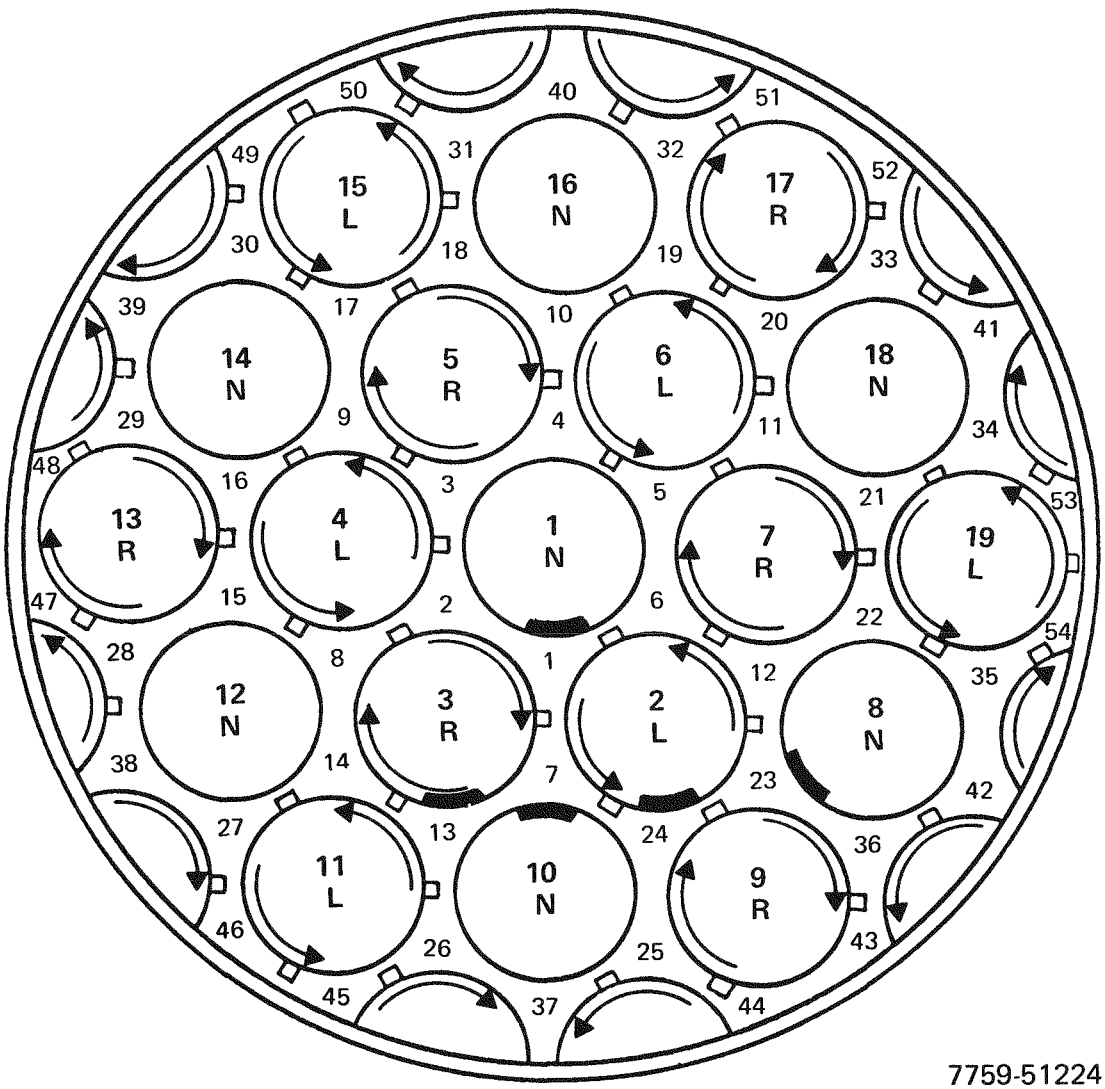

Figure 53. Initial Sensor Orientation for Preliminary R-L-N Tests

The preliminary tests were conducted using the Configuration 8 test bundle with the 4-in. -pitch, 0.018-in. -high plastic fin configuration. All tests were conducted with 110° F water flowing at a nominal 40 gpm (average bundle velocity of 10 ft/sec). No other flow settings were used as these tests were being conducted to evaluate instrumentation and analytical techniques.

The final R-L-N tests were conducted to provide sufficient data to verify an analytical mixing model which was based on a study of results from the preliminary tests. The test bundle for these tests was a 19- element bundle assembled, using elements with hobbed metal fins, to simulate an SPF reactor configuration. The test assembly incorporated those instrumentation and installation modifications suggested by the results of previous tests: three-channel $NaNO_3$ injection, inlet shroud tubes for all channels, additional and more closely spaced sensors in the instrumented elements, shielded instrument leads, and improved modulator detector circuitry. Because of the increased number of sensors, the data recording and reduction methods were also modified to include punched paper tape recording and computer data reduction.

These studies provided significant information on the characteristics of flow in a bundle of elements having the R-L-N finned element configuration. This improved understanding of bundle flow characteristics was used to develop the analytical model which was successful in describing the $NaNO_3$ concentration variations in the test bundle flow channels. Using the results of this analytical model, the mixing parameter could then be determined for these R-L-N configurations.

The original purpose of the preliminary tests was to obtain a mass balance (accounting) from the measured concentration data. The first of these tests, with the sensors oriented to measure the salt concentration in flow down a coolant channel (Figure 53) had unsatisfactory mass balances. Comparison of results from tests with some sensors reoriented to measure other channels indicated that the $NaNO_3$ distribution in a flow channel was not uniform—the measured $NaNO_3$ concentration depended on which element the sensor was located. Interpretation of the data from these tests indicated that there were two types of flow in a bundle of R-L-N elements: a rotating flow in the fin-wrap direction around the finned elements, and an axial flow along the surface of the

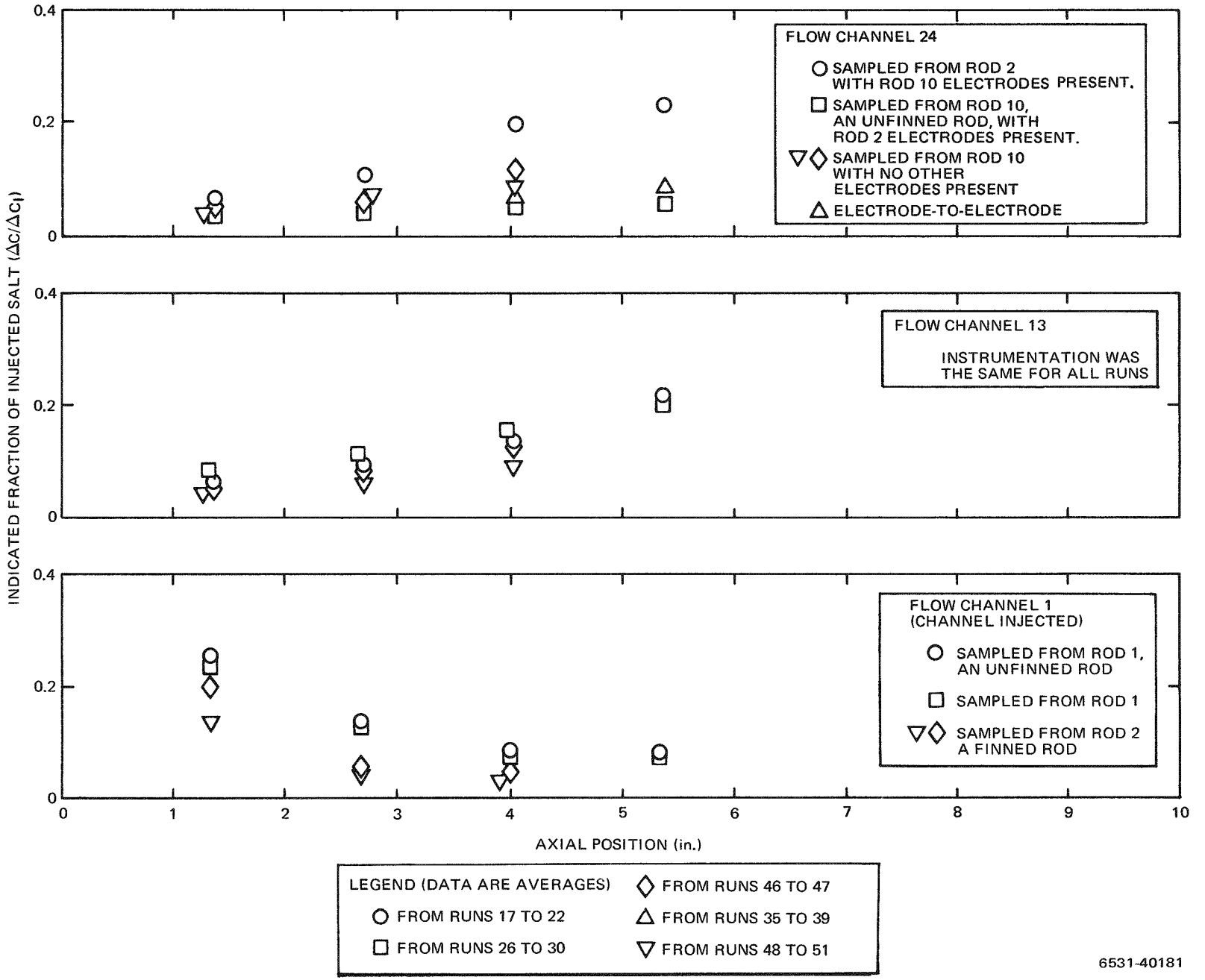

Figure 54. Effects of Sensor Orientation on Detection of Indicated Salt Fraction

unfinned elements. A sensor reading was apparently biased by the salt concentration near the surface of the instrumented element. Thus, if fins were sweeping "salty" water from an adjacent channel across the sensors on the finned element, these sensors would read a higher salt concentration than sensors at the same channel location but on an unfinned element. Conversely, if the fins were directing "fresh" water into a "salty" channel the sensors on the unfinned element would indicate the higher concentration. These effects are clearly indicated by the channel 24 and channel 1 data of Figure 54.

Because the flows in a channel were apparently separated into axial and spiral flows which were not mixed at the center of the channel, the instrumented elements were rotated slightly to locate the electrodes at the element gaps between channels (see Figure 55). This relocation, by increasing the likelihood of flow mixing, would allow measurement of a salt concentration more representative of the channel average concentration. Also, the shortest distance to ground for the electrode surface was across the ~0.024-in. gap between adjacent elements. Thus, these measurements, although not in a flow channel, would be more representative of concentrations at an axial position than those in the channel sample runs. Results of tests with the sensors located in this manner indicated that finned element spiral flows do not mix, even at the gaps between channels. The salt concentrations indicated by measurements from electrodes on a finned element sweeping "fresh" water into the gap were lower than those determined from measurements by an electrode on a finned element sweeping "salty" water into the gap.

As testing progressed, the observation and correlation of voltage changes which occurred in both the electrode calibration data and raw data indicated that interactions were occurring between signals from electrodes in the same instrumented element. Capacitive coupling between signal leads was suspected as the cause of these interactions, and changes in system connections were made to eliminate these interactions. These modifications consisted of:

1) Separation of the unshielded instrument lead wire to reduce capacitive coupling.

2) Reduction of probe excitation frequency from 200 kHz to 50 kHz.

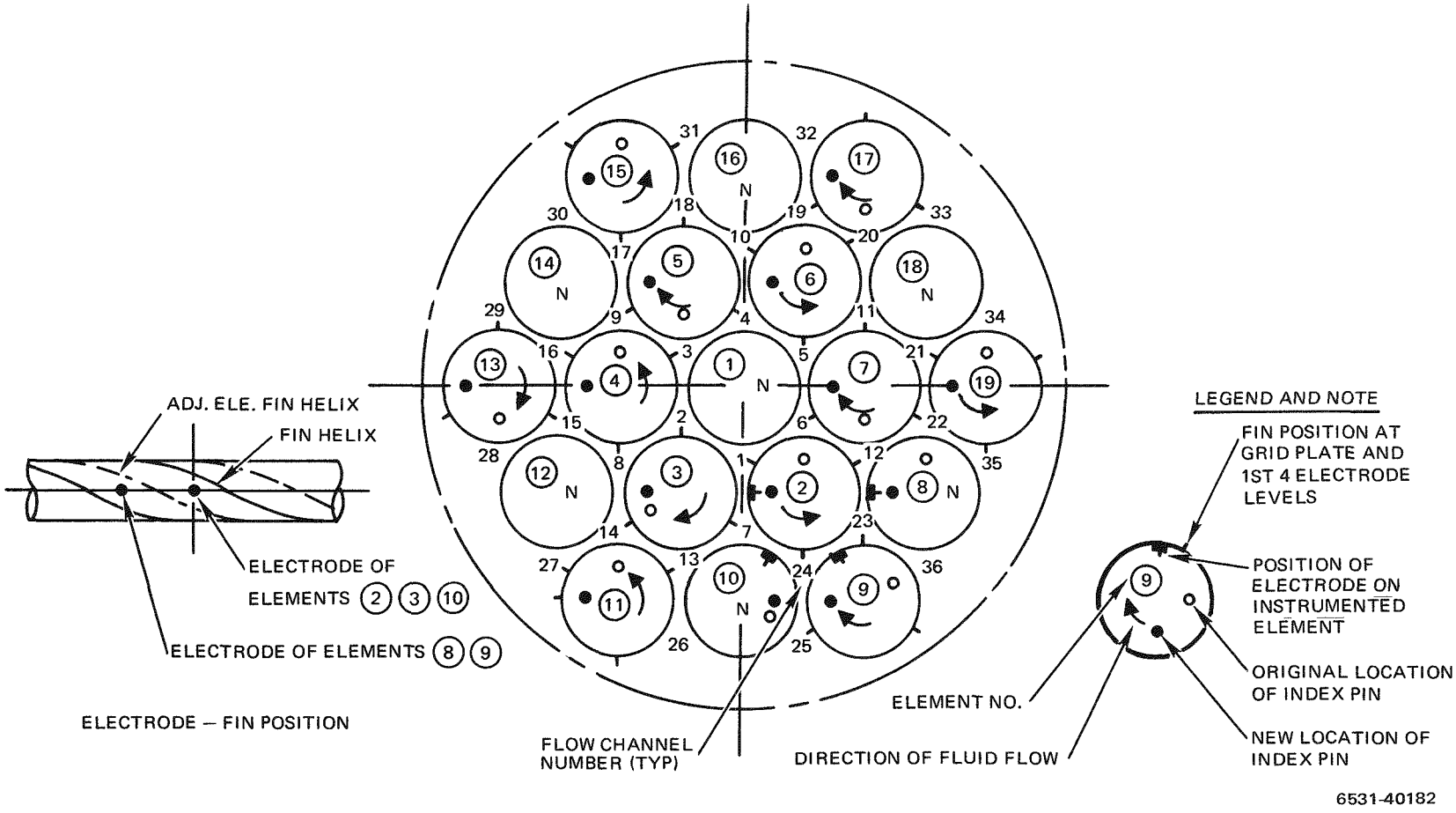

Figure 55. Orientation of Sensors at Channel Gaps

Checks of system operation and the results of injection tests performed after these modifications indicated that the modifications were successful.

The effects of these interactions, as they occurred in a somewhat random manner depending upon which leads were connected, cannot be evaluated. Comparison of results from tests prior to the elimination of interactions showed that the general trends and behavior of the injected salt solution were similar in each case. Thus, although the absolute magnitude of the measured concentration variations did not agree before and after the elimination of lead interactions, data with interactions present could still be used to interpret flow behavior in the test bundle.

The results from these preliminary tests were used to design the experimental and analytical approaches for tests of the R-L-N element configuration proposed for the SPF reactor. The observed flow characteristics and the signal interactions dictated changes in the injection system and the instrumentation systems. The discovery of two types of flow in the bundle was a major factor in the revision of the analytical model.

Testing of the SPF configuration provided data which could be correlated with the new analytical model. The relationship of flow characteristics to bundle geometry were determined by using the data from the nominal, 30-mil (0.026 in. actual) fin R-L-N bundle test data. Using the relationships developed from these data, the $\Delta C/\Delta C_I$ variations in the bundle channels were predicted for the 15-mil fin SPF configuration and for Configuration 8 of the preliminary R-L-N tests. Good agreement was obtained and the mixing parameter was calculated for all cases.

The test data for each SPF bundle configuration (Table 4) were obtained at three channel Reynolds numbers, 1.0×10^4, 1.5×10^4, and 2.0×10^4. Visual comparison of $\Delta C / \Delta C_1$ data showed that no significant resolvable difference existed between data sets at the three different Reynolds numbers (Figures 56 and 57). This indicated that the "best-fit" input parameter set for the analytical simulation would be independent of Reynolds number and, therefore, the mixing parameter for a given R-L-N configuration would be independent of Reynolds number.

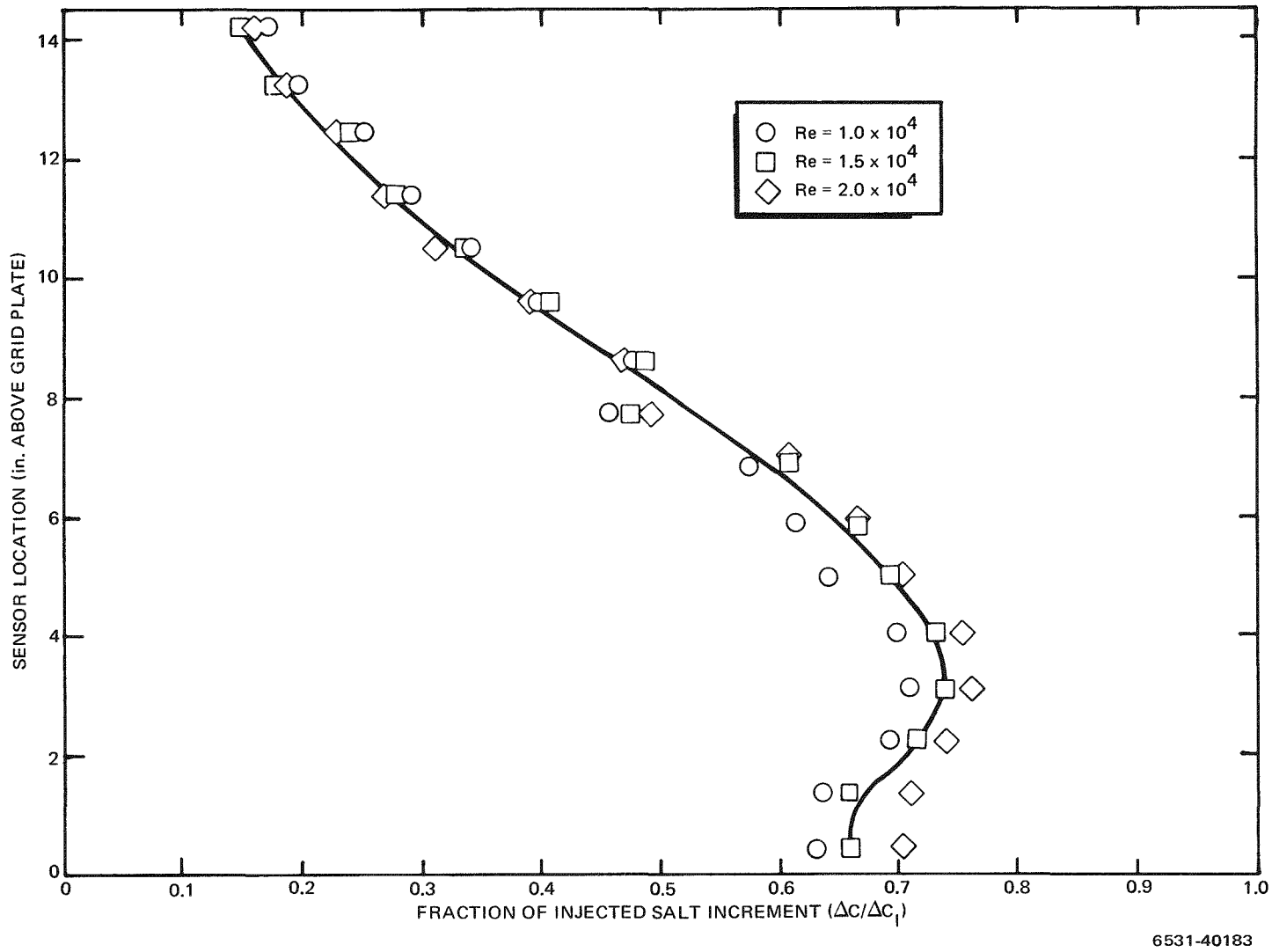

Figure 56. Absence of Significant Reynolds Number Effect on Flow Out of Injected Flow Channel – 15-mil Fin

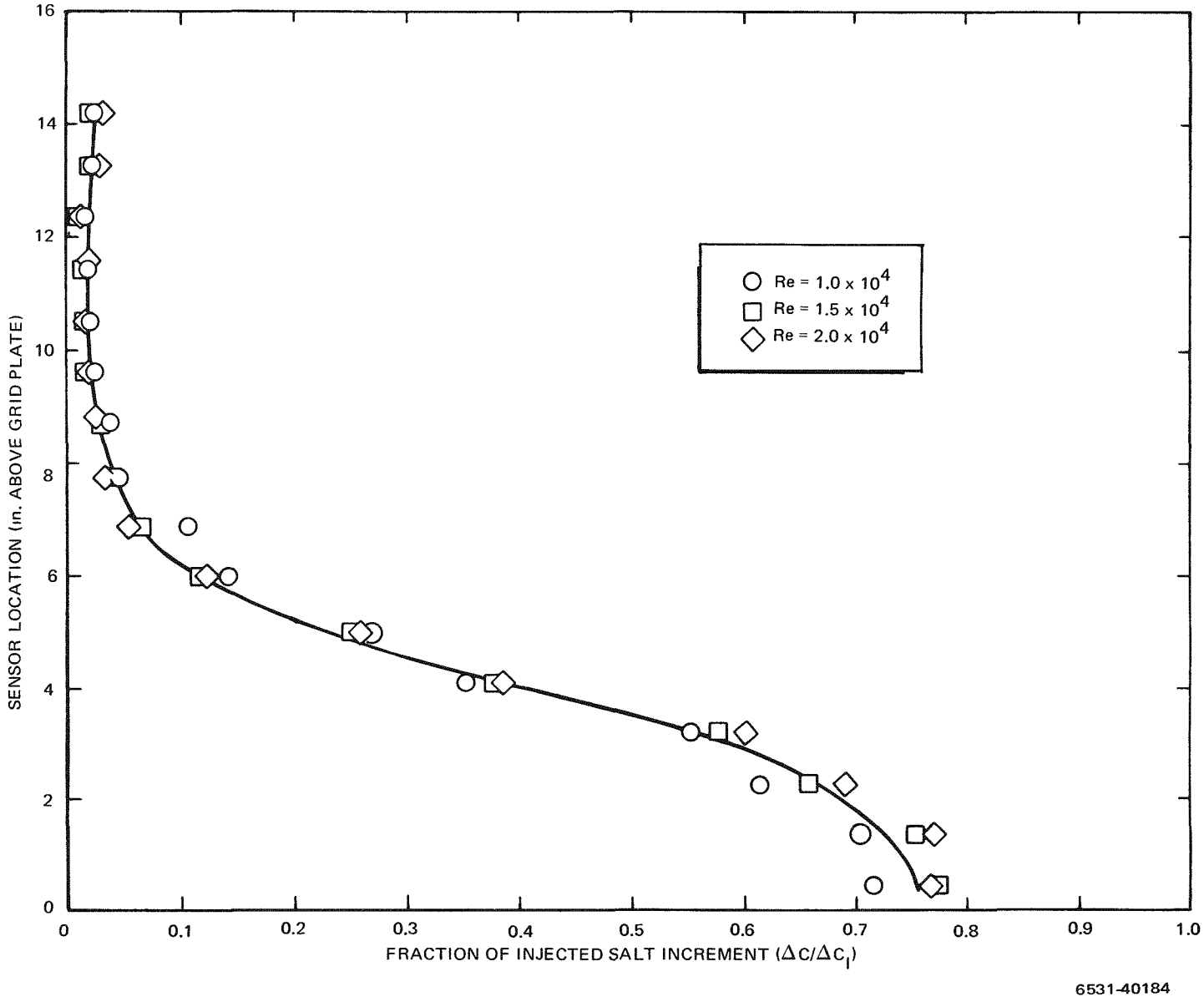

Figure 57. Absence of Significant Reynolds Number Effect on Flow Out of Injected Flow Channel — 30-mil Fin

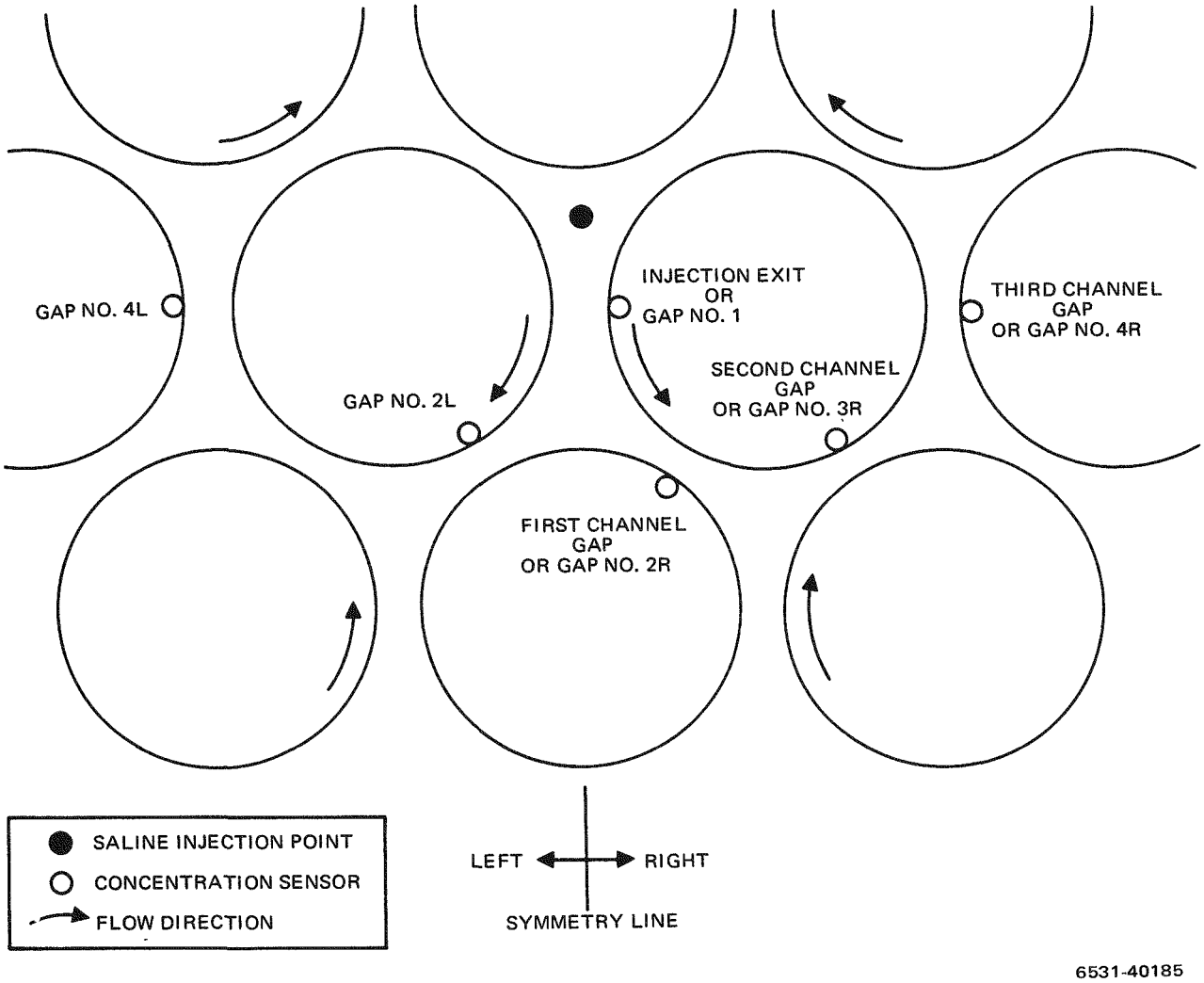

Figure 58. Identification of Channel Gaps for Analytical Model

Several element arrangements were necessary to define the $\Delta C/\Delta C_I$ values for the four channel gaps of interest (Figure 58). Because the data defining the $\Delta C/\Delta C_I$ variation in a channel gap were not recorded at the same time nor with totally identical configurations, there were certain data variations at given channels on repeated tests. Other data perturbations were caused by the $NaNO_3$ injection solution first encountering a "left" or "right" fin and assuming a preferred rotation state. Consequently, a simple method was devised to obtain a weighted $\Delta C/\Delta C_I$ variation for any given gap, independent of the gap being "right" or "left" of the injection tricusp channel.

This method of obtaining a weighted average $\Delta C/\Delta C_I$ was based on certain data points which were common to most measurement sets. The unnormalized data (Figures 59 and 60) were reduced to four, compatible, axial saline concentration distributions using these common data points, and then normalized to unit total concentration at that axial probe location where the injection exit gap (gap 1 in Figure 58) measurement peaked. This methodology was applied to the data from all the R-L-N tests where some form of improved data recording was used.

The excellent agreement of predicted and experimental concentrations for the 30-mil fin case (Figure 61) was to be expected. As these data had the most detailed concentration distributions (all gaps showed concentration peaking within the test bundle), they were used to determine the analytical model input parameters for the best-fit. The analytical concentration distributions for the 15- and 20-mil R-L-N finned cases were calculated using the linearized relationships between flow parameters and bundle geometry determined from the above best-fit data. Good agreement exists for the 15-mil hobbed fin data (Figure 62) but only fair agreement exists for the 20-mil plastic fin data (Figure 63). The latter is believed attributable to characteristics of the data acquisition system for this set of tests, and the relatively few data points available from this test.

The mixing parameters for these R-L-N configurations were evaluated using the expression giving the mixing parameter as a function of the geometry of a R-L-N array. Typically, the mixing parameter value increased from an initial value to some constant value (Figure 64). The calculated constant mixing parameter values are shown in Table 5.

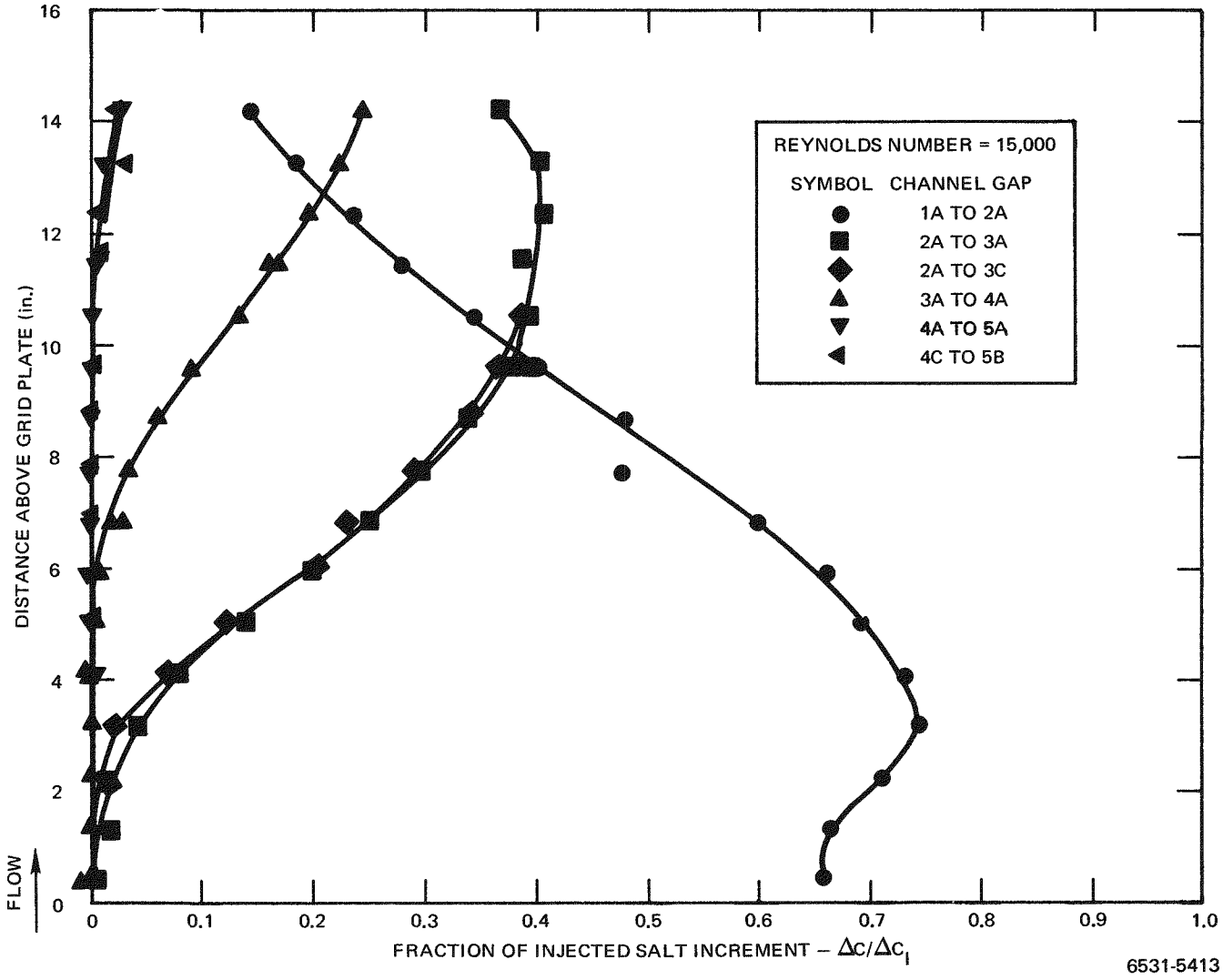

Figure 59. Tracer Salt Distribution, Mixing Model with Nominal 15-mil Fins

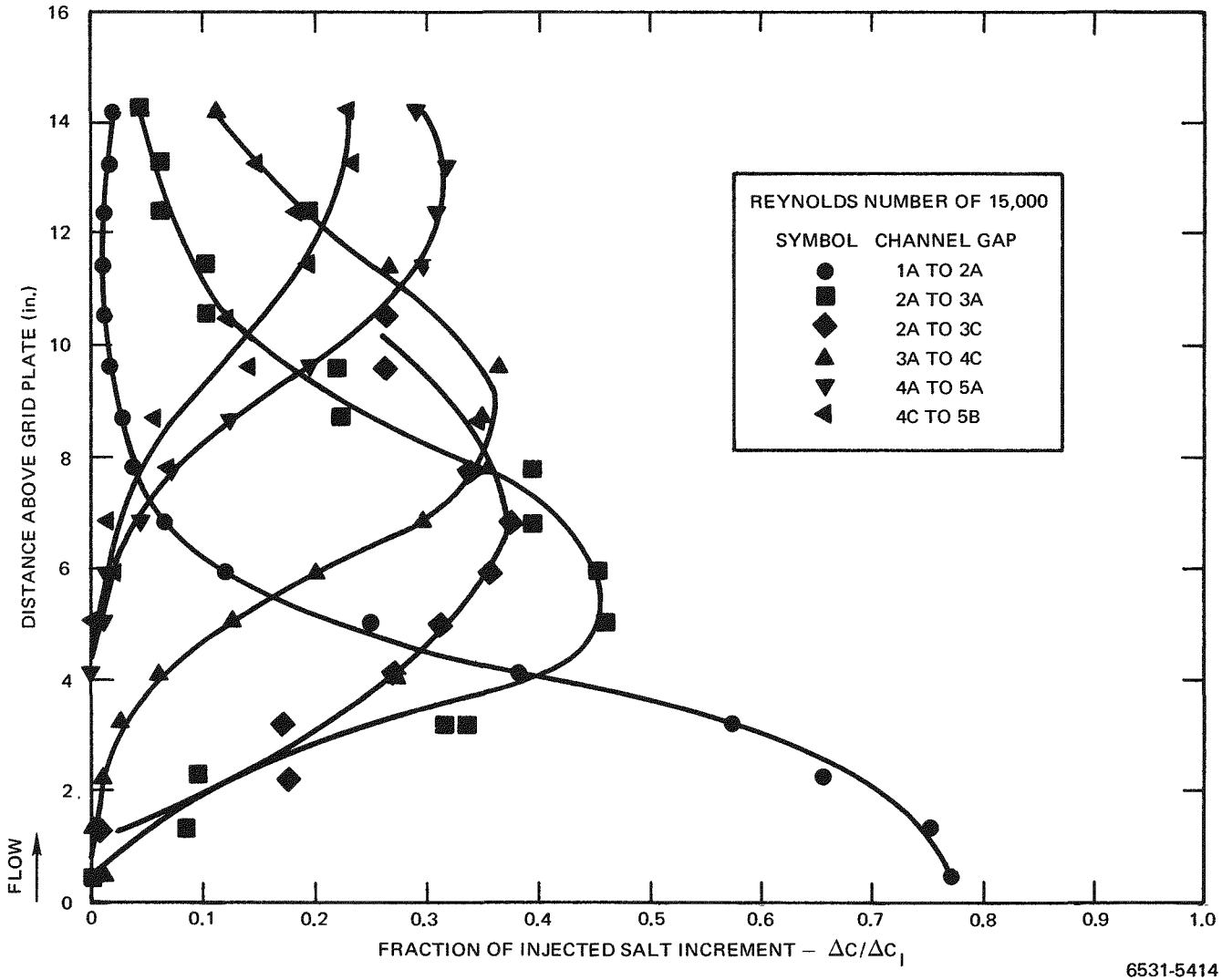

Figure 60. Tracer Salt Distribution, Mixing Model with Nominal 30-mil Fins

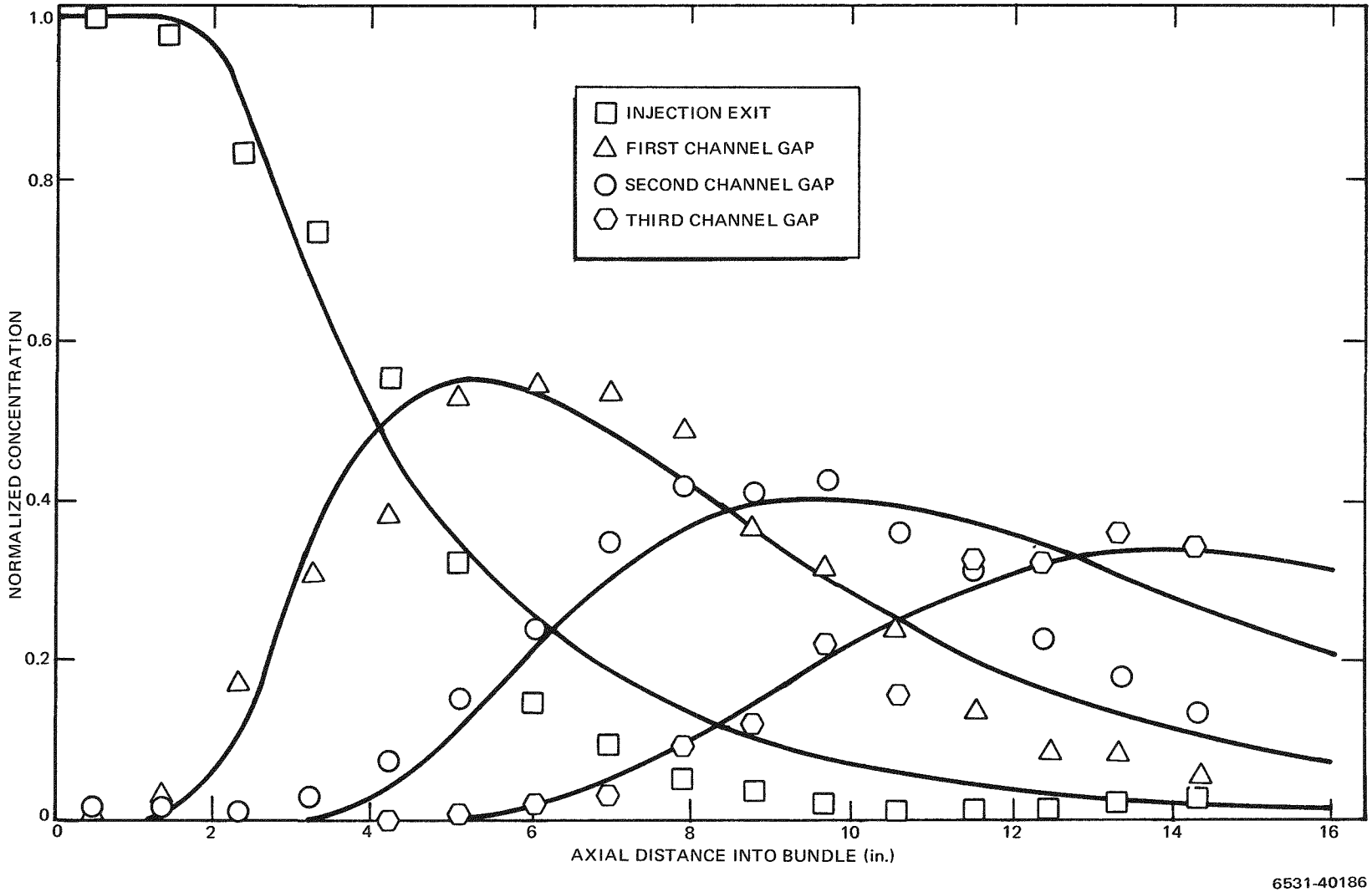

Figure 61. Theoretical-Experimental Comparison of Nominal 30-mil Fin Mixing Data (Best-Fit Input Parameter Set)

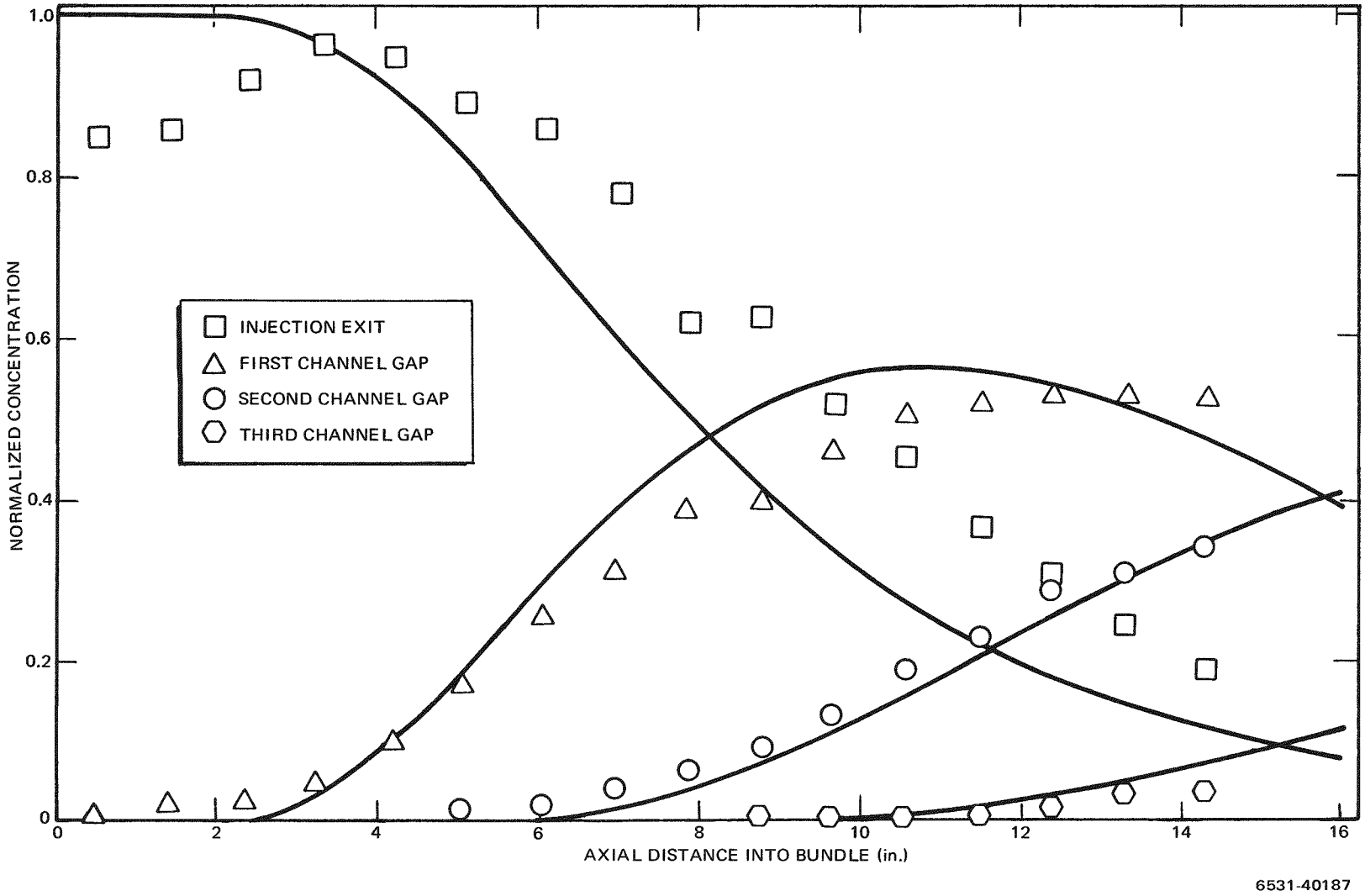

Figure 62. Theoretical-Experimental Comparison of Nominal 15-mil Fin Mixing Data

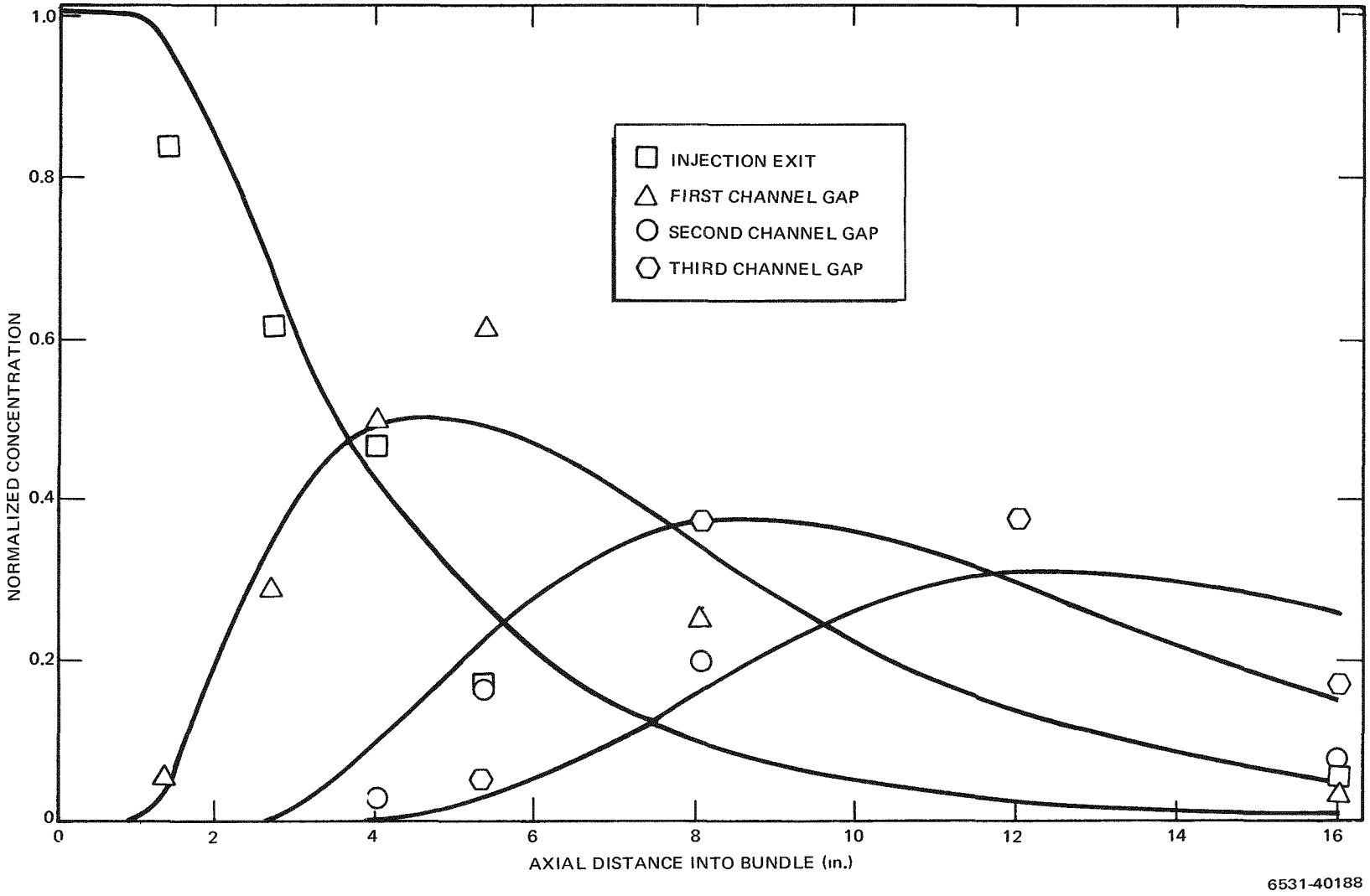

Figure 63. Theoretical-Experimental Comparison of Nominal 20-mil Fin Mixing Data

TABLE 5

VALUES OF MODELING PARAMETERS FOR FLOWS IN TEST BUNDLES

Parameter	Test Bundle – Nominal Fin Height		
	0.015 mil	0.020 mil	0.030 mil
$P_{flow,i}$ (in.)	20.0	15.2	20.0
$P_{flow,f}$ (in.)	10.5	7.6	10.5
t_{flow} (in.)	0.008	0.013	0.019
Z_{ent} (in.)	5.76	3.68	2.50
D_R/V (%)	3.50	3.50	3.50
D_A/V (%)	0	0	0
h_{mix}^* (%/in.)	13.7	26.6	24.8

*Final value given.

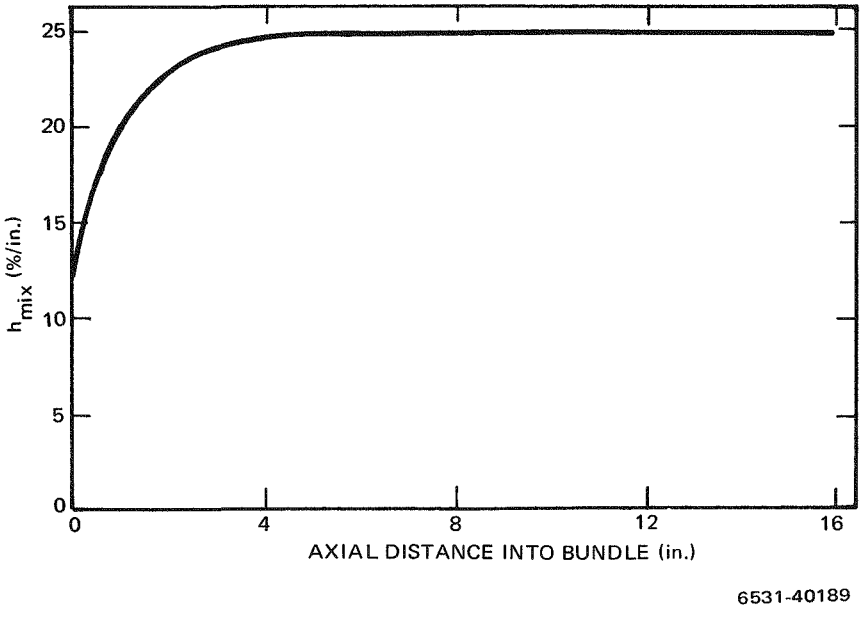

Figure 64. Variation of Mixing Parameter with Distance Downstream of the Flow Channel Entrance for 30-mil Fin Test Bundle

C. CONCLUSIONS

A combined analytical and experimental effort has resulted in the development of an experimental method for the measurement of mixing phenomena and a mixing theory for the R-L-N finned element array selected for use in the ZrH reactor. The experimental method of using in-bundle conductivity sensors to detect the distribution of an injected $NaNO_3$ solution proved adequate not only for determining this distribution in a test bundle but also for identifying the two types of test bundle flow: an axial flow down a channel and a spiral flow around the finned elements. Modeling of these two types of flow was an important facet of the mixing theory. This satisfactory modeling, and the use of first-order approximations to the dependence of flow parameters on array geometry allowed the advanced diffusion-dilution mixing theory to calculate, with good agreement to experimental results, the flow-channel axial $NaNO_3$ concentration distributions for several fin geometry dimensional variations. During this study, a mixing correlation was also developed which allowed calculation of channel-to-channel mixing in an R-L-N array as a function of several array geometrical constants.

IV. CORE PRESSURE DROP

During the sequence of mixing tests, pressure-drop measurements were made for all configurations tested. These measurements were made as the mixing test schedule allowed, with a minimum of interference with testing. The flow system used for these tests was identical to that used in the mixing tests except for the addition of two variable area flowmeters to allow testing at low flows (see Figure 41) for some configurations.

A. MEASUREMENT METHODS

The measurement methods used were generally chosen to cover the range of pressure differences expected with sufficient sensitivity to provide meaningful data. Data recorded during the initial tests for the mixing ability of various configurations used either pressure gages or mercury manometers. For subsequent tests with the elements with hobbed fins, the pressure tap locations (Figure 65) required greater sensitivity so manometers with indicating fluid specific

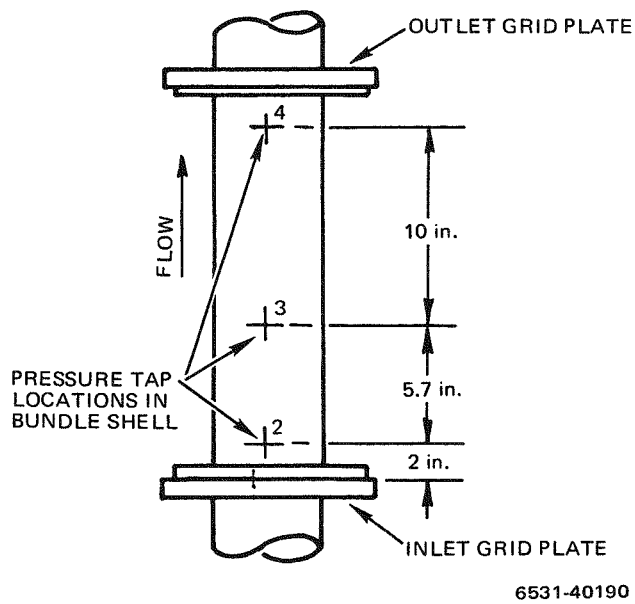

Figure 65. Bundle Pressure Tap Locations

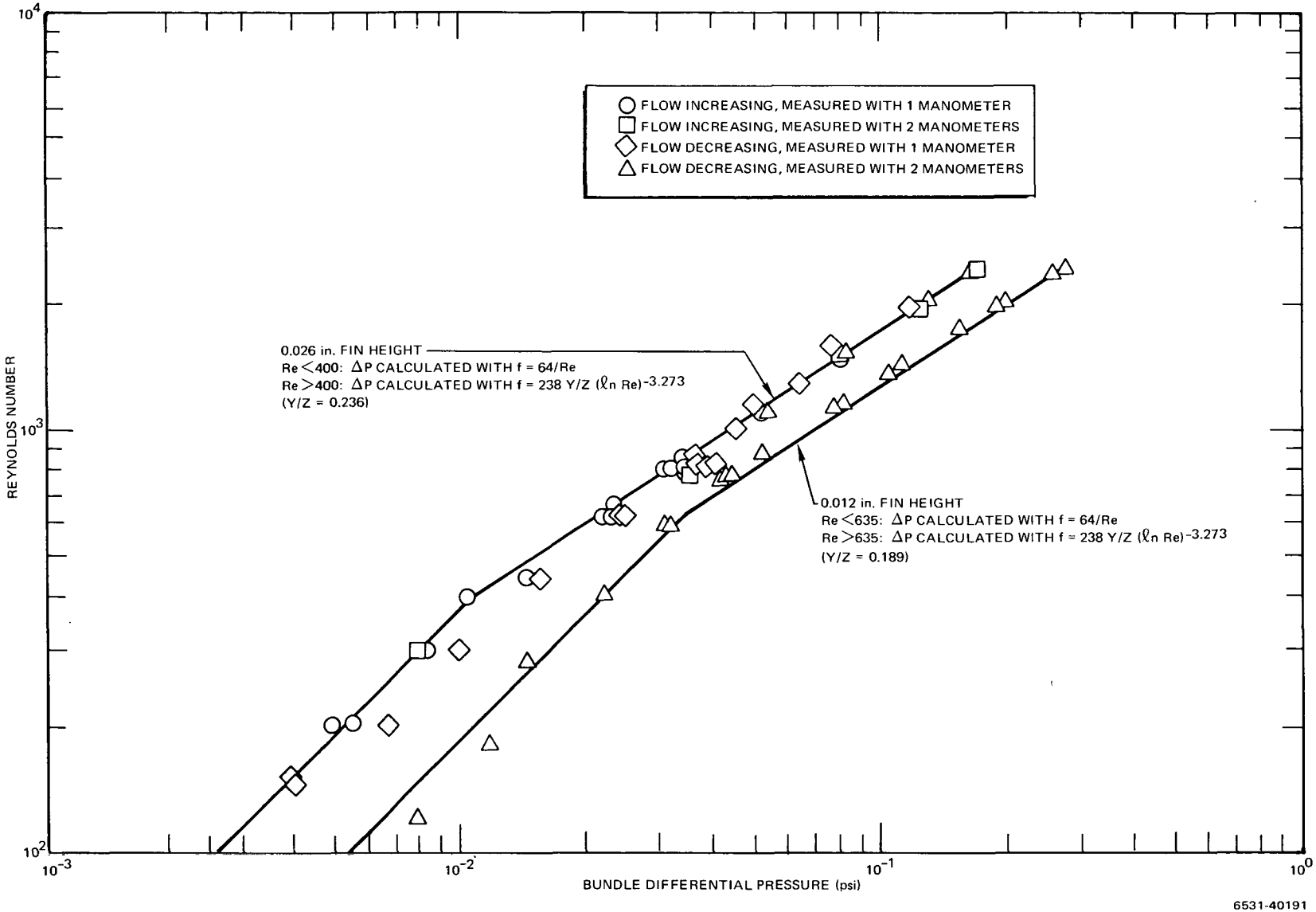

Figure 66. Test Bundle Pressure Drops with R-L-N Elements

gravities of 2.95, 1.75, and 1.20 were used as appropriate. For those tests where low Reynolds Number (i.e., $100 \leq Re \leq 3000$) pressure-drop data were desired, inclined manometers were used with low specific gravity indicating fluid.

The small differential pressures encountered at the low Reynolds number flows (see Figure 66) were apparently not great enough to overcome a measurement system surface tension and/or fluid inertia effect. This effect caused the measuring system to exhibit a "dead band" bordered by pressure-drop measurement made when system flow was increasing and when flow was decreasing. Artificially deflecting the inclined manometers by briefly venting one side while the system flow was constant demonstrated that the indicated pressure differential would never settle out at a value higher than that obtained when flow was being decreased, i.e., when manometer differential indications were approached from larger differential readings. Thus, only readings taken when the manometer fluid settled out from a higher differential reading were used in determining the low Reynolds number pressure drops.

B. RESULTS AND CONCLUSIONS

Using the measured pressure drops, the friction factor variation with Reynolds number was calculated for each test configuration. Based on the test results, qualitative observations were made of the relationship of bundle friction factor to mixing effectiveness. These friction factor versus Reynolds number data were also used to develop a correlation for the bundle friction factors for the finned element arrays as a function of Reynolds number.

Results of the early test data for finned configurations showed that any increase in flow mixing over the unfinned element case also resulted in an increase in bundle friction factor (see Figure 67). This increase in friction factor between different configurations was not necessarily directly related to the increase in mixing observed. For similar configurations, however, increased mixing produced increased pressure drop. Of the configurations tested in the evaluation phase of the program, the R-L-N arrays gave the best tradeoff between mixing and pressure drop.

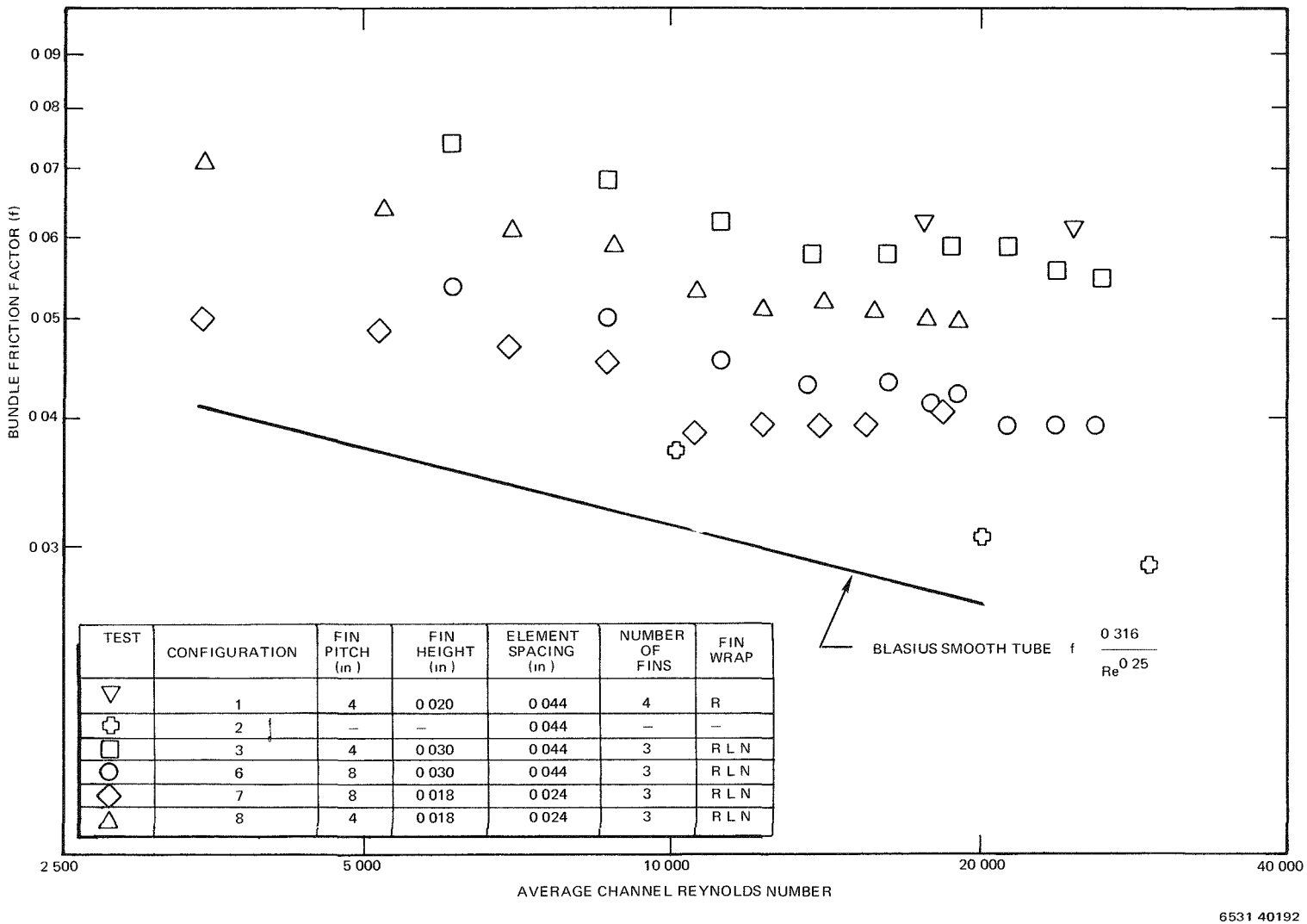

TEST	CONFIGURATION	FIN PITCH (in)	FIN HEIGHT (in)	ELEMENT SPACING (in)	NUMBER OF FINS	FIN WRAP
▽	1	4	0 020	0 044	4	R
✿	2	–	–	0 044	–	–
□	3	4	0 030	0 044	3	R L N
○	6	8	0 030	0 044	3	R L N
◇	7	8	0 018	0 024	3	R L N
△	8	4	0 018	0 024	3	R L N

Figure 67. Variation of Test Bundle Friction Factors with Channel Reynolds Number

The development of the correlation between friction factor and bundle Reynolds number for turbulent flow in the R-L-N finned array was originally based on a correlation for a triangular array of fuel pins each wrapped with a single wire.* As additional results became available from testing of the hobbed fin configuration (see Figures 68 and 69) the satisfactory correlation for laminar flow data was found to be 64/Re. However, further improvements were required in the correlation for the transition and turbulent flow regions. The final form of the correlation is:

$$f = 238 \frac{Y}{Z} (\ln Re)^{-3.273} \quad ,$$

where f is the bundle friction factor and Y and Z are functions of test bundle geometry. Y is a function of the ratio of element pitch to element diameter, P/D (see Figure 70). Z is given by

$$Z = \left(\frac{l}{d} \frac{0.5}{N} \frac{S}{h} \right)^{0.5}$$

where

l = fin pitch

d = fuel pin diameter

N = average number of fins per flow channel

h = average fin height

S = space between elements.

Friction factor values are plotted versus Reynolds number calculated as $Re = Vd\rho/\mu$ where

V = fluid velocity

d = bundle hydraulic diameter

ρ = fluid density

μ = fluid viscosity.

*W. A. Sangster, "Calculation of Rod Bundle Pressure Loss," ASME Paper 68-WA/HT-35

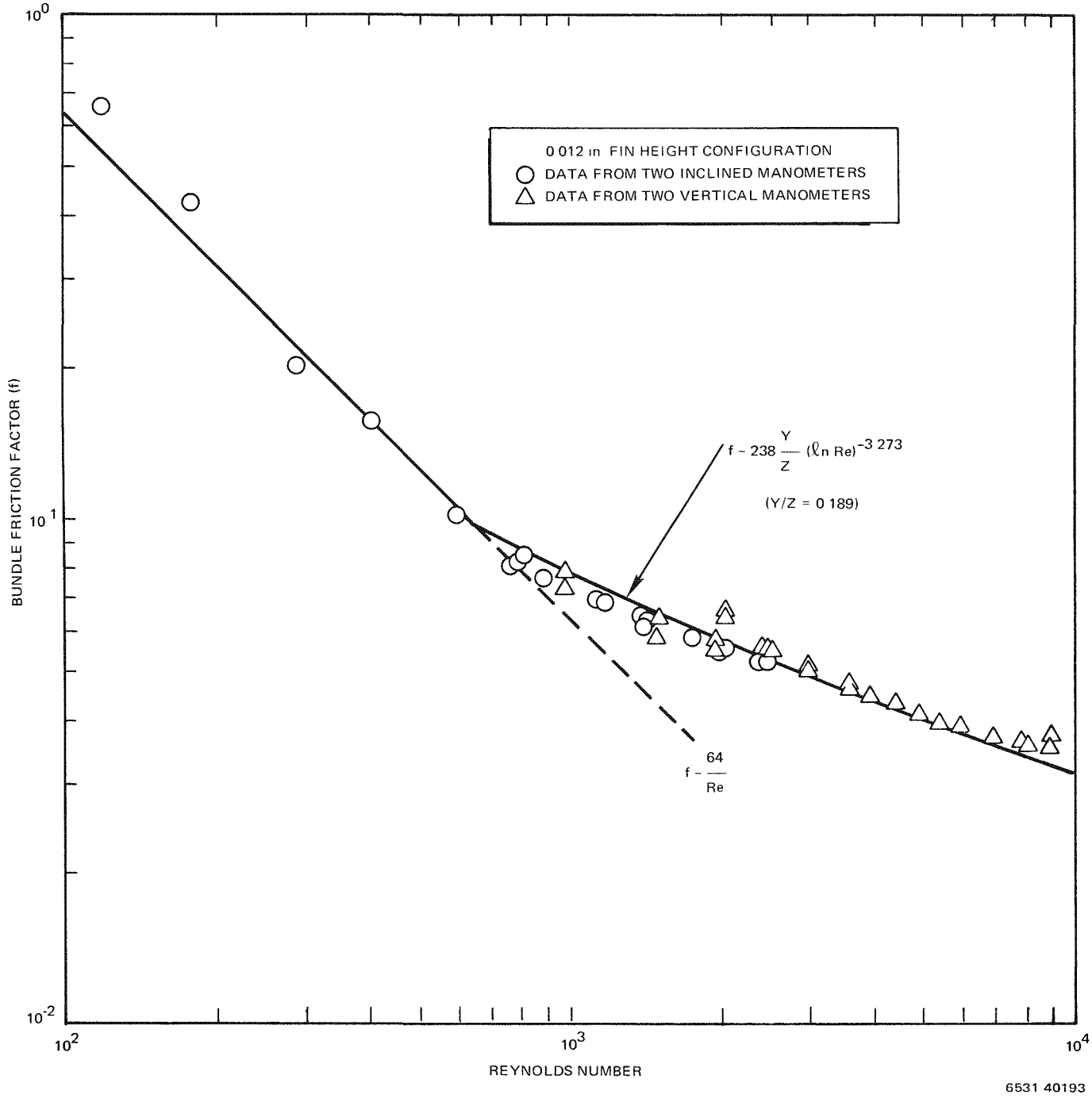

Figure 68. Friction Factor Variation with Reynolds Number

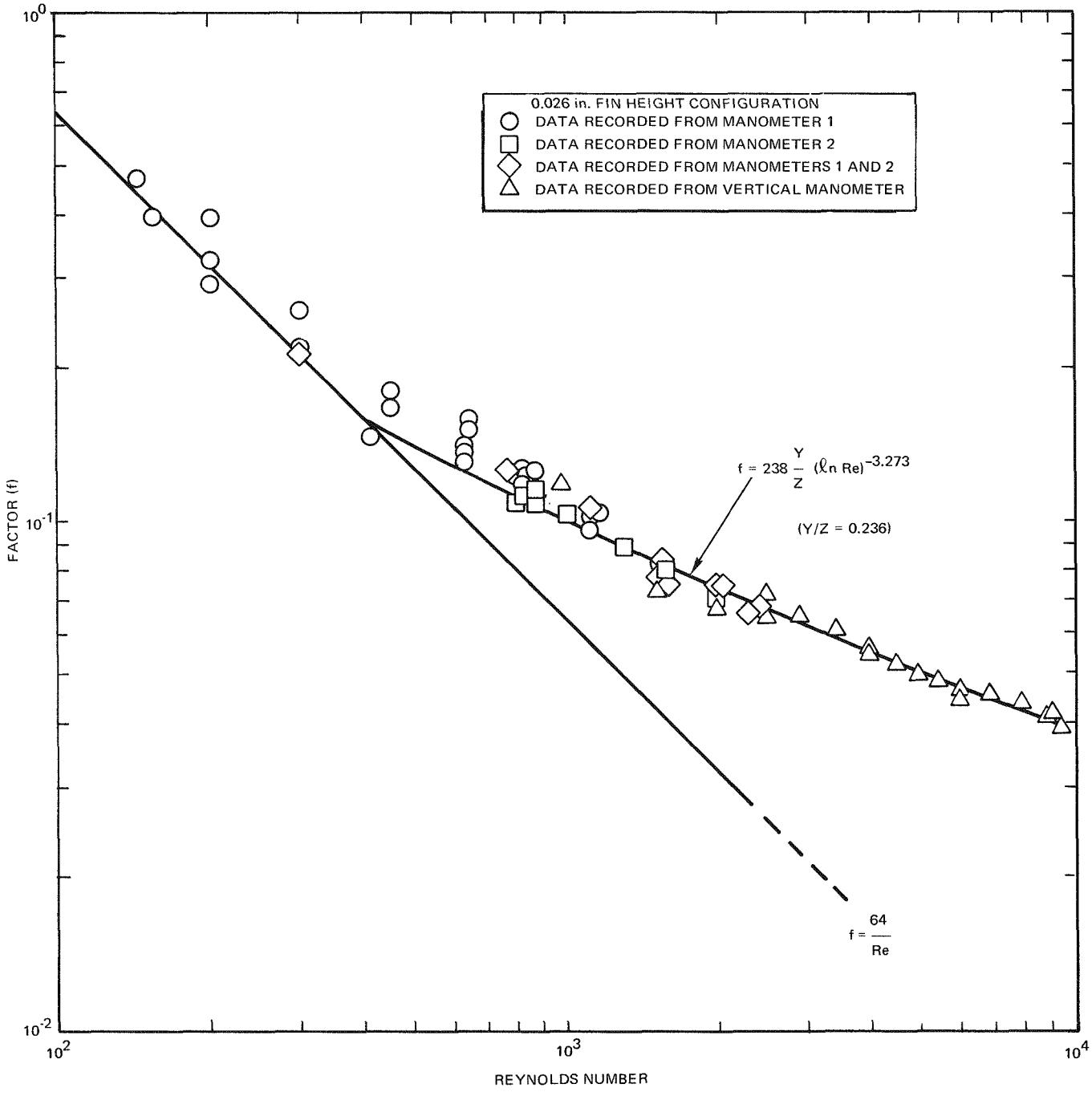

Figure 69. Friction Factor Variation with Reynolds Number

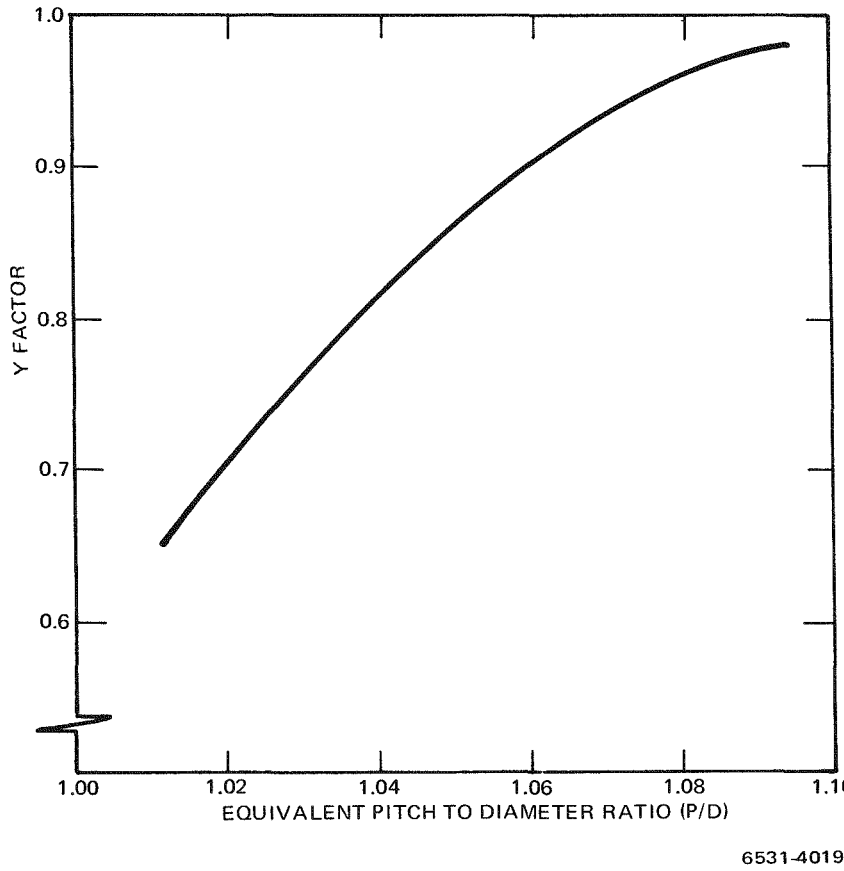

Figure 70. Variation of Y Factor with Bundle Element Pitch to Element Diameter Ratio